THE BEHAVIOR OF BEAMS SUBJECTED TO CONCENTRATED LOADS

by

Paul B. Summers

Joseph A. Yura

Sponsored by

American Iron and Steel Institute

Phil M. Ferguson Structural Engineering Laboratory

Department of Civil Engineering

University of Texas at Austin

PMFSEL Report No. 82-5

August 1982

A C K N O W L E D G M E N T S

The report herein, which is the M.S. thesis of Paul Summers, was sponsored by the American Iron and Steel Institute. Their financial support is greatly appreciated. The facilities of both the Phil M. Ferguson Structural Engineering Laboratory and the Department of Civil Engineering at The University of Texas at Austin were used. The computer analysis was done using the University computer system.

The authors also acknowledge the guidance of Dr. C. Phillip Johnson, who was the other member of Paul Summers' supervisory committee, Dr. Karl H. Frank and Dr. Richard E. Klingner. Special thanks are extended to graduate students John M. Joehnk and to David R. Wright who helped in this research.

The help of Hank Franklin and James Stewart in the preparation of the model beams, and the assistance of Dave Whitney and Bob Gedies in the photography is sincerely appreciated. Also acknowledged is the continual assistance of Laurie Golding and Maxine DeButts, and the friendly cooperation of both Tina Robinson who typed the complete manuscript and Deanna Thomas who so excellently drafted all of the figures.

A B S T R A C T

Tests on composite steel and concrete beams, continuous steel beams and simply supported plexiglass model beams, subjected to a concentrated load at midspan have demonstrated a buckling phenomenon where the bottom flange, which is primarily in tension, moves laterally. A complete parametric study was undertaken using a linear elastic finite element buckling analysis program to gain insight into this behavior.

Results are presented for beams under a single midspan concentrated load with varying end restraint in-plane. The phenomenon was found to be a combination of local web buckling and lateral-torsional buckling, the former effect being dominant in simply supported beams and the latter in fixed ended beams. For beams with end restraint in between these cases (including most continuous beams), an interaction of the two effects occurs.

It was found that bending stresses significantly influence the load at which there is a local web buckle between the top and bottom flange braces at the load point. Also observed was the fact that when the bottom flange was unbraced, the addition of a brace there did little to increase the buckling load if the beam was simply supported, but dramatically increased it when the beam was fixed ended.

Design recommendations for beams subjected to concentrated loads are provided along with a design example.

TABLE OF CONTENTS

N O T A T I O N

A_f	Area of flange
a	$\sqrt{EC_w/GJ}$
b	Width of flange
b_{eff}	Effective length of web used in calculation of spring stiffness
b_s	Width of stiffener
C_b	Distance from neutral axis of beam cross section to mid-thickness plane of bottom flange
C_w	Torsional warping constant
C_1	Coefficient for lateral-torsional buckling of a beam
d	Distance between flange centerlines
d_{wc}	Distance from web-compression flange junction to neutral axis
E	Modulus of elasticity
G	Elastic shear modulus
G, G_c, G_D	Joint bending stiffness ratio (subscripts apply to respective ends of the column)
h	Clear distance between flanges
I	Moment of inertia of cross section
I_f	Moment of inertia of flange for out-of-plane bending
I_w	Moment of inertia of unit width of web
I_y	Moment of inertia of cross section about Y-axis
J	Torsion constant
J_{tf}	Torsion constant of top flange

$[K_g]$	Out-of-plane geometric stiffness
$[K_i]$	In-plane structural stiffness
$[K_o]$	Out-of-plane structural stiffness
k	Stiffness of bottom flange lateral spring
k^*	Minimum spring stiffness required to force buckling into second mode of an axially compressed flange = $4P^*/L$
L	Length of beam
L_1	Length between inflection points of beam
ℓ	Length of beam between brace points
M_{cr}	Elastic buckling moment of beam
M_N	Negative end moment
M_{sm}, M_{la}	Smaller and larger end moments of a section of beam between braces. Ratio M_{sm}/M_{la} is moment coefficient for lateral-torsional buckling.
m	Uniformly distributed moment
P, P_X, P_Y	Applied concentrated load; in X,Y directions, respectively.
P_{BAS}	Buckling load given by Basler Theory
P_{BFU}	Buckling load for fixed ended beams with unbraced bottom flange
$P_{BFU\alpha}$	Buckling load for beams of end restraint defined by α with unbraced bottom flange
P_{cr}	Elastic buckling load of beam
P_E	Reference Euler buckling load of pinned-pinned web column = $\pi^2 E t_w^3/12h$
P_{LOC}	Load to cause local web buckling
P_{TFU}	Buckling load of simply supported beam with unbraced tension flange

P_{VC}	Buckling load of beam when only vertical stresses are present
P^*	Reference load at which an axially compressed flange would buckle in the second mode = $4\pi^2 EI_f/L^2$
R_1, R_2	Stiffnesses of rotational springs applied at ends of web column
$\{R_i\}$	Nodal forces due to in-plane loading
$\{r_i\}$	Nodal displacements due to in-plane loading
$\{r_o\}$	Out-of-plane displacements (buckled shape)
T	Stiffness of lateral spring applied at end of web column
t	Nondimensional spring stiffness = Th/P_E
t_f	Thickness of flange
t_s	Thickness of stiffener
t_w	Thickness of web
X,Y,Z	Coordinate axes
u,v,w	Displacements in X, Y, and Z directions, respectively
α	Coefficient representing negative end restraint = $M_N/(PL/8)$
Δ	Lateral deflection of bottom flange in buckled state
$\Delta_1, \Delta_2, \Delta_3$	Components of Δ due to translation of top flange, rotation of top flange, and bending distortion of web, respectively
δ	Lateral deflection of tension flange under unit midspan lateral load = $L^3/48EI_f$
θ	Rotation of the top flange at buckling
θ_X, θ_Y	Rotations about X,Y axes, respectively
λ	Constant used in computing lateral buckling load
ν	Poisson's ratio

π	3.1416
σ	Stress
σ_b	Bending stress at web-flange junction under critical load to cause local web buckling
σ_{bc}	Critical stress for web buckling in bending
σ_{fc}	Critical buckling stress in the bottom flange
σ_v	Vertical compressive stress under load in web
$\sigma_{v\ max}$	Maximum vertical compressive stress under load in web
σ^*	Reference stress = P^*/A_f

CHAPTER 1

INTRODUCTION

1.1 Structural Behavior

A beam subjected to gravity loads along a laterally supported top flange would be checked for yielding in bending and shear, local buckling of the compression flange and web behavior under any concentrated loads. The web would be checked for both buckling and yielding under each concentrated load. If the beam is simply supported, the above mentioned failure modes assume that the bottom (tension) flange does not move laterally. However, it has been observed experimentally that under certain circumstances, beams both simply supported and those with any degree of end fixity or continuity, can reach a state of instability in a mode that previously has been rarely acknowledged.

Tests at both Lehigh University and at The University of Texas at Austin have shown beams buckling with lateral movement of the bottom flange. In a continuous beam this flange is primarily in tension (with some compression near the supports), but in a simply supported beam it is purely in tension. These beams had sufficient lateral bracing of the "compression" flange to ensure that conventional lateral-torsional buckling had not yet occurred at the loads under which they failed.

Daniels and Fisher[11] conducted tests on simply supported composite beams with a span of 25 ft. between bearings. The beams consisted of a reinforced concrete slab 60 in. wide and 6 in. thick connected to a W21x62 steel beam by pairs of stud shear connectors. The beams were supported at their ends by steel rollers that were free to move as the lower flange extended during loading. Figure 1.1 shows the beam cut at midspan after the test. At the failure load

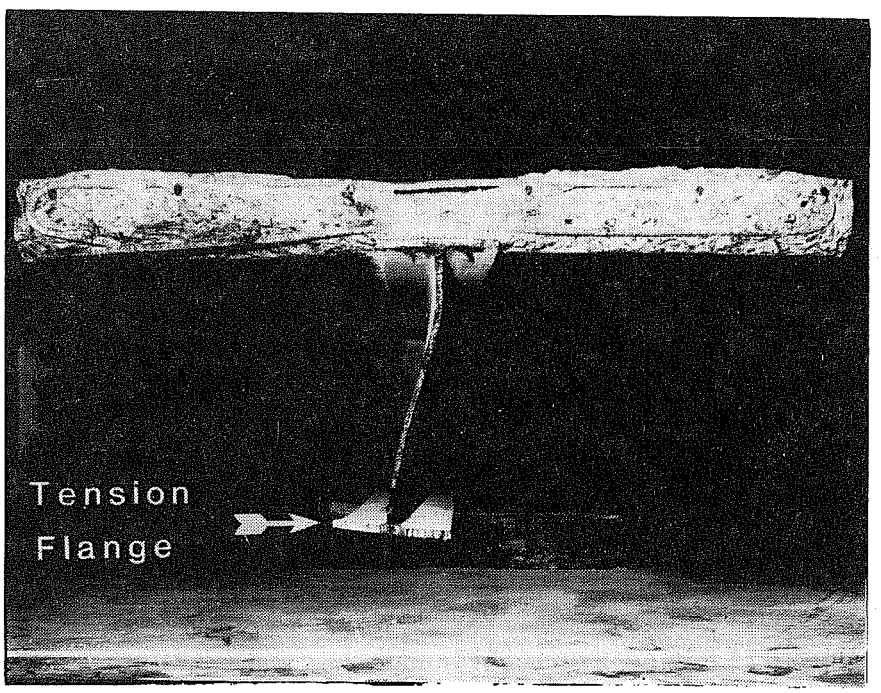

Fig. 1.1 Lateral movement of tension flange in composite beam of Daniels and Fisher[11] test

crushing of the concrete had progressed to full depth of the slab and considerable yielding of the steel beam had occurred, but astonishingly, the tension flange had deflected laterally.

Bansal[4] and Yura[18] have reported the results of a research program of over forty tests on three-span continuous steel beams. The loading and support conditions for the test beams were so arranged as to simulate a real beam in a rigid building frame. The loads on the beams were applied to the bottom flange and upwards rather than in the gravity load orientation for ease of testing, and were only applied in the central span (20 ft.). The side spans (4 ft.-6 in.) provided continuity to the beam at the interior support points where vertical stiffeners were welded to the web. Lateral bracing was provided at supports and load points.

Figure 1.2 shows an M14x17.2 steel beam loaded vertically upwards at midspan between the central supports, with lateral bracing on the bottom flange, which is primarily in compression, at the load point and at the 1/4-points of the central span. Furthermore, twist of the flange about the longitudinal axis is prevented under the load point by the loading mechanism itself. The photograph shows the lateral movement of the top flange, which is primarily in tension, at the failure load. Figure 1.3, although from a different test beam, shows this movement in more detail. It is a photograph of the beam cut at midspan where the load was applied. Once again, as in the Daniels and Fisher test, this movement of the "tension" flange can be seen. Both inelastic and elastic buckling in this mode were observed in the series of tests. The phenomenon also occurred in beams with two or three equal loads, symmetrically applied within the central span. In all cases in which the lateral movement of the tension flange in the positive moment region occurred, the failure was catastrophic. There was very little post-buckling strength.

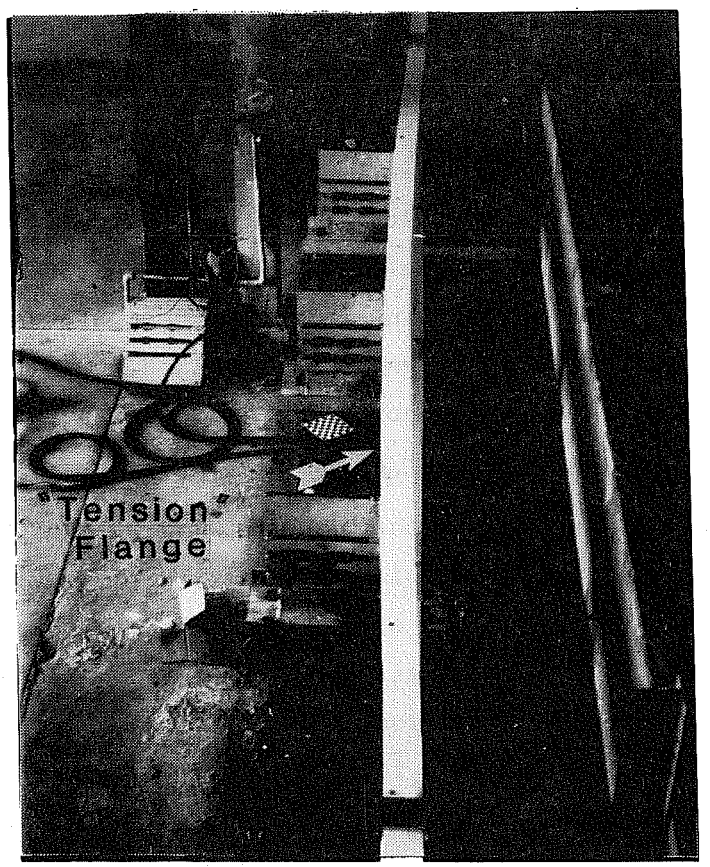

Fig. 1.2 Lateral movement of "tension" flange in three-span continuous beam[18]

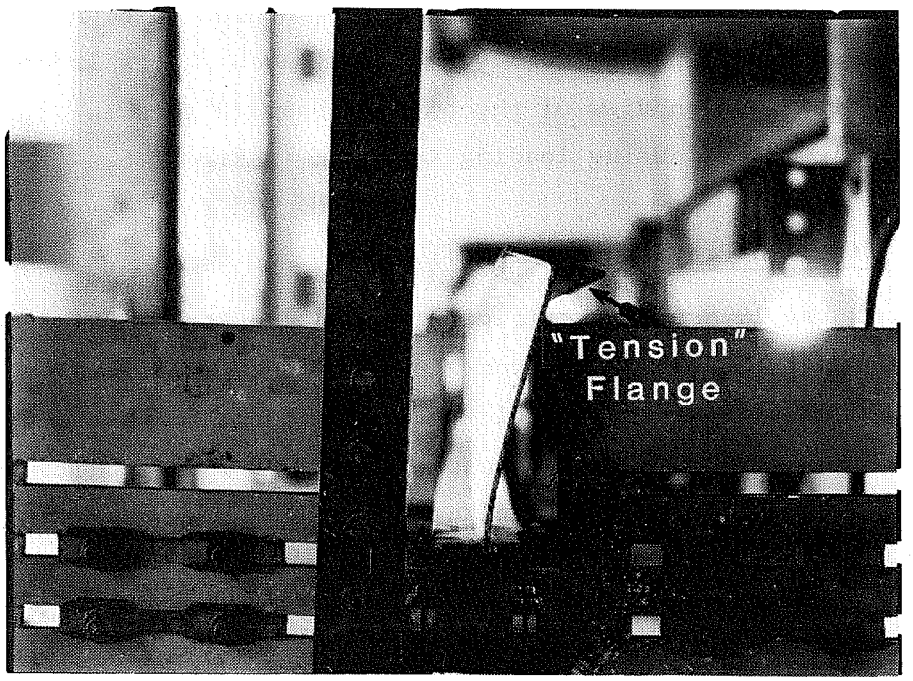

Fig. 1.3 Cross section at load point of three-span continuous beam[4] showing lateral movement of "tension" flange

A third observation of the phenomenon was an acrylic (plexiglass) model beam of wide-flange shape developed by Oral, a graduate student of The University of Texas at Austin. The beam was simply supported over a 24 in. span and was 1-1/2 in. deep. The bracing and loading arrangements were the same as those for the continuous beam of Fig. 1.2.

Figure 1.4 shows once again that the phenomenon of a failure mode, in which the flange primarily in "tension" deflects laterally, clearly exists. A plan view of the buckled beam is seen in Fig. 1.5, and a side view of it during loading is shown in Fig. 1.6.

1.2 Specification Provisions

Both the 1978 AISC Specification[3] and the Structural Stability Research Council (SSRC)[17] Guide contain provisions enabling the designer to approximate the elastic buckling moment for I-beams, wide-flange sections or doubly symmetric plate girders when such members are loaded by end couples in the plane of the web, or by transverse loads applied in the plane of the web. The load to cause lateral-torsional buckling of the beam can be obtained from the following equation:

$$M_{cr} = C_1 \frac{\pi}{\ell} \sqrt{EI_y GJ} \sqrt{1 + \frac{\pi^2 a^2}{\ell^2}} \qquad (1.1)$$

where M_{cr} = elastic buckling moment

C_1 = buckling coefficient dependent on loading and support conditions obtained from information reported by Clark and Hill[9] and Salvadori[16]

ℓ = unbraced length of beam

E = modulus of elasticity

G = shear modulus

I_y = weak-axis moment of inertia

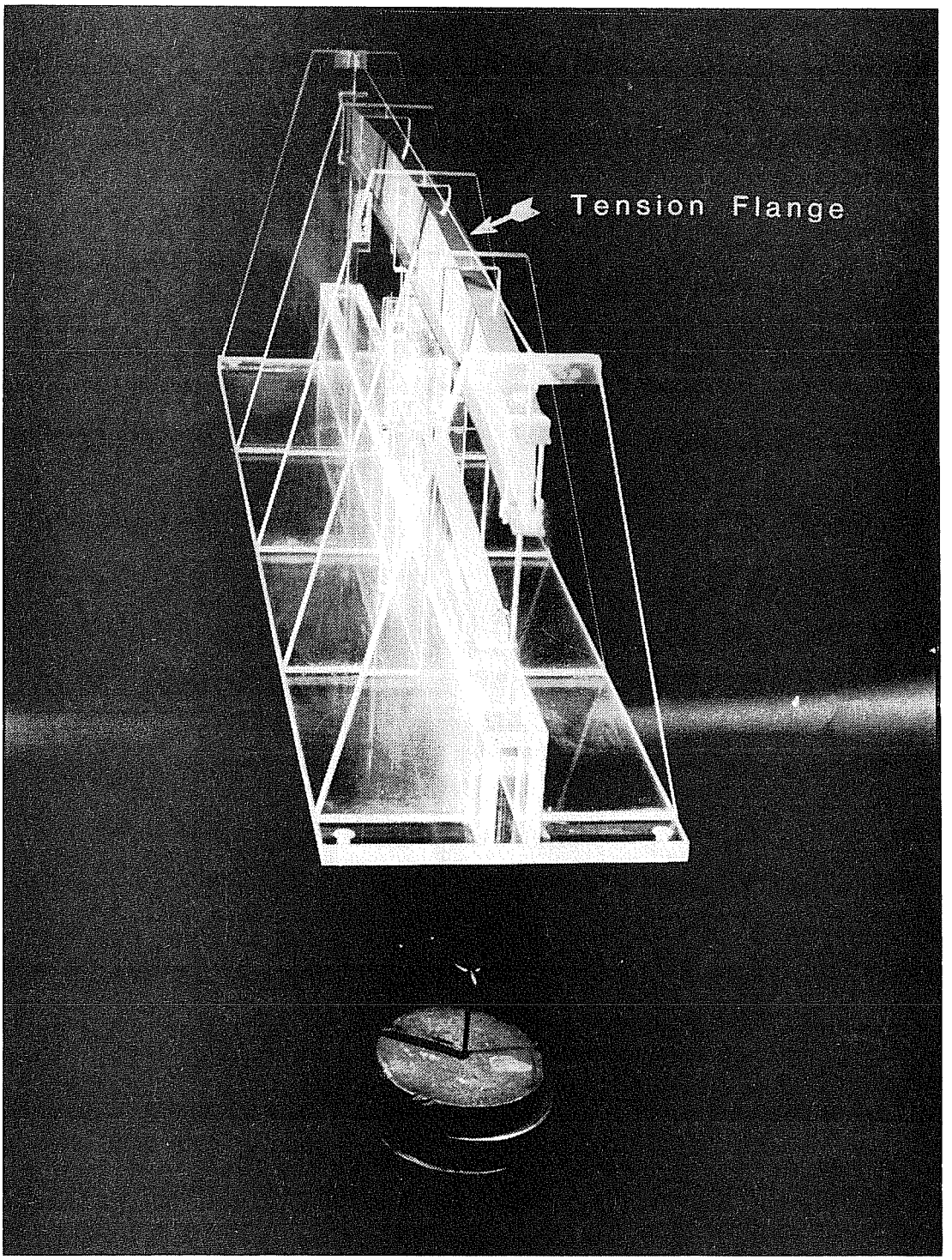

Fig. 1.4 Lateral movement of tension flange in plexiglass model beam

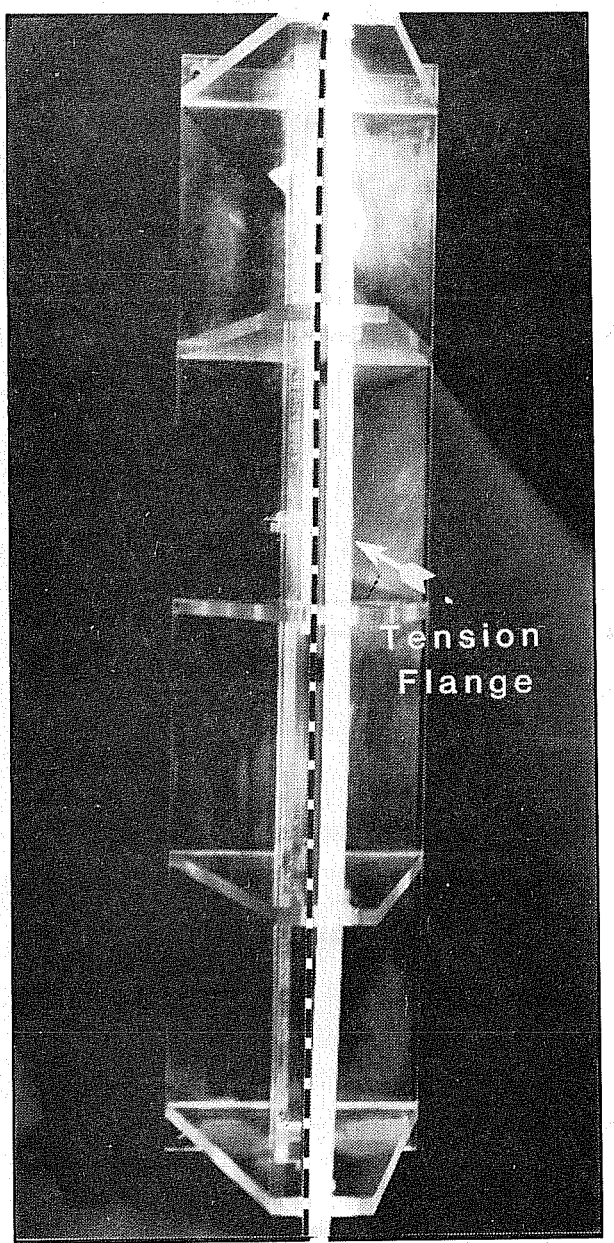

Fig. 1.5 Plan view of buckled plexiglass model beam showing lateral movement of tension flange

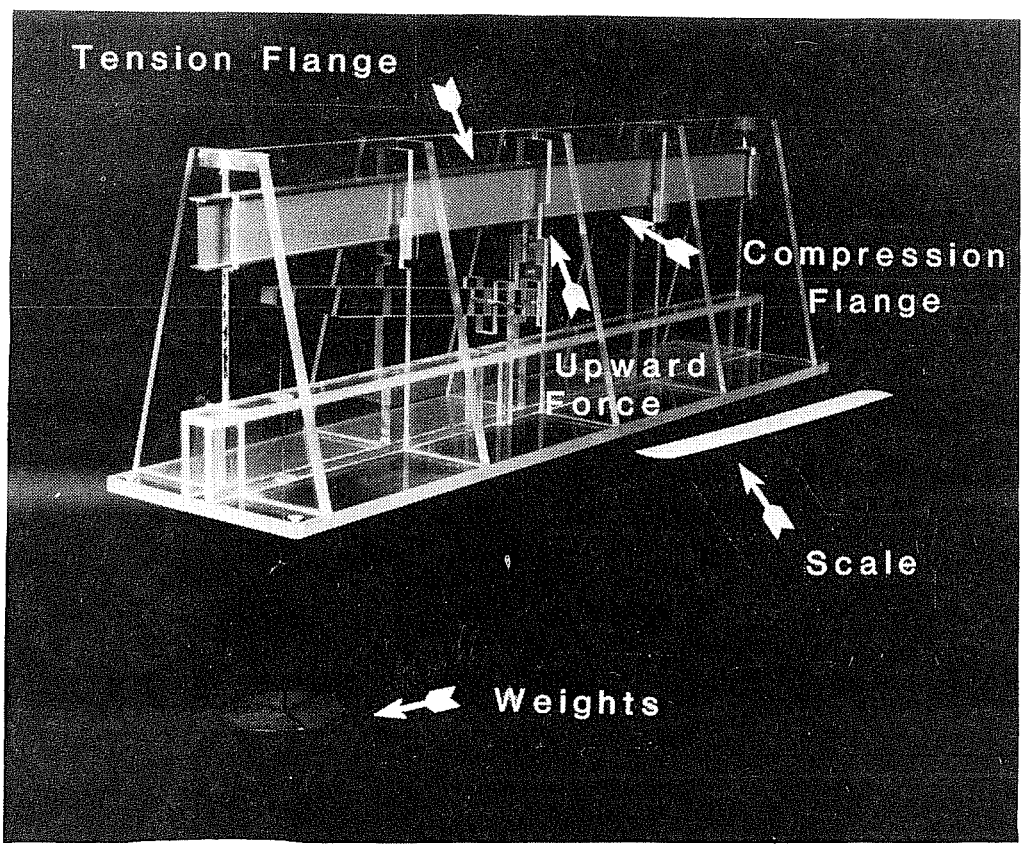

Fig. 1.6 Plexiglass model beam during loading

$a^2 = EC_w/GJ$

C_w = warping constant

J = torsional constant

Use of Eq. (1.1) in this form requires that both flanges are free to warp at the supports (i.e., pinned laterally).

The 1978 AISC Specification also contains provisions, based on development by Basler,[5] to guard against web buckling due to concentrated transverse loading. For the case where there are no transverse stiffeners and the flange, on which the concentrated load P_{cr} is applied, is restrained both laterally and torsionally about its longitudinal axis,

$$P_{cr} = \frac{5.5\pi^2 E}{12(1 - \nu^2)} \left(\frac{t_w^3}{h}\right) \tag{1.2}$$

where ν = Poisson's ratio

h = clear distance between flanges

t_w = web thickness

This check on web buckling underneath a concentrated load assumes that the other (unloaded) flange is braced laterally against movement. To develop the formula Basler assumed (Fig. 1.7) that the loaded area of the web underneath the concentrated load can be represented by a uniform column (of web), width h, under a triangular stress distribution (maximum stress under concentrated load and zero stress at other flange). Equation (1.2) then gives the buckling load of this fixed-pinned column. For complete details see Appendix 1.

Since the failures presented in Sec. 1.1 are ones where the "tension" flange moved laterally and the "compression" flange remained relatively straight, it would appear neither Eq. (1.1) nor Eq. (1.2) is suitable to estimate the buckling load for these circumstances.

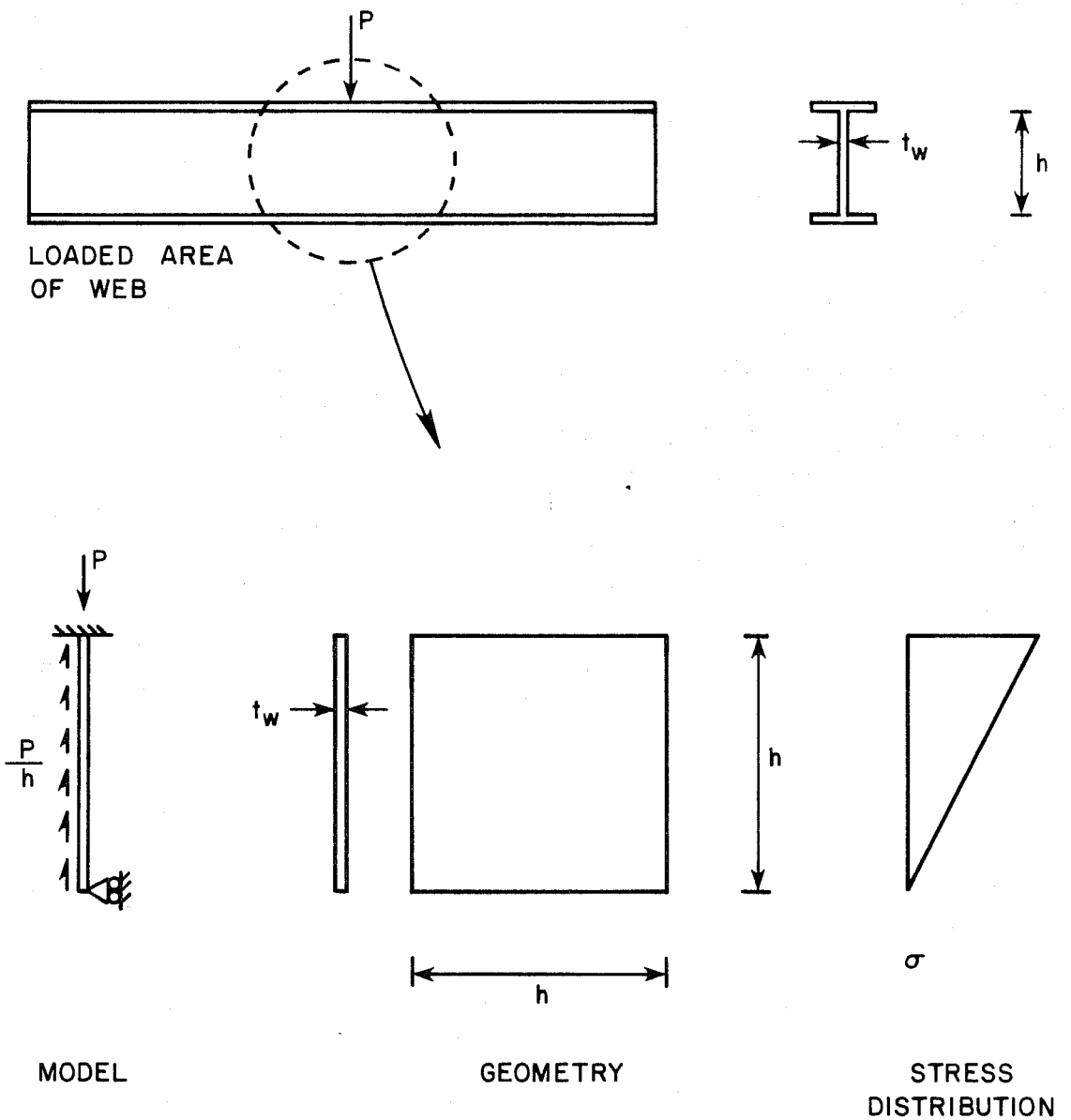

Fig. 1.7 Basler's Model[5]

Furthermore, use of these equations can result in a considerable overestimate of the buckling load.

1.3 Yura Theory

The previous observations led Yura[18] to develop a theory that permits the bottom (tension) flange to move under the action of the concentrated load. The same assumptions as Basler with regards to stress distribution in the web were used, but the bottom flange lateral stiffness controls the movement of point "B" (Fig. 1.8). The flange acts like a brace for point B, and the bottom flange can be replaced by a spring of stiffness,T. (In Basler's theory, this was an immovable hinge support). For full details see Appendix 2.

This theory proved to be remarkably successful in the prediction of the buckling loads for the continuous beam tests described previously. However, it did not accurately predict buckling loads for the simply supported plexiglass model. The results are shown in Fig. 1.9, which is a plot of nondimensional buckling load P_{cr}/P_E versus nondimensional spring stiffness, $t = Th/P_E$. P_E is the reference Euler buckling load of the pinned-pinned column given by

$$P_E = \frac{\pi^2 EI}{L^2} = \pi^2 E\left(\frac{1}{h^2}\right)\left(\frac{ht_w^3}{12}\right) = \frac{\pi^2 Et_w^3}{12h}$$

where I = moment of inertia in plane of bending

L = length of the member

1.4 Purpose and Scope

The purpose of this study is to explain the phenomenon of bottom flange movement, and to determine whether or not the movement of the flange significantly affects the strength of the beam. Design

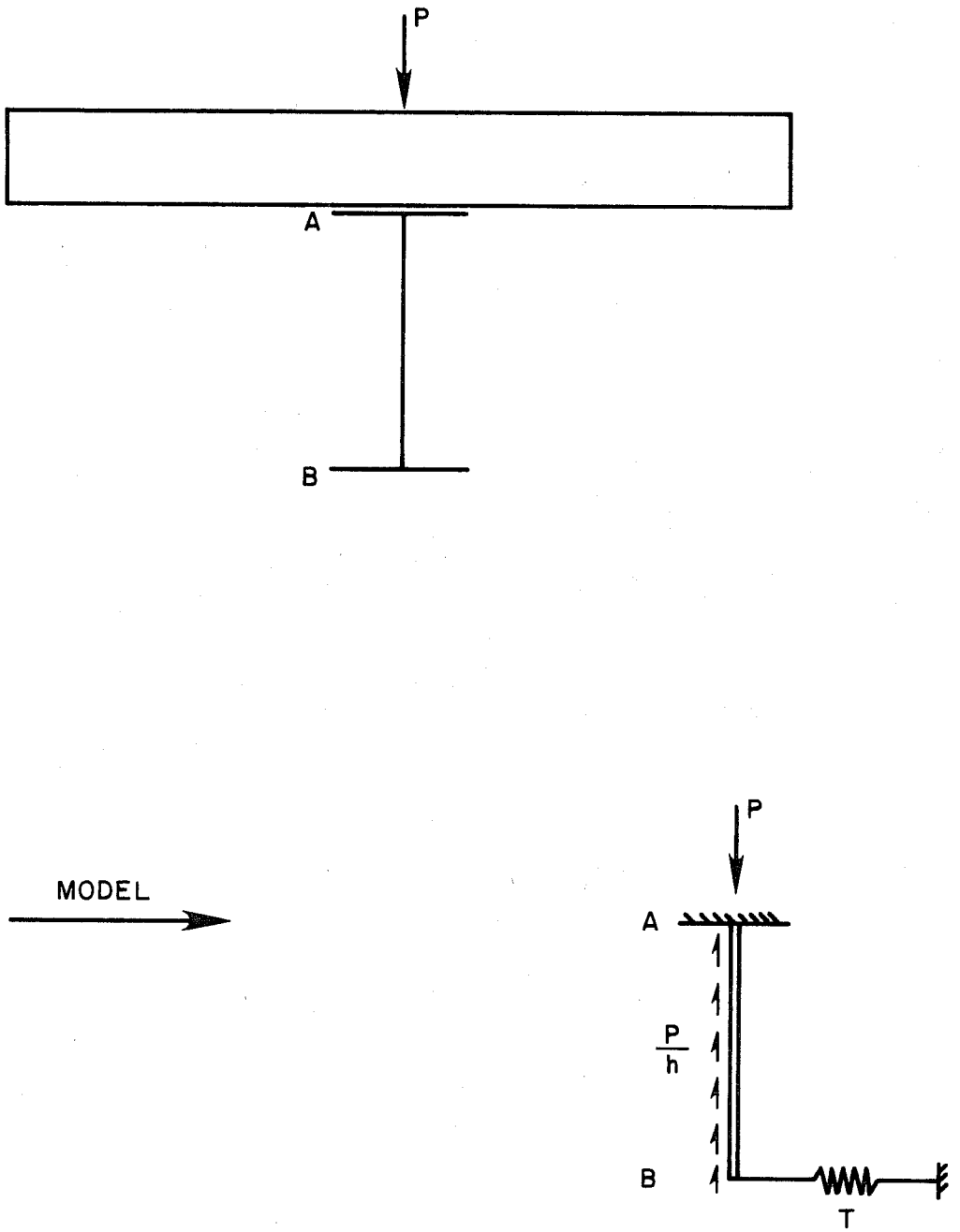

Fig. 1.8 Yura's change to Basler's model[18]

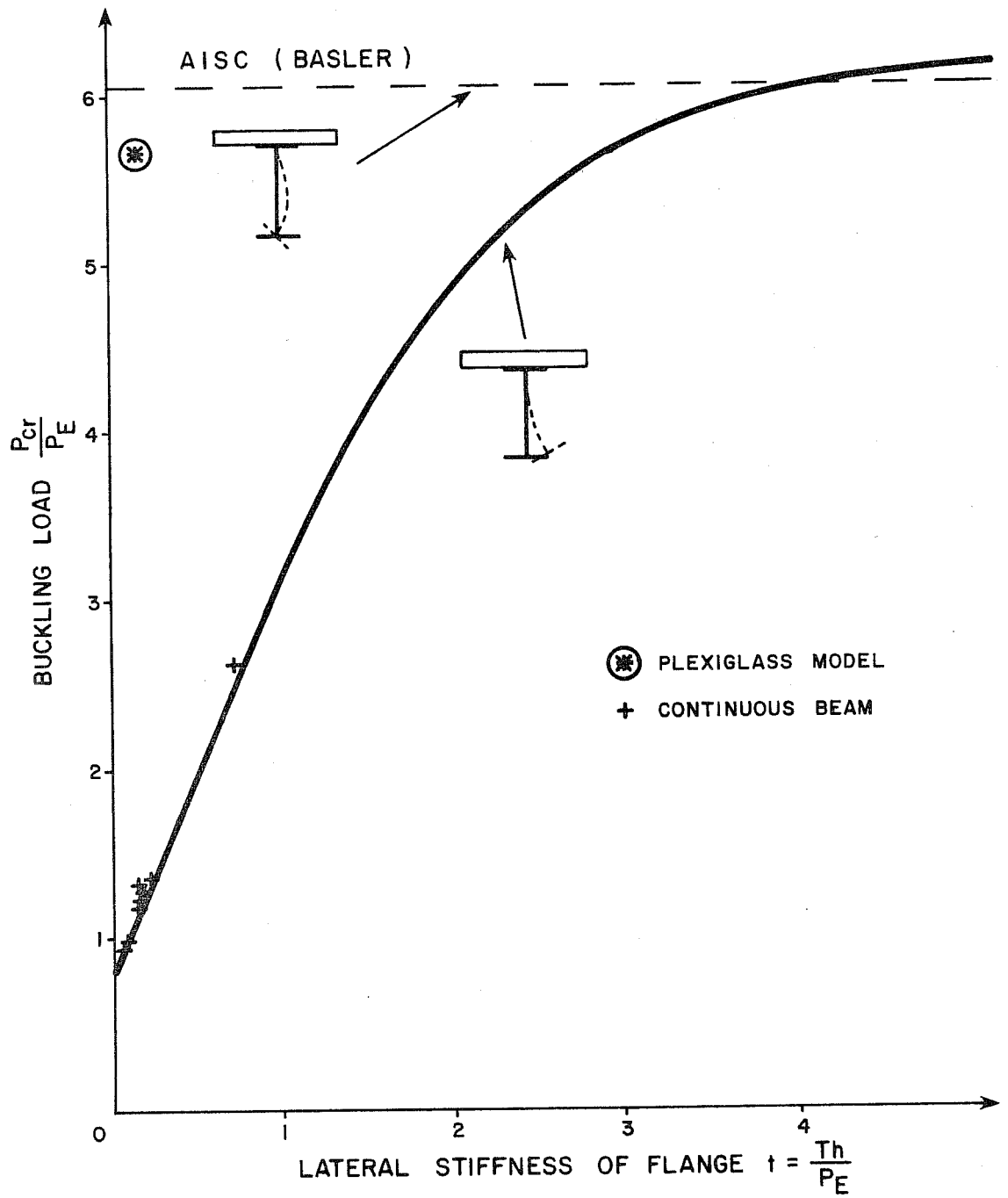

Fig. 1.9 Yura's buckling curve and test results[18]

recommendations for control of this behavior in both simply supported and restrained beams will be provided.

Only beams symmetric in both loading and boundary conditions are considered. They may be simply supported or have any degree of end fixity (to simulate restrained or continuous beams). As shown in Fig. 1.10, the beams are loaded at midspan by a single concentrated load applied on the top flange, which is braced at this point both laterally and torsionally about its longitudinal axis. In order to provide an explanation of the phenomenon in question, braces were often provided at various other points along the length, L. The beams are restrained at each end on the top flange laterally, and, on the bottom flange also against twist. The cross section is always free to warp (rotate about the vertical axis) of both ends.

Chapter 2 presents some details of the finite element elastic buckling analysis program used in this study, a description of the initial plexiglass beam experiment, and some comparisons of the results with Yura's theory. A detailed parametric computer study was undertaken in Chapter 3 to develop a fundamental understanding of the phenomenon. Chapters 4, 5 and 6 present design recommendations for simply supported beams, fixed ended beams, and beams with a varying amount of end moment respectively, for both laterally braced or unbraced bottom flanges under the load point. A complete sample design problem is included.

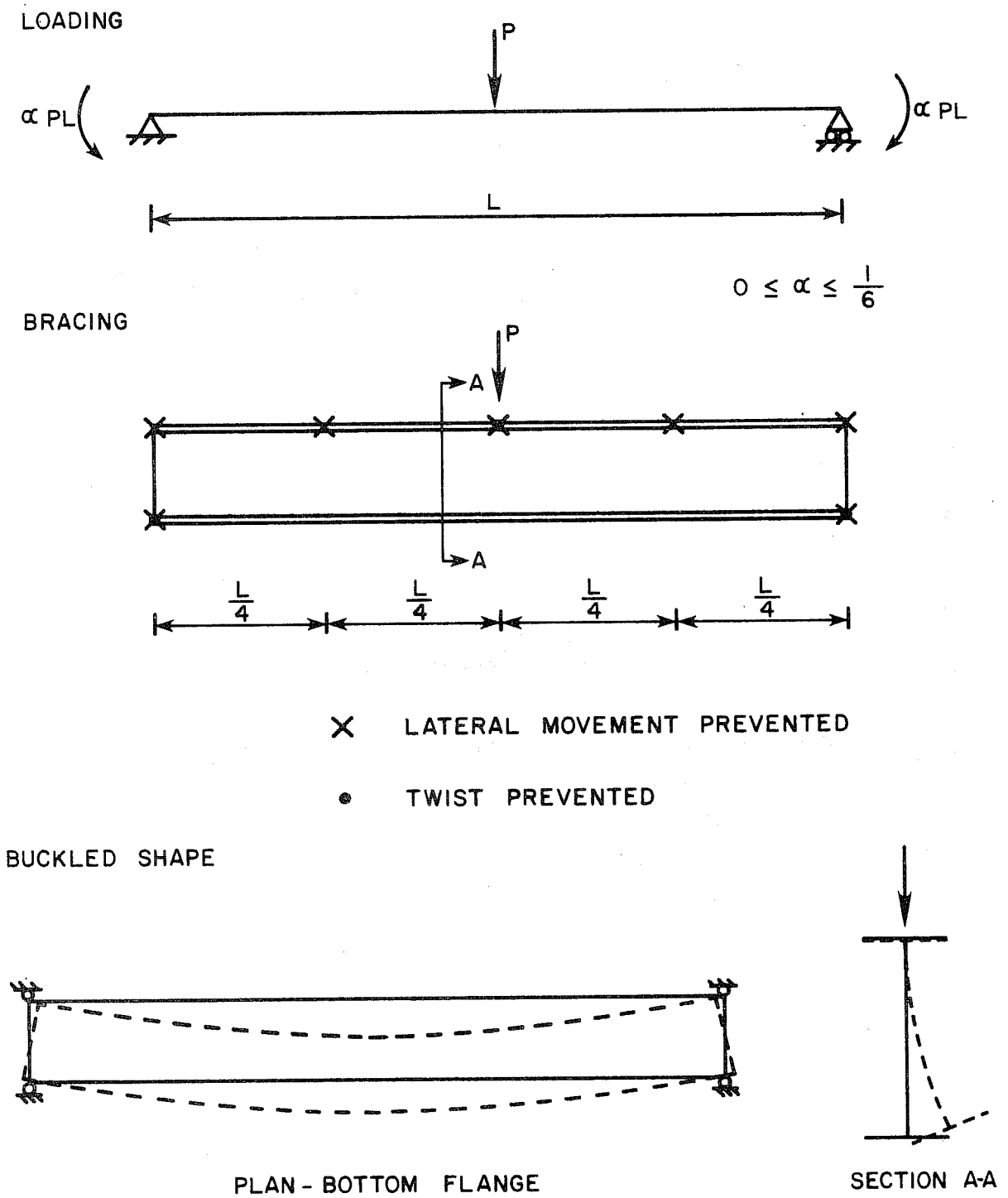

Fig. 1.10 Typical study problem

CHAPTER 2

PRELIMINARY STUDIES

This chapter presents some details of the finite element buckling analysis program BASP, developed by Johnson, Akay and Will[1,13,14] and used to conduct the computer analyses of this study. The program idealizes the web by two-dimensional finite elements and the flanges by conventional one-dimensional elements. In this manner, the cross section can distort. The buckling load and buckled shape are given as output. Also presented is a description of Oral's original plexiglass model and comparison of test results with both theoretical and computer predictions. Extensions and refinements are made to Yura's theory in an attempt to fit it to both plexiglass model and computer results.

2.1 Analysis Program

The finite method is recognized as an effective tool for predicting buckling loads for thin-walled members. Historically, these members have been treated as one-dimensional or line elements in determining their critical buckling stress. Valuable insight into the buckling phenomenon has been established in this way, however, the influence of cross-sectional distortion is not accounted for due to the simplifying assumption that cross sections do not distort during buckling.

To provide for more generality, a three-dimensional assemblage of thin plate elements having both membrane and bending stiffness was developed.[13,14] Since both the web and the flanges and stiffeners were represented by the plate elements, the cross section was permitted to distort. Studies based on the three-dimensional

assemblage indicated that deep sections with top or bottom restraints did in fact exhibit significant cross-sectional distortion. The critical load was in turn substantially affected. This procedure has the advantage of simulating complex structures, however, the ensuing computational times are significant.

The computer program used in this study, BASP (Buckling Analysis of Stiffened Plates), is specialized for the lateral buckling of beams (and frames) that have a plane of symmetry about the midsurface of the web.[1] The structural idealization (Fig. 2.1) is two-dimensional in which plate elements are used for the web (depth between flange centerlines d and thickness t_w). One-dimensional elements are used for the flanges (width b and thickness t_f) and, if present, stiffeners (width b_s and thickness t_s). The use of plate elements for the web (four divisions over the depth in this study) maintains the ability to account for cross-sectional distortion including local behavior. The use of one-dimensional elements for the flanges reduced the computational effort substantially, however, no significant differences in accuracy have been observed.

Arbitrary planar loadings, geometry, support conditions and elastic springs are easily represented (Fig. 2.2). Out-of-plane supports or elastic springs may be specified at nodal points to prevent or inhibit lateral movement out of the plane (w), rotation about the longitudinal axis (θ_x) and rotation about the vertical axis (θ_y). Furthermore, the two-dimensional state of stress in the web is represented.

In-plane and out-of-plane behavior are assumed to be uncoupled and buckling is assumed to be linear-elastic. The beam is first analyzed for loads applied in the plane of the web by use of

$$[K_i]\{r_i\} = \{R_i\} \tag{2.1}$$

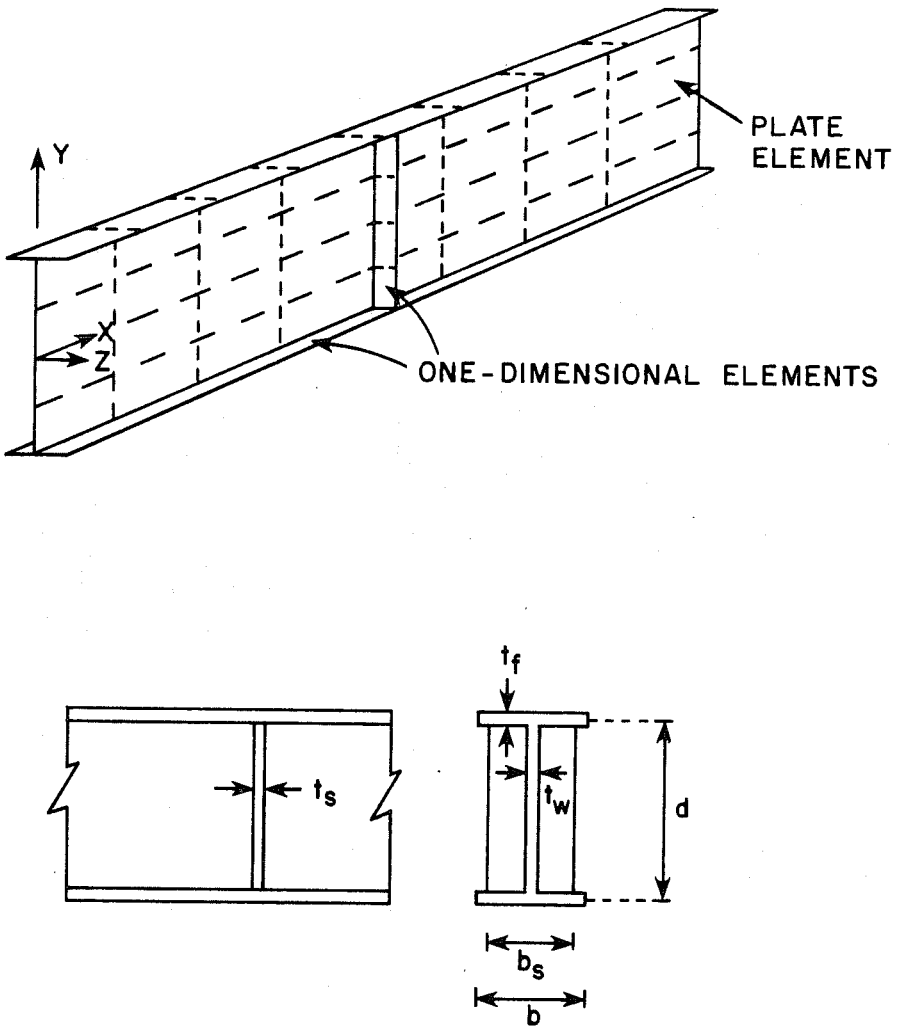

Fig. 2.1 Structural idealization in BASP

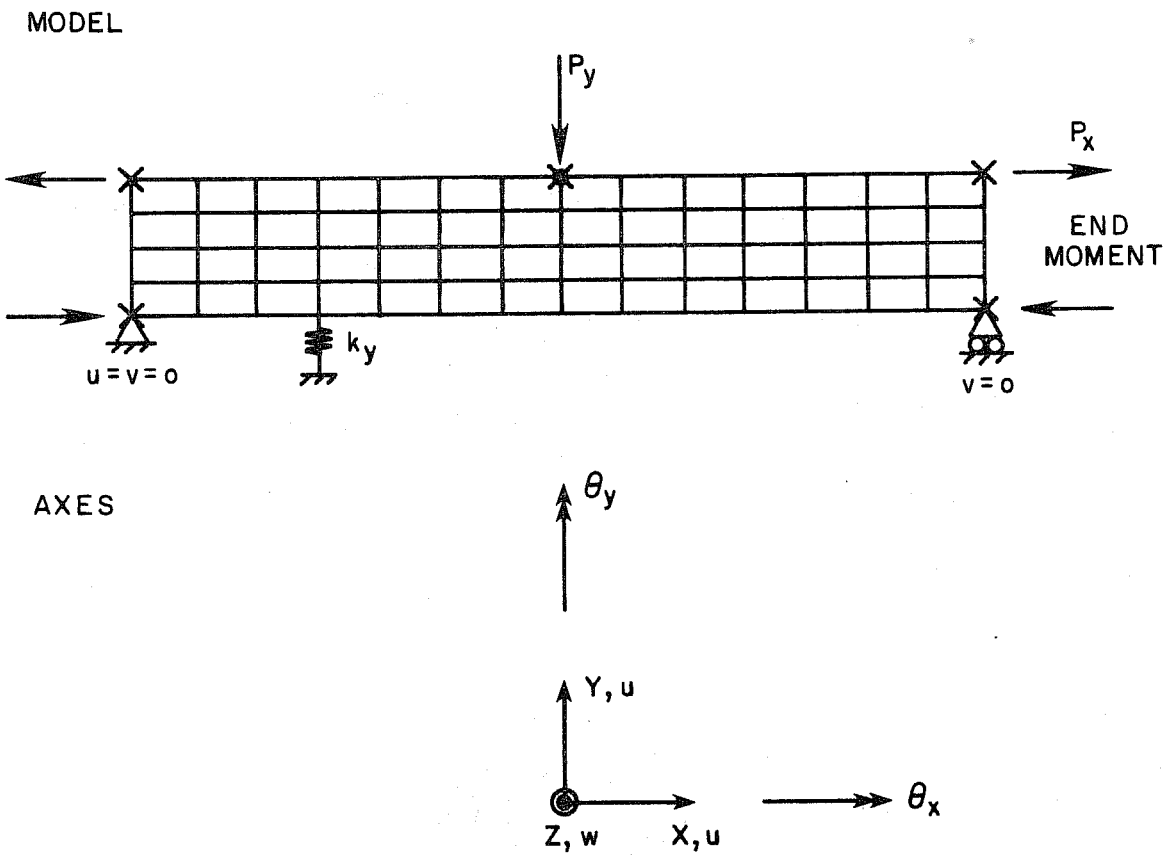

Fig. 2.2 Some BASP options

in which K_i represents the in-plane structural stiffness while R_i contains nodal forces due to in-plane loading. Equation (2.1) is used to calculate in-plane displacements, r_i, which are subsequently used to calculate in-plane stresses. These stresses give rise to an out-of-plane geometric stiffness, K_g, which is used to calculate the buckling load from the following equation:

$$[K_o]\{r_o\} + \lambda[K_g]\{r_o\} = \{0\} \tag{2.2}$$

in which K_o is the out-of-plane structural stiffness while r_o represents the out-of-plane buckled shape. The buckling load is λ times the applied loading. In Eqs. (2.1) and (2.2), K_i and K_o are uncoupled. This formulation is equivalent to the classical linearized buckling theory in which displacements are assumed to be small, therefore the buckled mode shape may be determined while the actual magnitude of the buckled shape remains undefined. Inverse iteration is used to solve the resulting eigenvalue problem, Eq. (2.2). This yields the smallest load causing buckling normal to the plane of the web. Buckling in the plane of the web is ignored.

As a sample problem, consider Oral's plexiglass model (henceforth referred to as Model 1). The geometric details follow in Sec. 2.2. Figure 2.3 shows both the input for BASP and the output. The beam is braced laterally and against twist at the supports ($w = \theta_x = 0$) and braced laterally ($w = 0$) under the load. It is simply supported with a midspan concentrated load, and has four web elements over the depth of the beam.

The theoretical critical moment given by Eq. (1.1) is $M_{cr} = 77.2$ lb.-in. That is, a critical concentrated midspan load $P_{cr} = 12.9$ lb. BASP predicts $P_{cr} = 12.5$ lb., which is in good agreement with the theoretical buckling load. Output from BASP can include the input data, the in-plane stresses and displacements, the eigenvalue and buckled shape at each iteration, and the final eigenvalue and buckled shape. Plots can be obtained for input geometry, bottom flange in-plane stresses, and buckled mode shape.

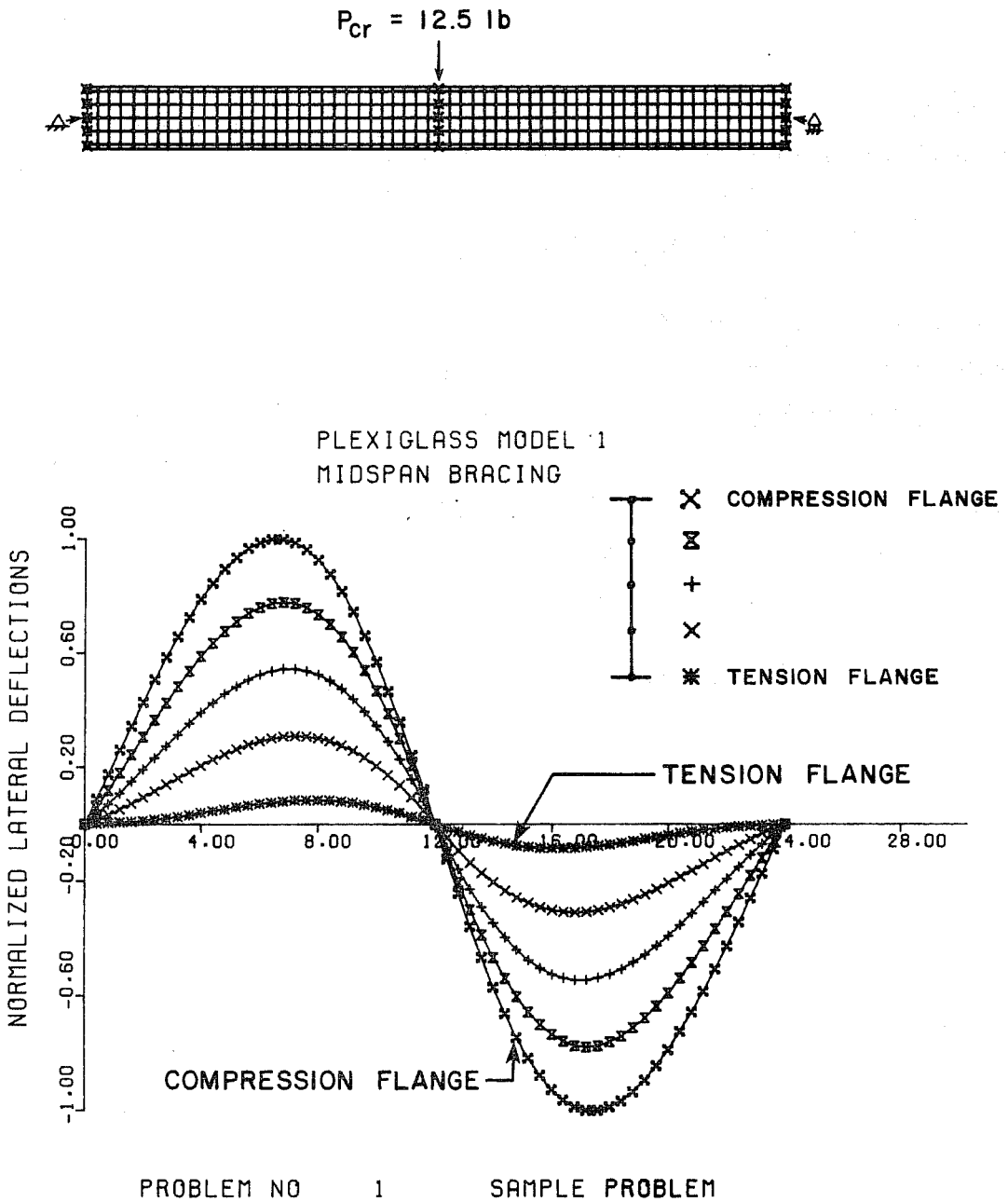

Fig. 2.3 BASP output--lateral torsional buckling of simply supported beam between ends and midspan brace

The buckled-shape plot for Model 1 is shown on Fig. 2.3. The five lines plotted correspond to the five nodes across any beam section (for the four web divisions). Each data point represents a node along the beam length. The lateral deflection, w, is normalized and plotted at each of the five node levels. For the beam described above, the plot indicates a lateral-torsional buckle between brace points, with lateral movement primarily of the compression flange.

2.2 Oral's Plexiglass Model

2.2.1 Test Set-Up. A test was conducted with a plexiglass model which was designed and fabricated to demonstrate the movement of the tension flange. The plexiglass test frame is shown on Fig. 2.4. The loading mechanism applies a vertical upwards concentrated load at midspan on the lower flange of the beam. The force is applied via weights which are hung from a lever with a mechanical advantage of 4:1 (Fig. 2.5). The beam was simply supported over a 24 in. span. The frame end supports were filed to represent a pinned condition laterally (warping permitted) at both flanges. The beam was braced laterally and torsionally as shown in Fig. 2.6. Figure 1.6 shows the beam inserted in the test frame, under load and braced at the 1/4-points on the compression flange. The cross section of Model 1 is shown in Fig. 2.7. The beam was made from methyl methacrylate (commonly known as acrylic or plexiglass). For this material, Hendry[12] suggests E = 500,000 psi and ν = 0.38. The modulus E was also verified in separate tests.

2.2.2 Testing. The beam was loaded in both bracing configurations. Because of the small scale of the model and the presence of initial imperfections, it was quite difficult to visually determine the buckling load. The beam did not just suddenly buckle, but rather there was slight lateral movement during initial loading followed by a substantial increase in the rate of lateral movement indicating buckling. Creep effects were

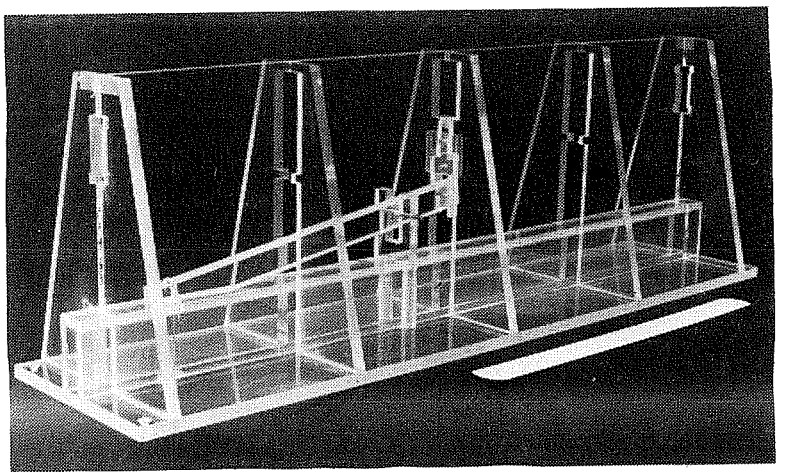

Fig. 2.4 Loading frame

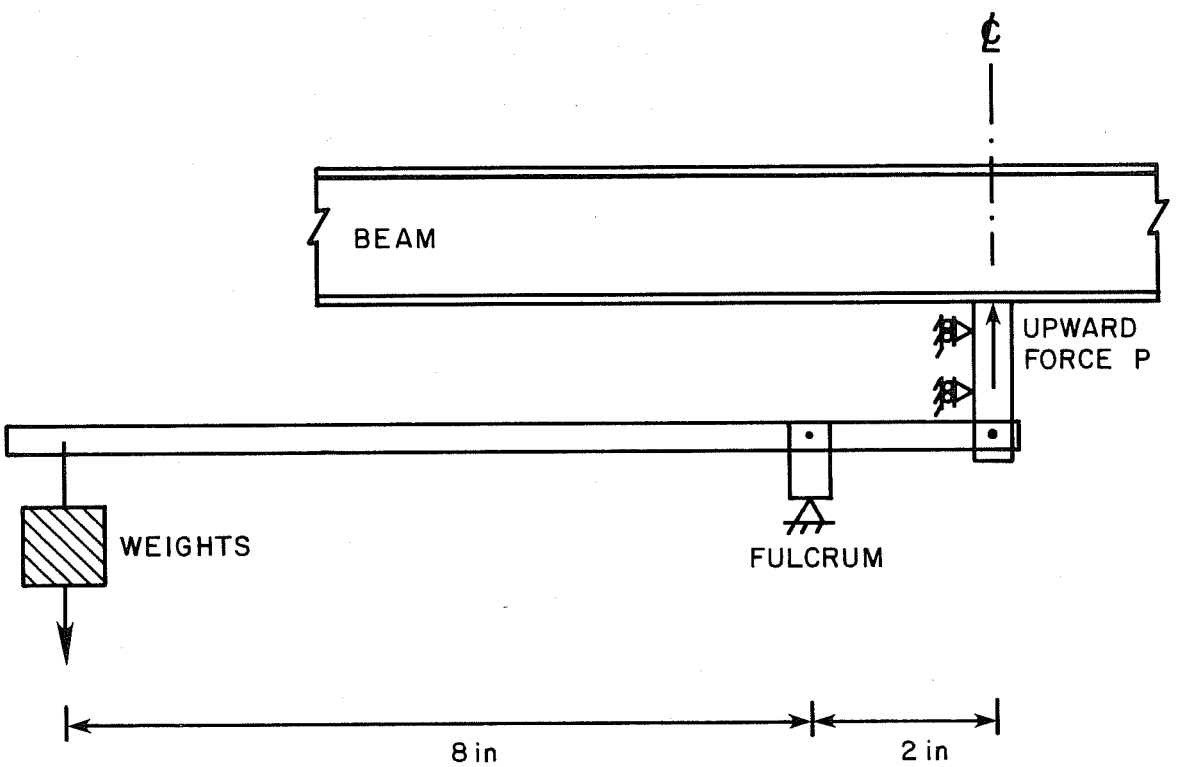

Fig. 2.5 Load application mechanism

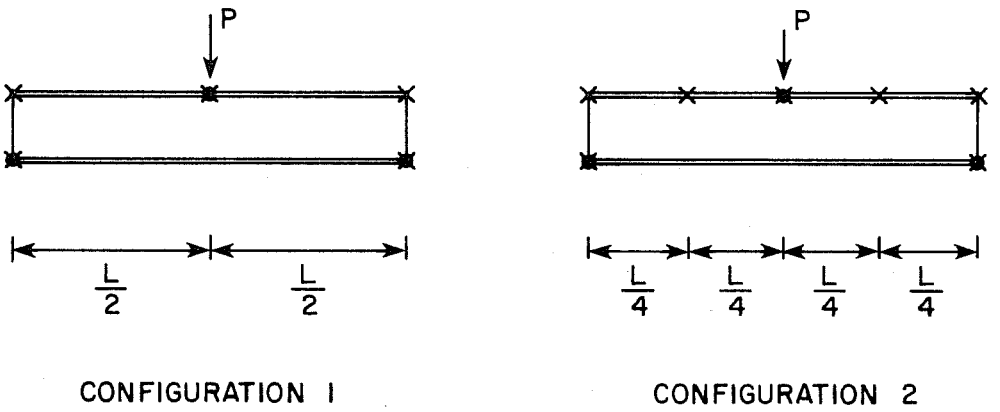

Fig. 2.6 Plexiglass model bracing configurations

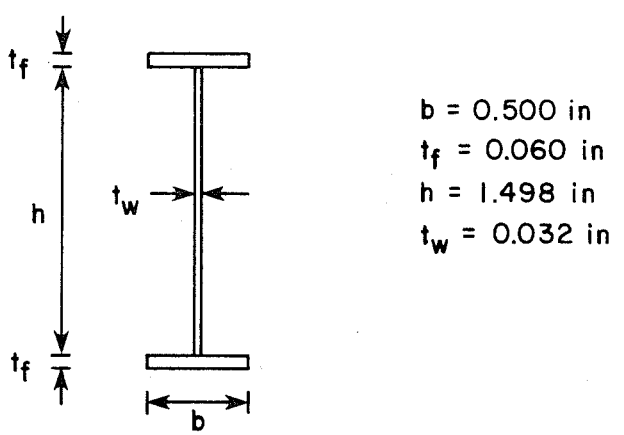

Fig. 2.7 Plexiglass Model 1 cross section

present and so load application and observations had to be made quickly.

The beam was designed with the intention of it buckling in the conventional lateral-torsional S-shape when in configuration 1 (midspan brace only). The addition of 1/4-point braces (configuration 2) was supposed to force the failure mode to that of tension flange movement as opposed to usual lateral-torsional double S-shape buckle between 1/4-point compression flange braces. The theoretical buckling loads predicted this behavior:

(1) Lateral-torsional buckling, configuration 1 Eq. (1.1)

M_{cr} = 77.2 lb. in. ~ P_{cr} = 12.9 lb. (Appendix 3)

(2) Lateral-torsional buckling, configuration 2, Eq. (1.1)

M_{cr} = 207 lb.-in. ~ P_{cr} = 34.6 lb. (Appendix 3)

(3) Movement of tension flange (Yura theory)

P_{cr} = 11.3 lb. (Appendix 2)

To be precise, Yura's theory suggested that movement of the tension flange should occur even before conventional lateral-torsional buckling in configuration 1.

The experiments, however, did not show this behavior. In configuration 1 there was a clear lateral-torsional buckle between compression flange brace points at about 13 lbs. as expected, but with no hint of tension flange movement. An end view of this is shown in Fig. 2.8 and a plan view in Fig. 2.9. In configuration 2, however, a full 35 lb. was applied to the beam before there was any sign of instability. At this load there was a lateral-torsional buckle between 1/4-point braces on the compression flange, when flange A was the compression flange. When, however, the beam was

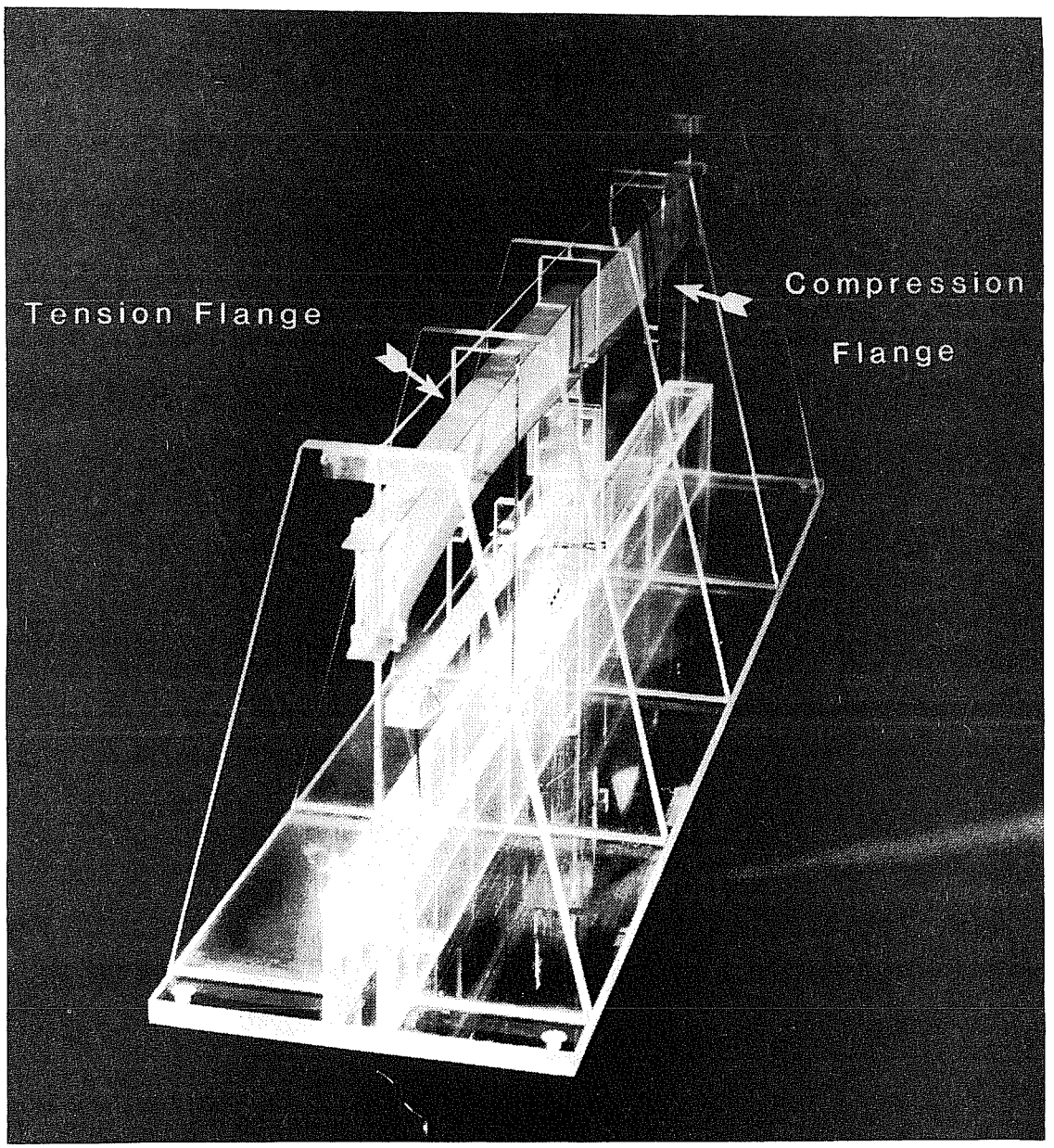

Fig. 2.8 Lateral torsional buckling of plexiglass model beam

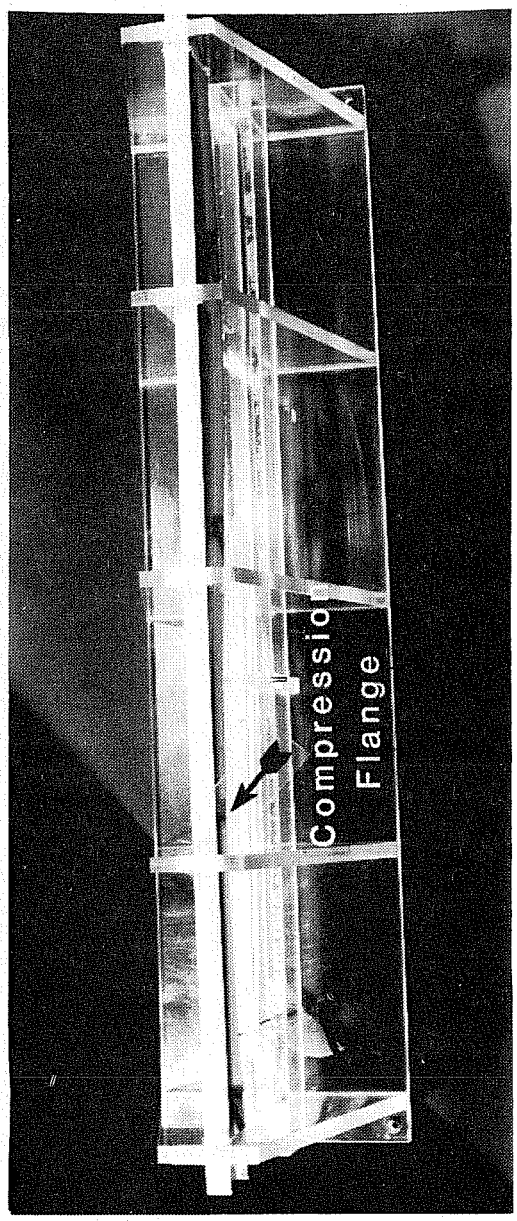

Fig. 2.9 Plan view of buckled plexiglass model beam showing lateral-torsional buckling

reversed in the loading frame, flange A in tension, the tension flange movement was visible, as in Fig. 1.4 at approximately the same load of 35 lb.

The experimental results indicate that the load to cause tension-flange movement was significantly higher than that suggested by Yura's theory[18] (Fig. 1.9). Furthermore, this load could even be significantly higher than the load to cause lateral-torsional buckling in configuration 2, and may be visible only after the onset of this lateral-torsional buckling. Also, initial lateral deflection (sweep) may result in premature movement of the tension flange, especially if it is this flange that is considerably out of alignment.

2.2.3 Computer Analysis. The computer program BASP was used to possibly resolve this dilemma. Results of the analyses were:

(1) Lateral-torsional buckling, configuration 1 (Fig. 2.10)

P_{cr} = 12.4 lb.

(2) Lateral-torsional buckling, configuration 2 (Fig. 2.11)

P_{cr} = 35.2 lb.

(3) Tension flange movement, configuration 2 (Fig. 2.12)

P_{cr} = 51.8 lb.

The BASP results show that the load to cause tension flange movement is significantly higher than that suggested by Yura's theory. This load caused substantial local web distortion underneath the load point, and thus, web buckling may be a related phenomenon. The computer results agree excellently with the theoretical lateral-torsional buckling results.

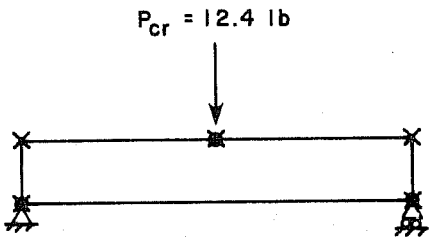

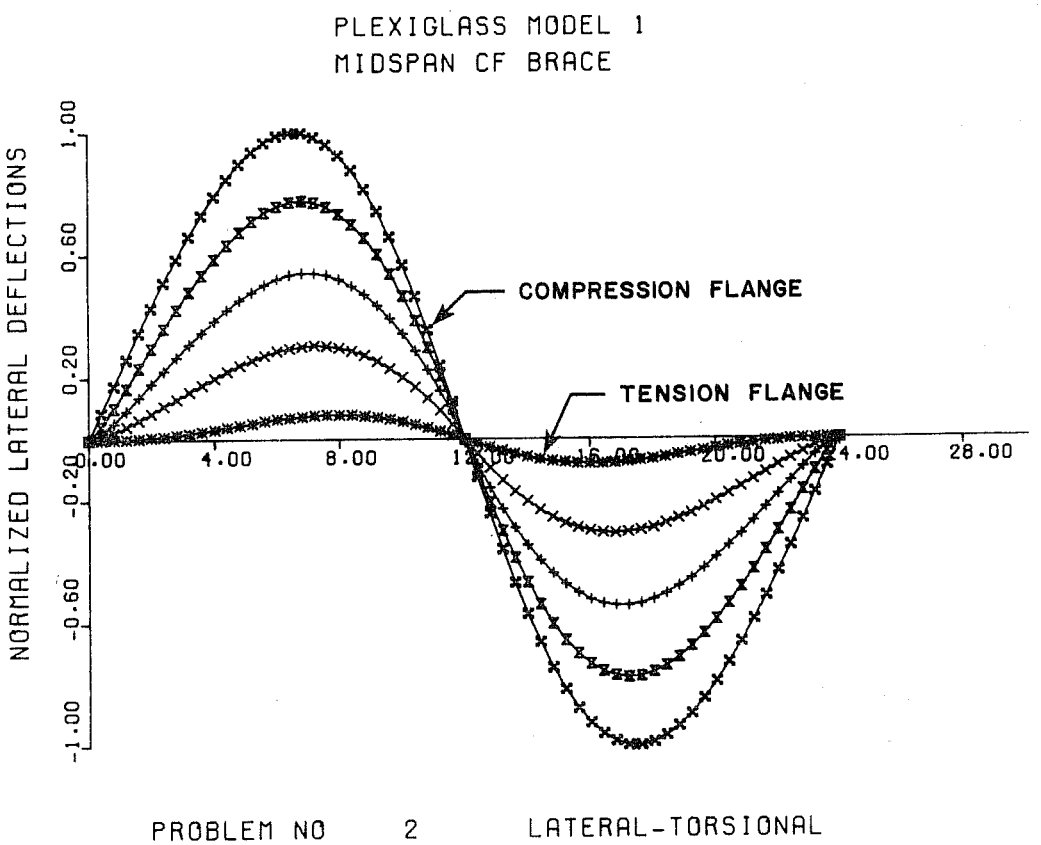

Fig. 2.10 BASP output--lateral-torsional buckling of plexiglass Model 1 in configuration 1

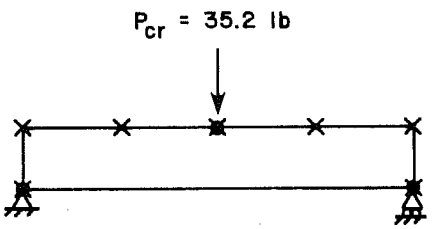

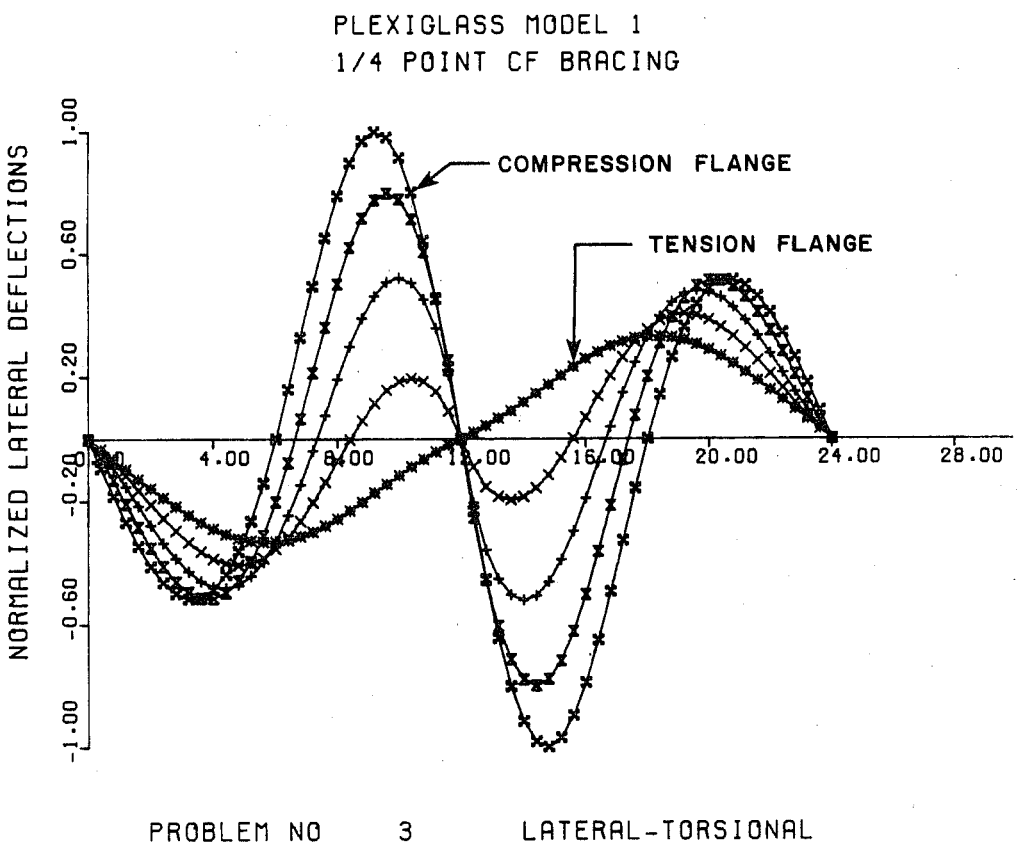

Fig. 2.11 BASP output--lateral-torsional buckling of plexiglass Model 1 in configuration 2

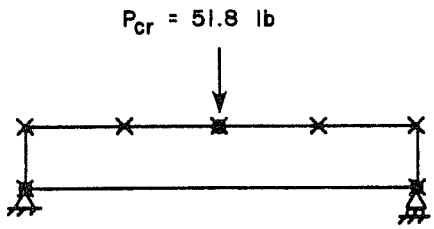

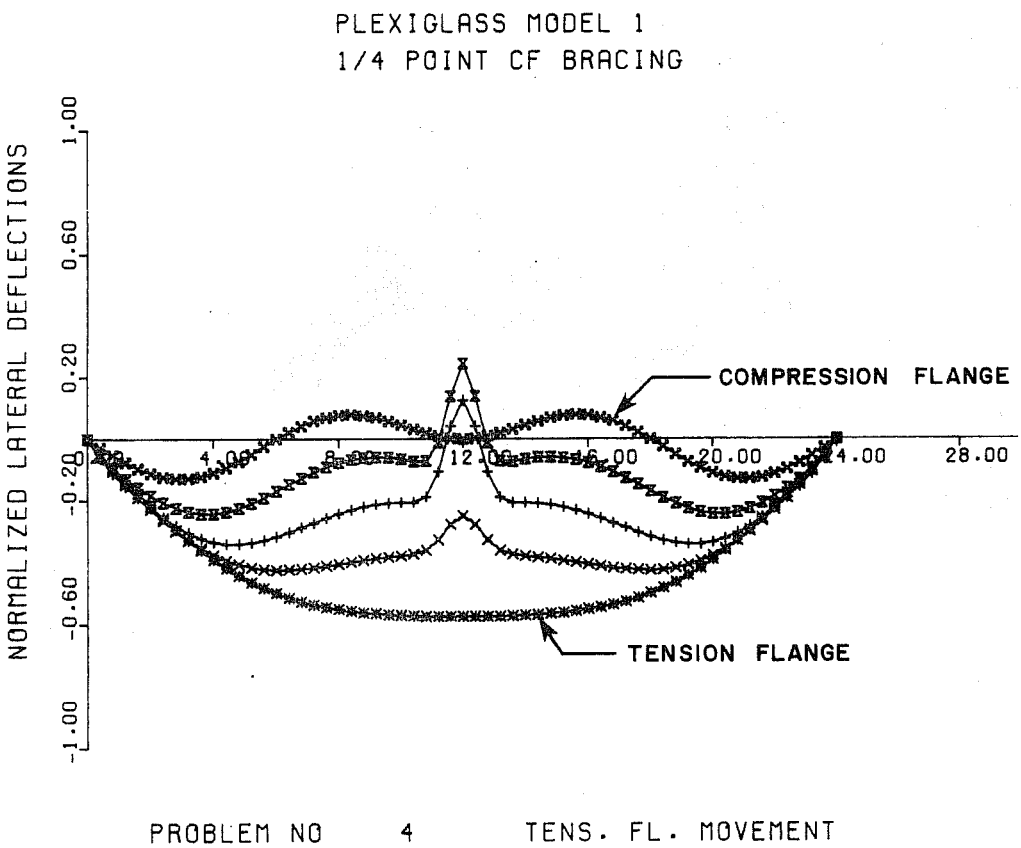

Fig. 2.12 BASP output--tension flange movement of plexiglass Model 1 in configuration 2

2.3 Extensions of Yura's Theory

Figure 1.9 and the results of the previous section show that Yura's theory does not accurately predict the load at which the plexiglass model exhibits a movement of the tension flange. So, the theory was altered in two ways in an attempt to get better correlation with the model test. First, a detailed stress analysis was undertaken in order to determine the actual stress distribution in a region under the concentrated load (Fig. 2.13a), since Yura's theory assumes (as does Basler's[5]) that the loaded area of the web can be represented by a uniform column under a triangular stress distribution. Second, rotational springs (stiffnesses R_1,R_2) were applied at the ends of the web column as shown in Fig. 2.13b, in addition to the lateral spring used by Yura. The rotational springs represent the torsional restraint provided by the flanges or by boundary conditions.

2.3.1 Stress Analysis. In order to accurately determine the vertical stress distribution under a concentrated load, a short beam with L/h = 4 was analyzed using the finite element program SAP IV[6] (Fig. 2.14). The dimensions of the cross section were those of the plexiglass model. A fine mesh was used to model half of the beam, taking advantage of symmetry. The load was applied over a small length of beam, 0.3 in., to simulate loading on the actual plexiglass model.

The results of the analysis in Fig. 2.15 show the distrubution of vertical stresses under the concentrated load. The region where the vertical compressive stress, σ_v, is greater than 10 percent of the maximum vertical compressive stress, $\sigma_{v\ max}$, is nearly of width h, and so it appears reasonable to take this as the column width. Vertical stresses of any significance occur in the upper 60 percent of the web, not over the full depth as assumed by Yura.

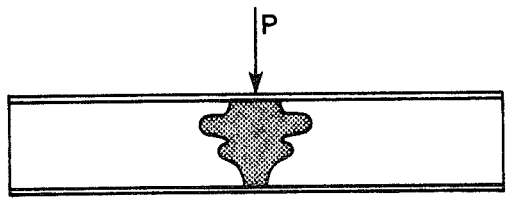

(a)

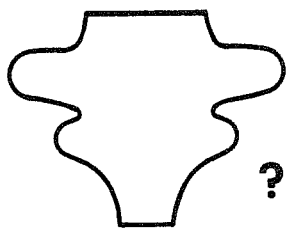

LOADED AREA OF WEB

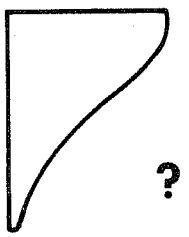

STRESS DISTRIBUTION

(b)

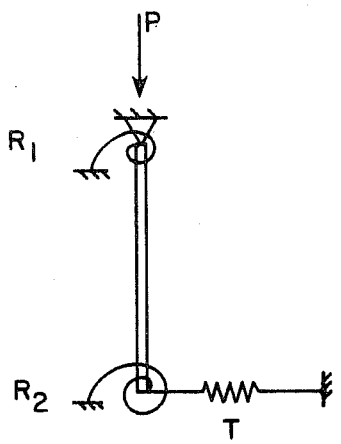

MODEL

Fig. 2.13 Refinements of Yura's theory

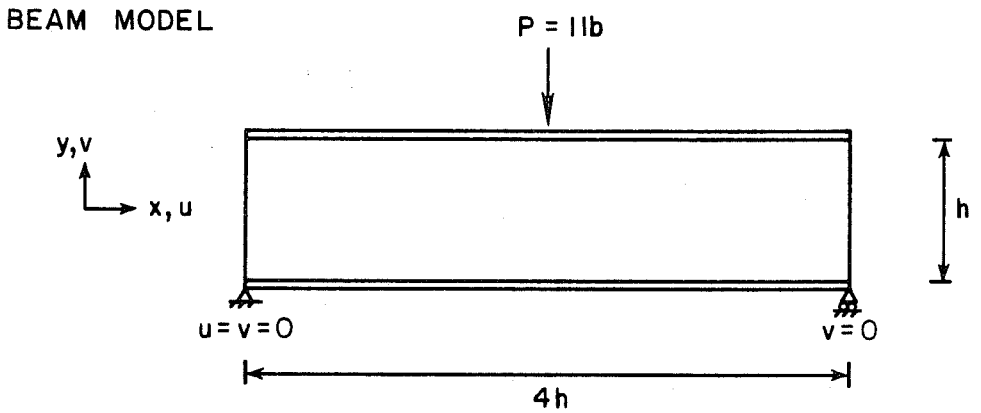

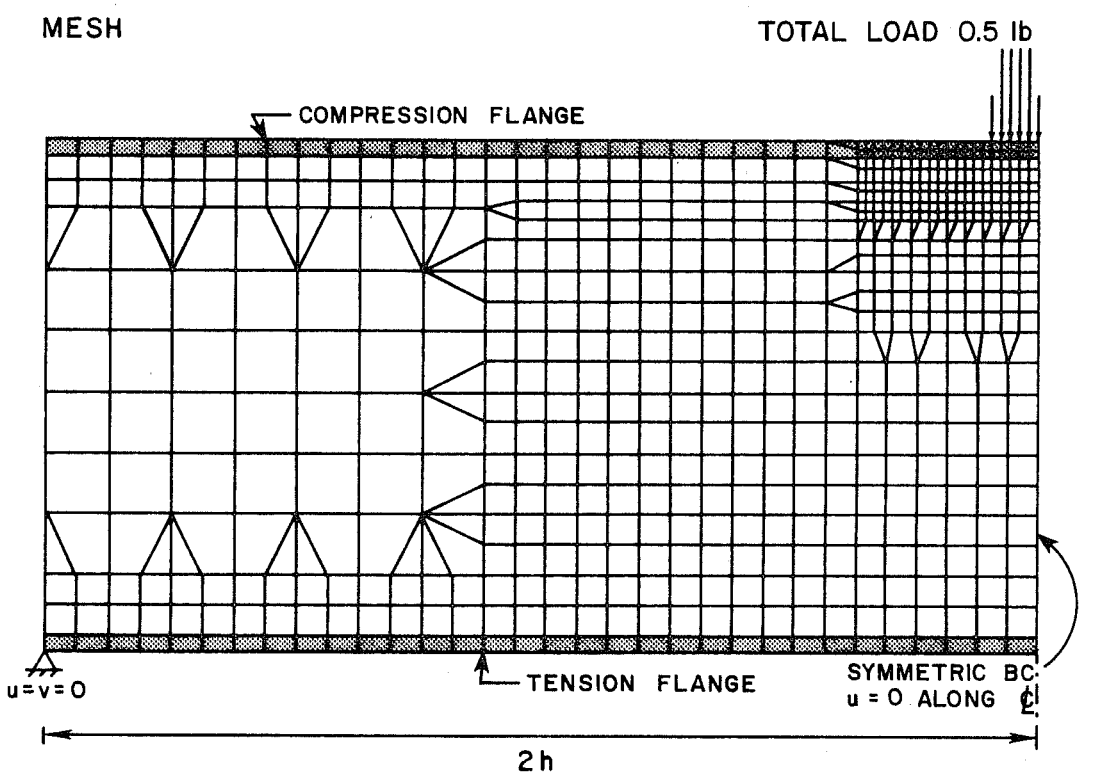

Fig. 2.14 SAP IV[6] finite element model

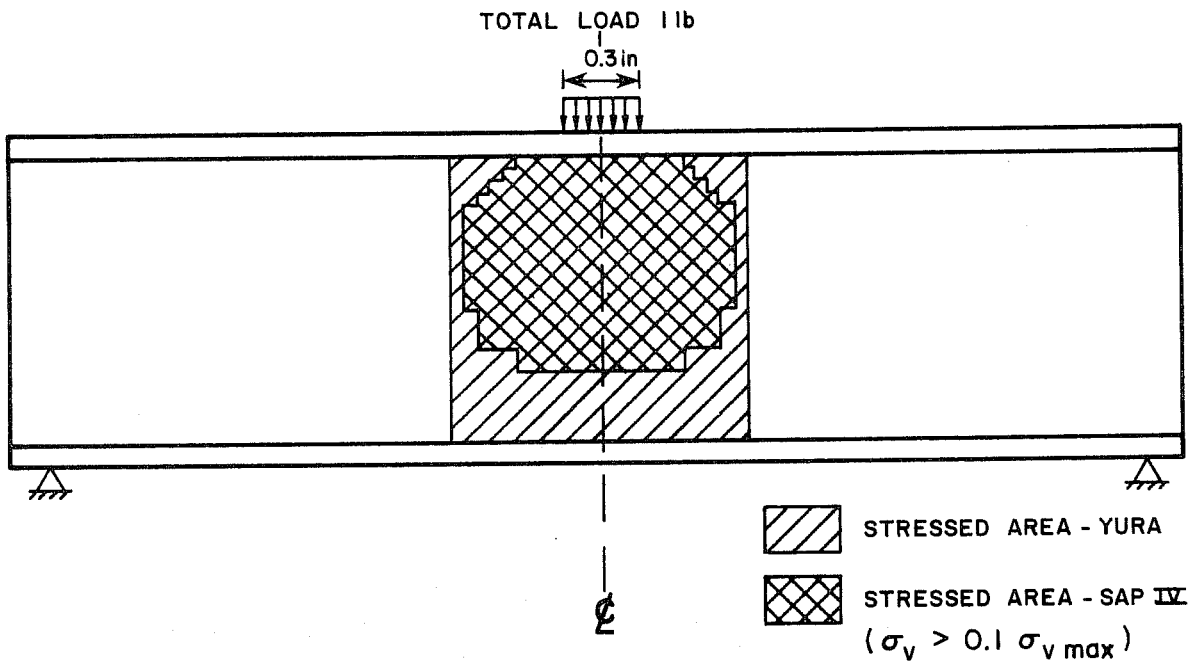

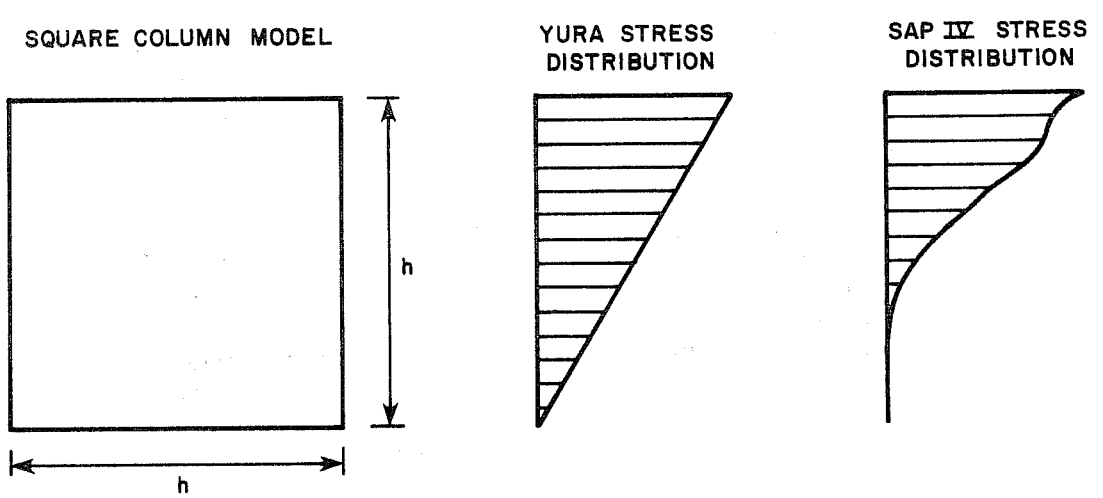

Fig. 2.15 Results of SAP IV analysis

2.3.2 Generation of Theory. Figure 2.16 shows curves of nondimensional buckling load, P_{cr}/P_E, versus nondimensional spring stiffness of bottom flange, t. The curves were generated using the buckling program BASP. Curves are plotted for both Yura and SAP IV stress distributions in the web column.

The curves show the small effect of the stiffness of the lower rotational spring. This is because this spring only controls the rotation of portions of the web that are not highly stressed and hence, is not an important factor in the determination of the buckling load. However, the stress distribution chosen in the column has a significant effect on the buckling load. The SAP IV stress distribution predicts higher buckling loads than the Yura stress distribution, since relatively more of the highly stressed region of the column has its lateral movement controlled by the support at the top of the column. That is, as the stress distribution is shifted upwards on the column towards the load point, the buckling load increases because of the lateral and rotational control of the column at this point. The third observation made is that none of the curves are able to predict the buckling load for the plexiglass model. A number of possibilities exist. The bottom flange stiffness alone may be an inaccurate gauge of the spring stiffness, T, or perhaps some other entirely different parameters control the buckling load. A complete parametric study using BASP is undertaken in Chapter 3 in an attempt to gain understanding of the phenomenon.

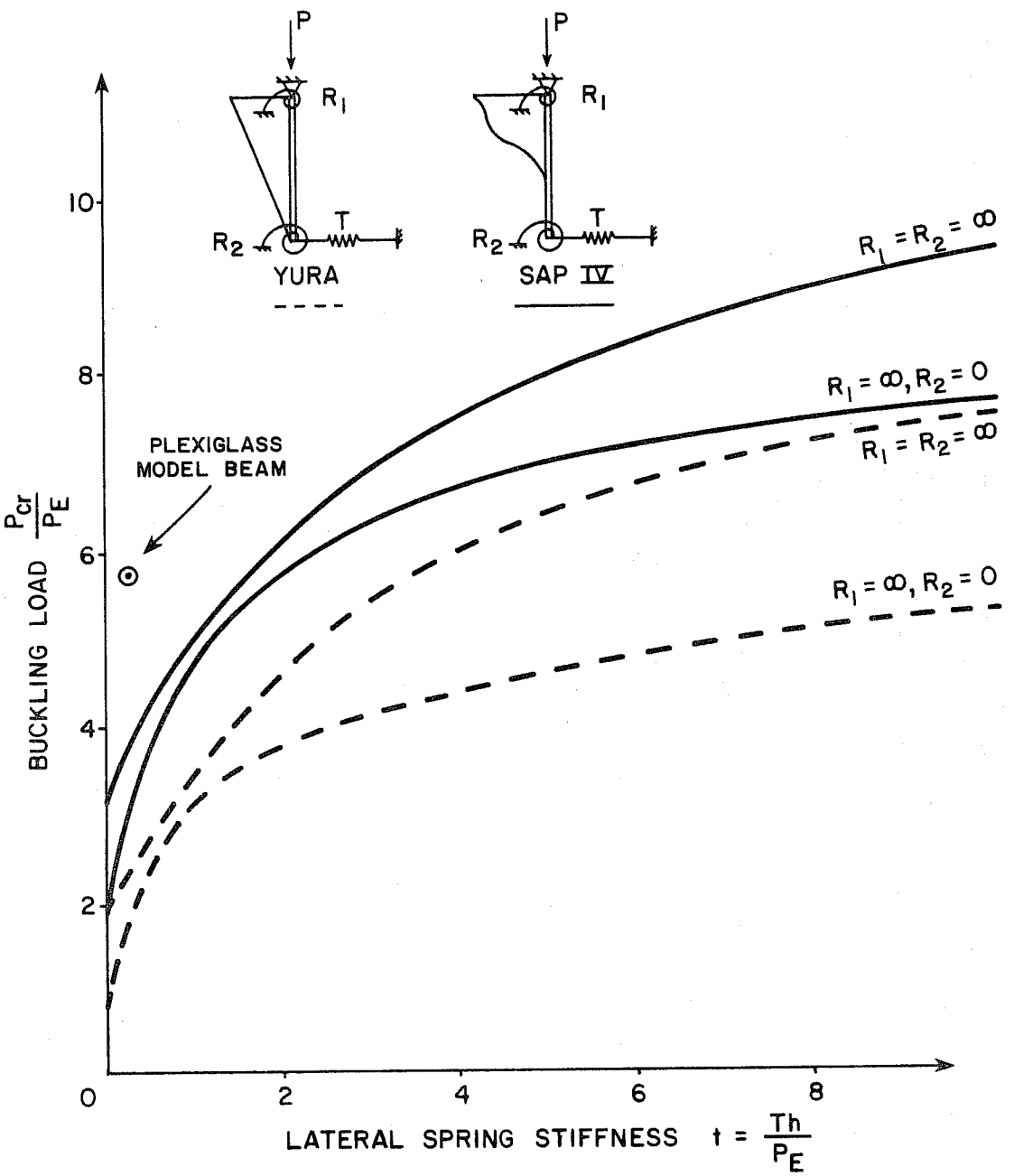

Fig. 2.16 Buckling curves for refinements to Yura's theory

CHAPTER 3

PARAMETRIC COMPUTER ANALYSIS

3.1 Background

The Yura theory (or extensions of it) shows a large effect on the buckling load depending on the existence of a bottom flange lateral brace at the load point, especially if the flange is laterally quite flexible. A lateral brace on the tension flange at the load location corresponds to t = ∞ in Fig. 2.16.

Figure 3.1 shows that a local buckle forms in the web of the plexiglass model at P_{cr} = 62.4 lb. when both flanges are braced laterally. The bottom flange brace increases the buckling load from 51.8 lb. (Fig. 2.12) to 62.4 lb. This is not a large increase. Figure 3.2 shows that no curve similar to those of Fig. 2.16 goes through these two points 1 and 2. If the Yura theory is to be valid, the value of "t" for the plexiglass model must be larger than originally anticipated. Point 1 would then be shifted to the right. That is, the tension flange and the rest of the beam must offer considerably more restraint to the buckling web than originally expected, and the addition of a brace on the tension flange would do little to increase P_{cr}. The dotted curve could then give solutions to both problems, provided proper means of measuring restraints and stress distributions were available.

To verify this postulate, further computer analyses were undertaken with the lateral stiffness of the tension flange considerably reduced. It was necessary to obtain some results where the addition of the tension flange brace would markedly increase P_{cr}, since the Yura theory suggests that the lateral stiffness of the bottom flange significantly affects the buckling

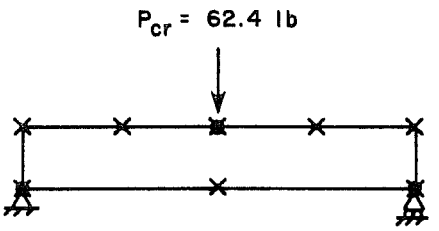

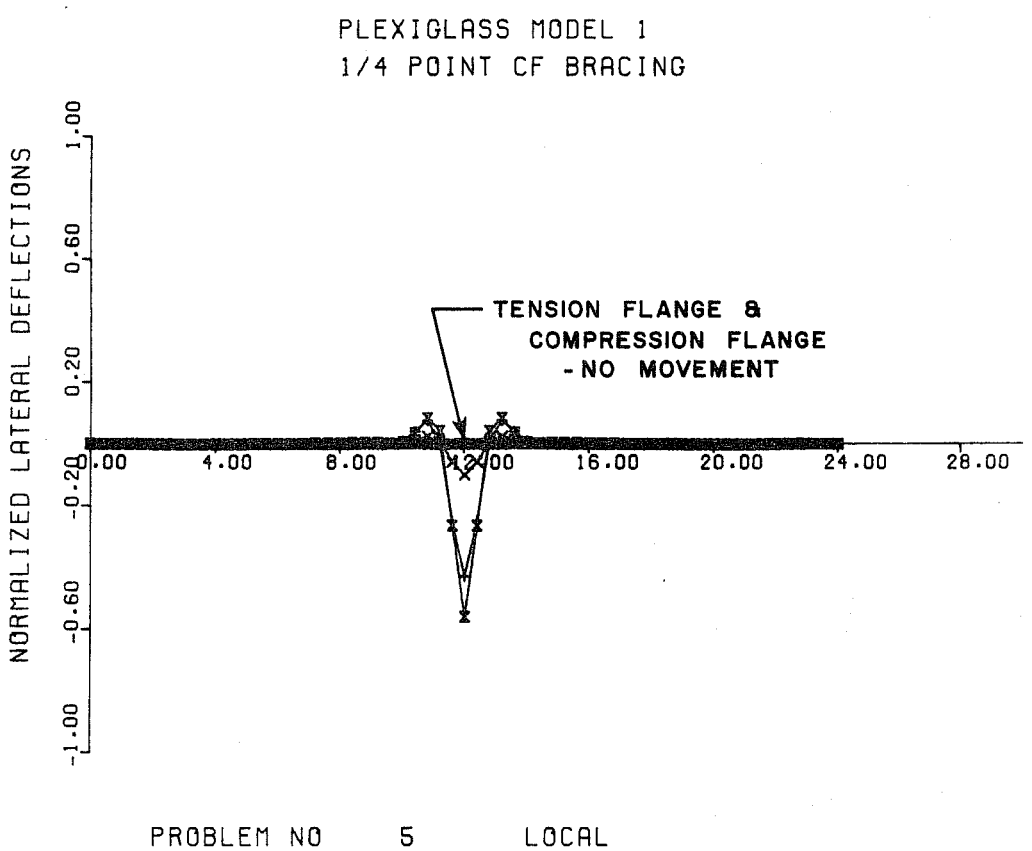

Fig. 3.1 BASP output--local buckling of plexiglass Model 1

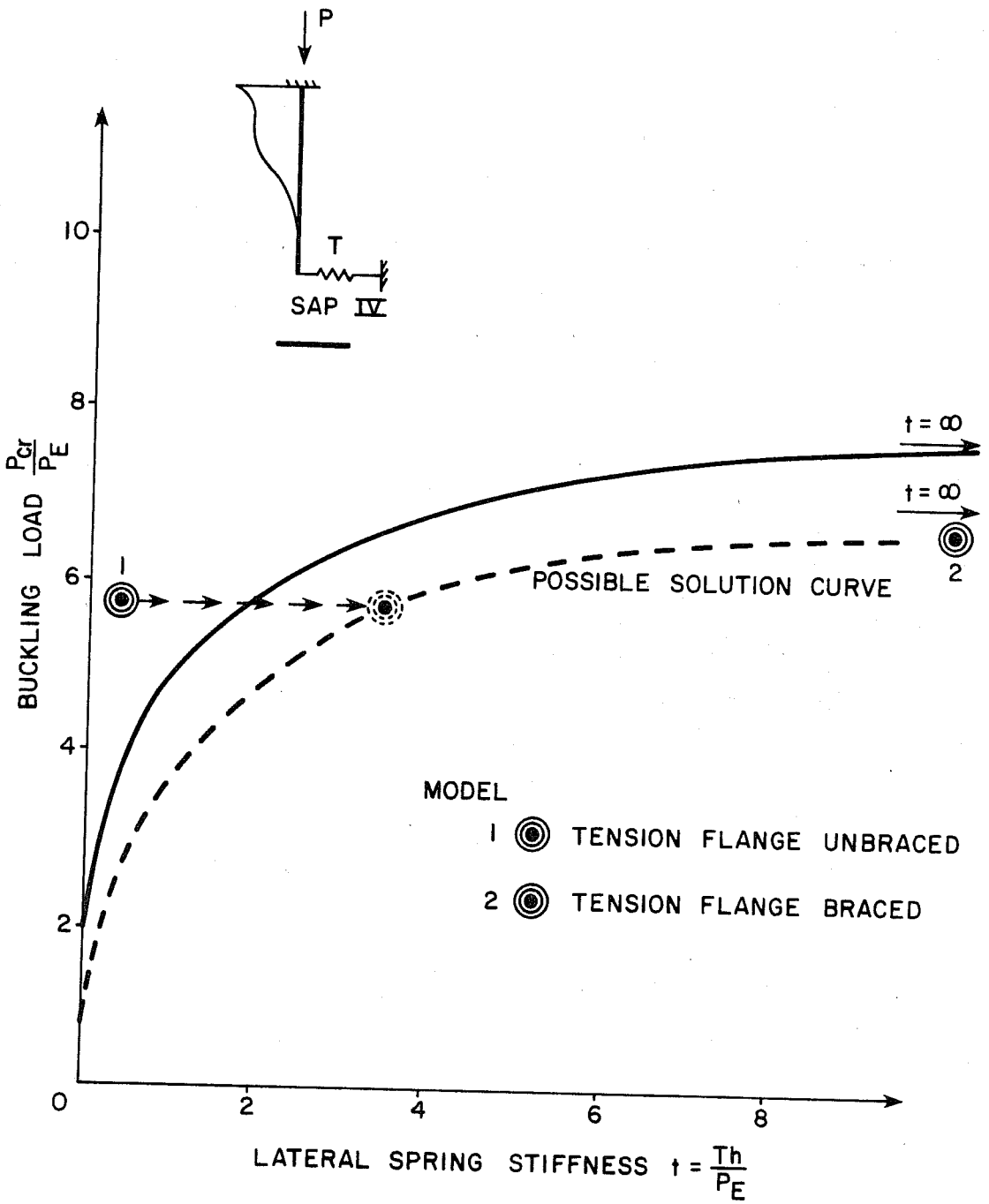

Fig. 3.2 Problems associated with Yura's theory and possible solution curve

load. The reduction of the lateral stiffness, T, can be accomplished in several ways. First, the length of the beam, L, can be increased since $T = f(L^{-3})$. Second, the width of the tension flange, b, can be decreased since $T = f(b^3)$. Both approaches were considered. When the flange width was altered, the thickness of the flange was also adjusted so that all beams studied would have the same moment of inertia and bending stresses. Naturally, when the length of the beam was varied, so was the bending stress distribution.

The following section presents a detailed study of these parameters and others. The plexiglass model beam configuration is used with changes to one or more parameters.

3.2 Analyses

All analyses were made with web element aspect ratios (length of element to height of element) between 0.5 and 2.0. In this manner, errors due to inaccurate element behavior are minimized. Bracing under the load, either on the top or bottom flange, was employed not just at one single node, but rather at five consecutive nodes (Fig. 3.3). The braced length along the flanges of the load point was approximately equal to the depth of the beam. The reasons for the multiple braces were twofold. First, to better represent engineering practice, where the load point is braced over a small length, and second, to enhance the characteristics of the buckled shape without significantly altering the buckling loads. In-plane supports consisted of pins at mid-depth of the beam. The ends of the beam were sometimes fully braced laterally when it was necessary to prevent slight local buckling over the supports. Again, the load was virtually unaffected while the buckled shape only showed the characteristics of interest.

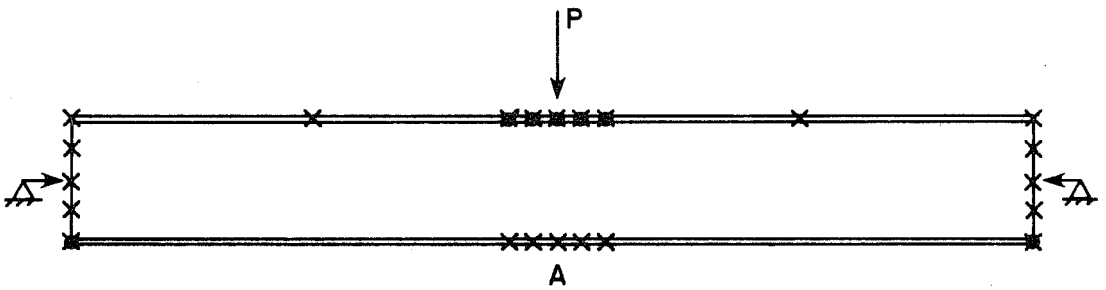

Fig. 3.3 Boundary conditions for beam of parametric study

3.2.1 Variation in Length. The cross-sectional properties of plexiglass model 1 given in Fig. 2.7 were used for all analyses. Beam length is varied from 12 to 48 in. to obtain results for the range L/h = 8 to 32. The bracing configuration of Fig. 3.3 was adopted except the tension flange was either braced or unbraced at location A. Buckled shapes are similar to those shown previously in Figs. 2.12 and 3.1. Results are given in Appendix 4 as problems 6 to 15, and plotted in Fig. 3.4.

The BASP solutions indicate there is not a large difference in buckling loads between the braced and unbraced cases despite a large variation in lateral stiffness of the tension flange, from a stiffness of T/8 to a stiffness 8T relatively. The length of the beam affects the buckling load for both bracing cases. Basler's theory[5] (and thus AISC[3]) assumes that bending stresses do not affect the local web buckling load. These results show otherwise: the longer the beam, the higher the bending stresses and the lower the buckling load.

Other BASP results (not presented) show that a 24 in. beam can be used to model all lengths with reasonable accuracy. This is done by simply superimposing additional bending stresses on the 24 in. beam in the region near the load point so that the bending

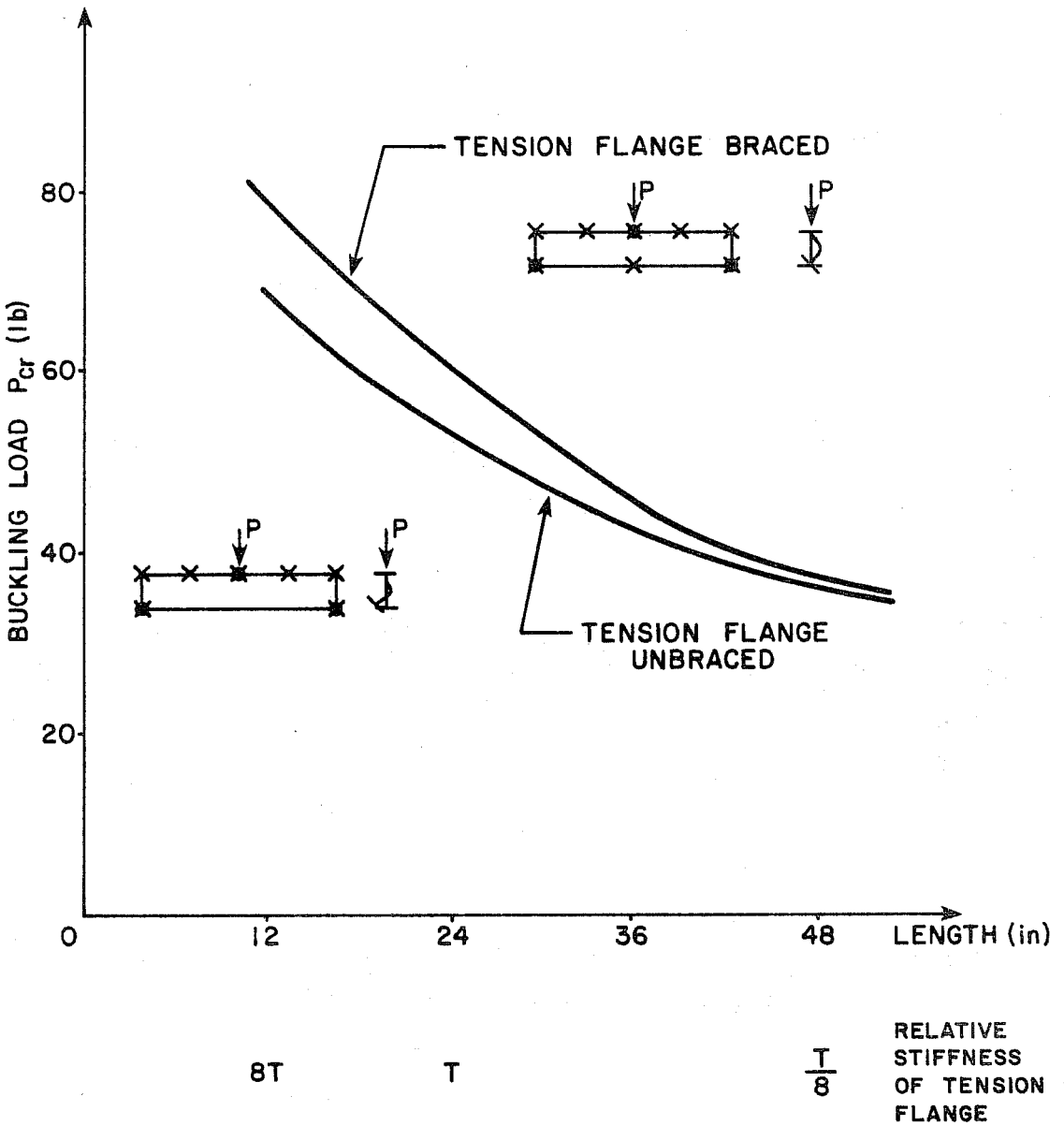

Fig. 3.4 Effect of beam length on buckling load

stress distribution there is the same as that existing in the other length beam. The tension flange stiffness remains that of a 24 in. beam. These results further suggest that the important parameters are both bending stress and vertical stress distributions in the vicinity of the load point. Furthermore, bottom flange stiffness seems insignificant, with tension flange bracing only slightly increasing the buckling load.

3.2.2 Variation in Tension Flange Width. Four different beam cross sections were used to study the effect of width of the tension flange on the buckling characteristics under a concentrated load. The same plexiglass beam (Model 1) section was used (Fig. 2.7) except for changes in the bottom flange. The width and thickness were altered, but the area of the bottom flange remained equal to the area of the top flange. In this manner, the neutral axis was kept at mid-depth of the beam, and the moment of inertia about this axis was virtually unchanged. Thus, the bending stress distribution in the 24 in. long beam remains the same for all tests. The bottom flange dimensions are varied over the range b/t_f = 0.5 to 34. The bracing and support conditions of Fig. 3.3 were used with the tension flange either braced or unbraced. Results are given in Appendix 4 as problems 8, 13 and 16 to 21, and are plotted in Fig. 3.5.

These results confirm the previous observations. Despite vast changes in the lateral stiffness of the tension flange (from a stiffness of T/16 to a stiffness of 4T relatively), there is less than 7 percent difference in the buckling loads when there is no tension flange brace. There is, of course, no difference in the buckling loads when there is a tension flange brace, since the bending stress distribution is the same for all beams.

The lateral stiffness of the top (compression) flange was found not to be a factor in the buckling load when the beam is simply supported for either braced or unbraced tension flanges. The cross section of the beam "b" shown in Fig. 3.5 was changed

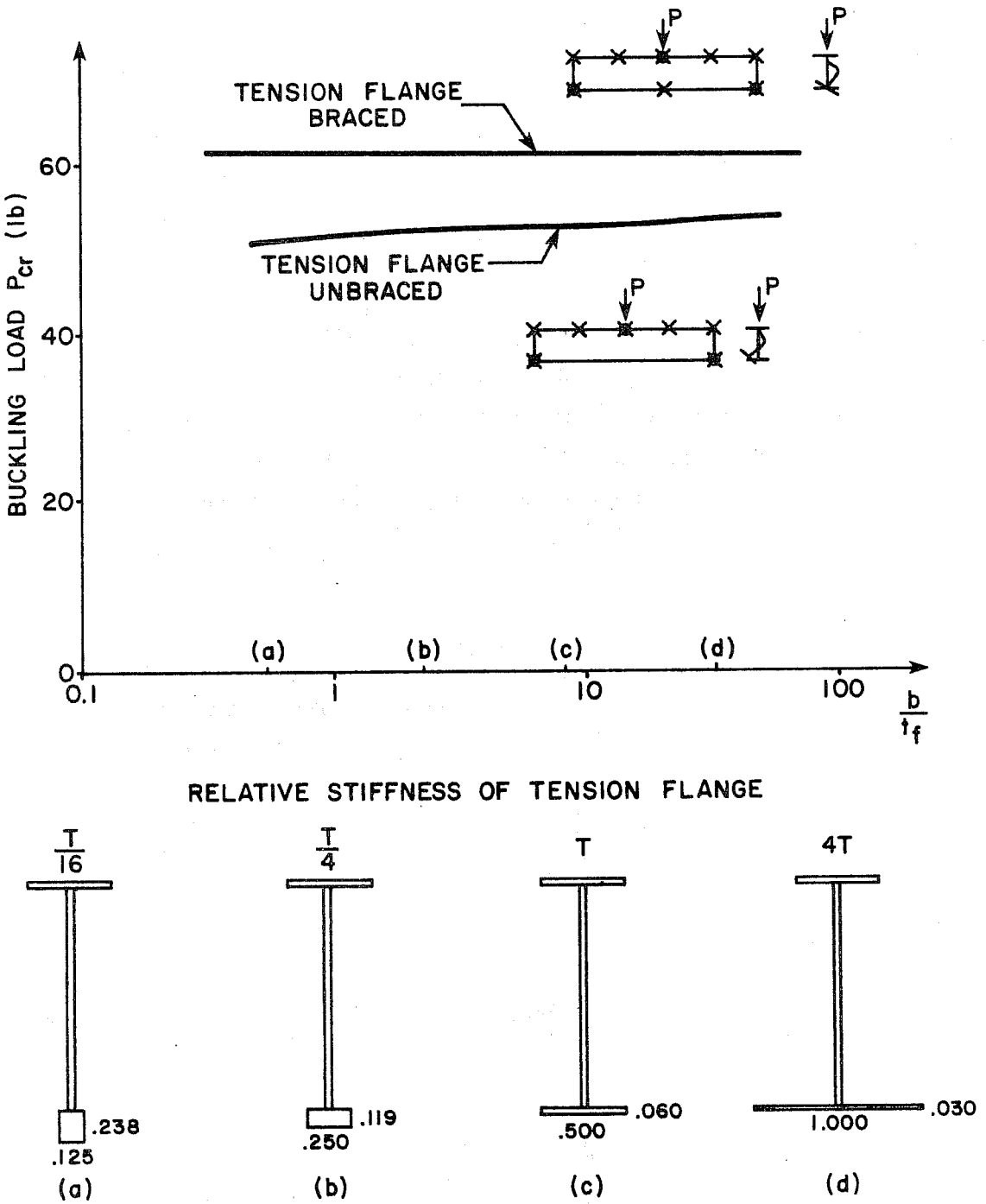

Fig. 3.5 Effect of lateral stiffness of tension flange on buckling load (dimensions in inches)

so that the compression flange dimensions were like those of the tension flange. There was a negligible effect on the buckling load. The results are reported in Appendix 4 as problems 32 and 33.

3.2.3 Variation of Other Parameters. Web depth, h, affects the web buckling load for two principal reasons. The depth influences the magnitude of the flexural stresses and it is directly related to web slenderness. The bending stress is a function of h^{-1} and the web column buckling load is a function of h^{-2}. The Model 1 cross section is used (Fig. 2.7) for variation in web depth studies and the configuration of Fig. 3.3 with tension flange either braced or unbraced adopted. The web depth is varied so as to obtain results for beams of relative depth between flange centerlines of d/2, d and 2d. Length is varied between 12 and 48 in. The combination of changes in L and h gives a range of L/h from 8 to 32. Results are reported in Appendix 4 as problems 6, 8, 10, 11, 13, 15 and 34 to 41. They confirm the importance of web depth as a parameter involved in the determination of P_{cr}. The variation is almost linear. That is, as Basler suggests, P_{cr} is a function of h^{-1}.

The moment of inertia of a web section buckling out of its plane is a function of $(t_w)^3$. Hence, slight variation in this parameter is likely to result in marked differences in P_{cr}. Model 1 cross section (Fig. 2.7) is used with web thickness variation such that a stocky web of slenderness ratio h/t_w from 31 to 62 is maintained. Results are reported in Appendix 4 as problems 8, 13, and 42 to 45. As expected, there was a rapid variation in P_{cr} with change in web thickness.

A singly symmetric cross section, shown in Fig. 3.6, is considered. It has a reduced tension flange area resulting in a higher neutral axis, a smaller moment of inertia and smaller section moduli at both the top and bottom flanges. Thus, it has higher bending stresses under unit loading. The beam has a pinned-roller simple support system in the plane, as the neutral axis is not

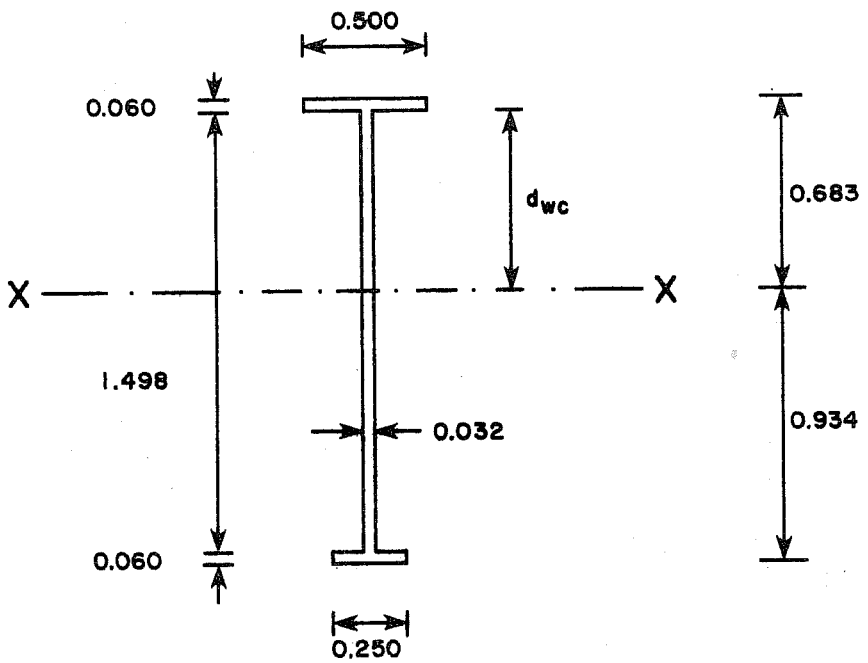

Fig. 3.6 Singly symmetric beam cross section (dimensions in inches)

at mid-depth of the beam (where the supports are). Apart from this change, the configuration for the 24 in. long beam is as in Fig. 3.3, with tension flange either braced or unbraced. The results, problems 46 and 47 in Appendix 4, show a increase in buckling loads over the standard doubly symmetric cross section, problems 8 and 13. This increase, despite higher bending stresses, can be attributed to the fact that the distance from the web-flange junction to the neutral axis, d_{wc} (depth of web in compression) is only 0.623 in. In the doubly symmetric beam, it is h/2 = 0.745 in. Since a smaller length of web is in compression, it takes a higher load to buckle it. For singly symmetric beams, d_{wc} seems to be a relevant parameter in predicting P_{cr}.

Two further problems were considered. First, all dimensions of the beam of Fig. 2.7 were multiplied by ten as was the length. The results (problems 48, 50 of Appendix 4) were that the buckling loads were exactly one hundred times those of the standard beam (problems 8, 13). This is because dimensionally

$$P_{cr} \sim \text{Young's Modulus, E} \times (\text{characteristic length})^2$$

Second, these increased dimensions were all maintained except the web thickness which was reduced from 0.32 in. back to 0.048 in. This resulted in a web slenderness ratio, h/t_w, of 312 (problems 49, 51 of Appendix 4). The buckling loads were dramatically reduced from those of the increased size beam, which had a stocky web. Furthermore, the tension flange bracing does little to alter the buckling load or buckled shape (Fig. 3.7). This is because the web is so slender that the flange is relatively stocky and stiff and will not move laterally, even if unbraced, under the action of the slender web.

3.2.4 Rotational End Restraint. The studies on lateral stiffness of the tension flange presented in the previous sections indicate that the Yura theory, or any extension of it, is invalid

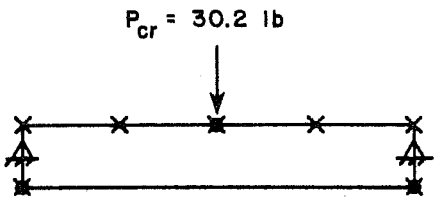

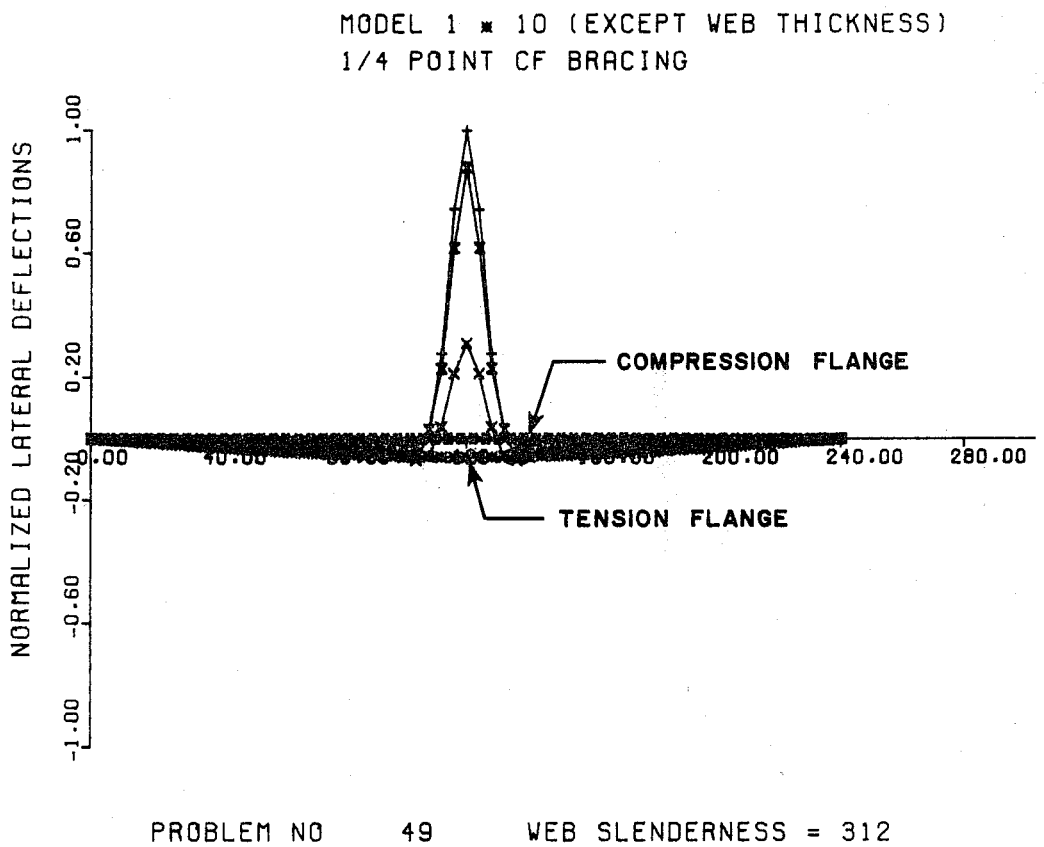

Fig. 3.7 BASP output--local buckling and slight tension flange movement of simply supported beam with slender web and unbraced tension flange

for simply supported beams. However, Yura obtained excellent correlation between his theory and tests on continuous beams. Since the only difference between simply supported beams and continuous beams is end restraint and because of this, bottom flange compression, a study was undertaken to determine the interaction between bottom flange compression near the supports and concentrated load effects on the web. The addition of varying amounts of negative end moment, M_N, can simulate all forms of beam continuity, up to and past complete fixity. Pinned ends out of the plane were used which permitted the beam to warp at the supports. Figure 3.8 shows how complete fixity can be modelled using the simply supported beam.

The cross section and length of plexiglass Model 1 (Fig. 2.7) were kept constant for the following analyses. As usual, both braced and unbraced bottom flanges were considered. The only variable parameter was M_N which ranged between 0 and PL/6. The fixed end moment for this beam is PL/8. Results are given in Appendix 4 as problems 8, 13, and 22 to 31 and are plotted in Fig. 3.9. The buckled shape for the fixed end case is shown in Fig. 3.10. Note how the bottom flange has completely "kicked out" and there is almost no local buckle effect at the concentrated load point. The results show an increase in the buckling load with increase in negative end moment when the bottom flange is braced. This is explained by the reduced positive moment (and bending stresses) at midspan under the load, with increasing M_N. However, when the bottom flange is unbraced, the buckling load drops dramatically with increasing M_N. Perhaps the bottom flange itself is on the verge of buckling due to the compression of its ends. This compression effect in beams with any degree of end restraint will be discussed in Chapters 5 and 6.

Similar variation of parameters, as carried out in the previous sections on simply supported beams, was also undertaken on beams with fixed ended restraint. Only one parameter was varied for any given

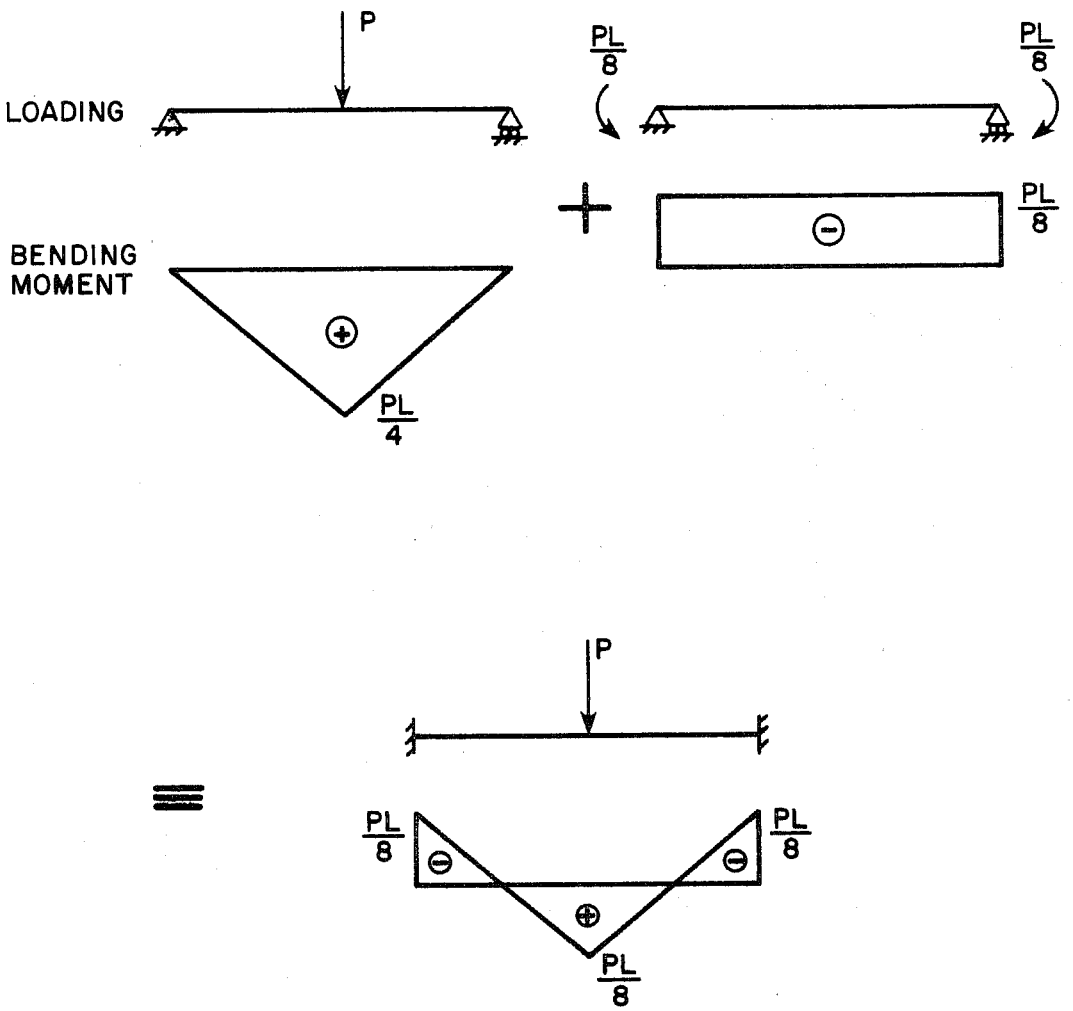

Fig. 3.8 Modelling of fixed ended beam

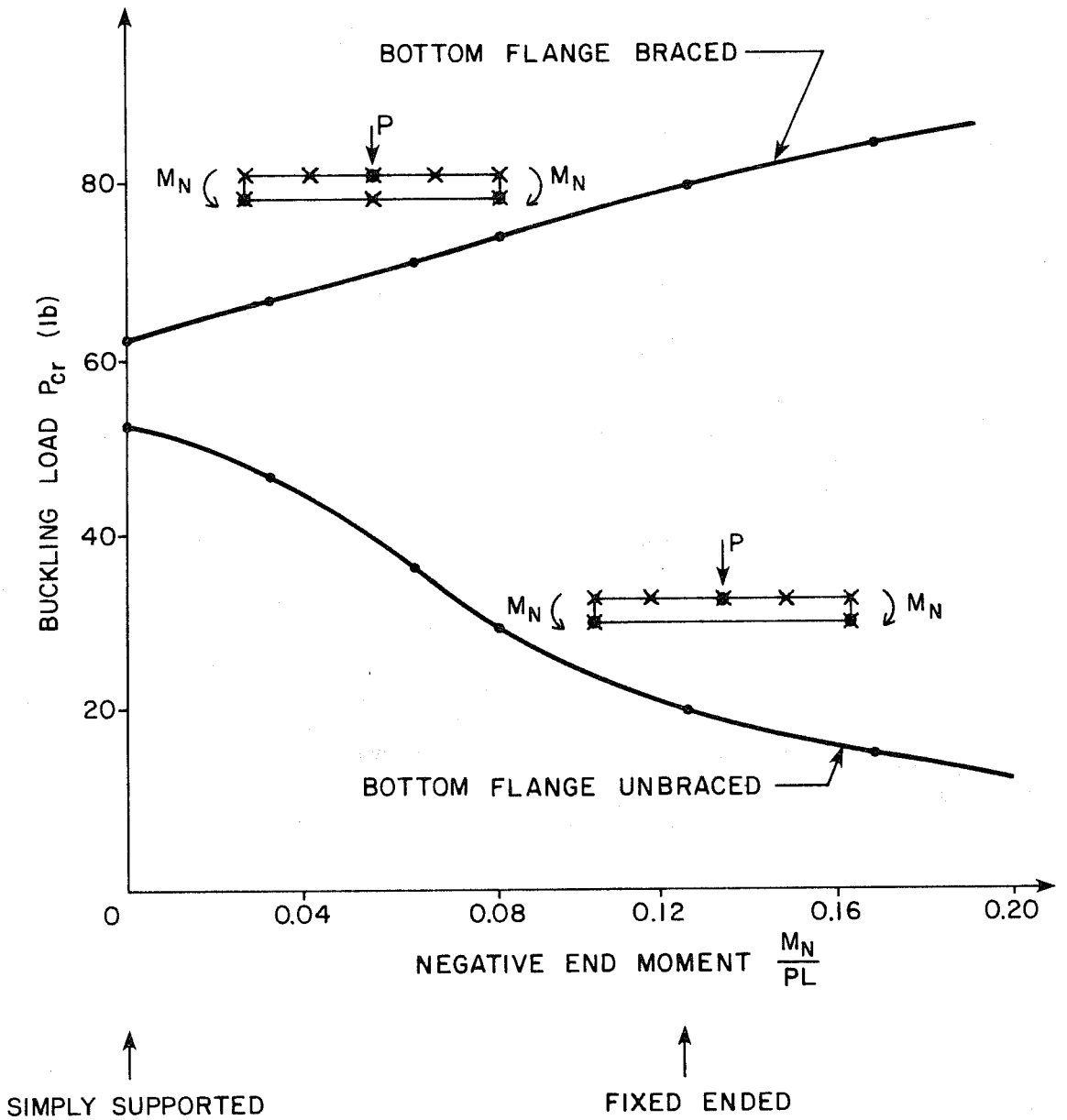

Fig. 3.9 Effect of negative end moment on buckling load

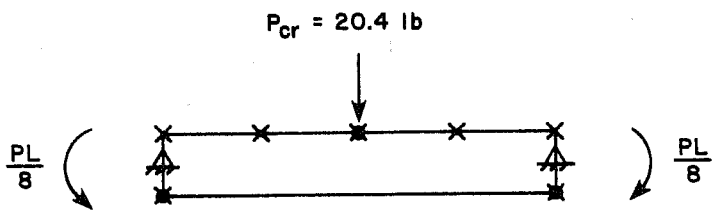

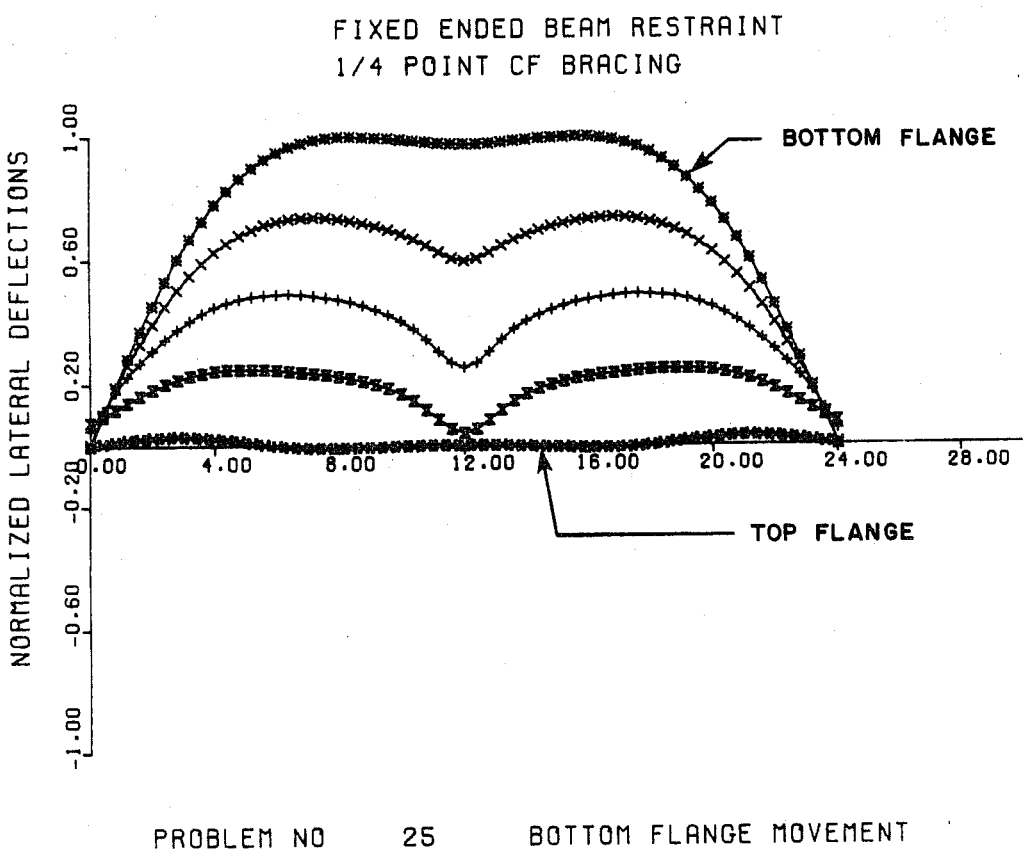

Fig. 3.10 BASP output--bottom flange movement of plexiglass Model 1 in fixed ended beam configuration

analysis. Both braced and unbraced bottom flanges were considered. There was variation in length and depth of the beam such that L/h ranged from 8 to 32, variation in web thickness such that web slenderness h/t_w ranged from 16 to 300, and also the singly symmetric section of Fig. 3.6 was studied. The results are reported in Appendix 4 as problems 25, 30 and 52 to 69. They show that similar trends are observed to those for simply supported beams. The presence of end moment, however, increased the buckling load when the bottom flange was braced, but decreased it otherwise. Very slender webs (L/h = 150 to 300) exhibit local buckling even when the bottom flange is unbraced, as discussed in the previous section and shown on Fig. 3.7. Stocky webs (L/h = 15 to 30), however, will not buckle locally at reasonable load levels. Other forms of instability occur earlier. If the bottom flange brace is removed, the stocky web acts as a restraining member for the "buckling" bottom flange. The stockier the web, the better the restraint and the less the movement of the bottom flange underneath the load (Fig. 3.11).

3.3 Interpretation

The previous analyses raise points that were not earlier recognized.

(1) The length of the beam, and thus the flexural stresses, play an important role in the determination of P_{cr} for both local buckling (bottom flange braced at the load point) and bottom flange movement (unbraced bottom flange).

(2) The lateral stiffness of the bottom flange does not significantly affect the buckling load for simply supported beams with unbraced tension flanges.

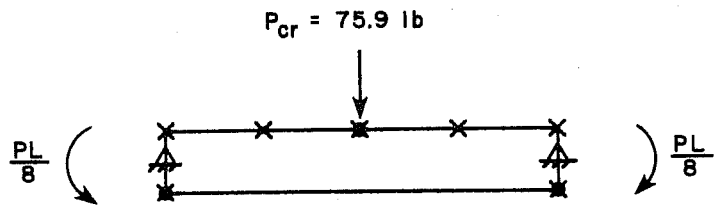

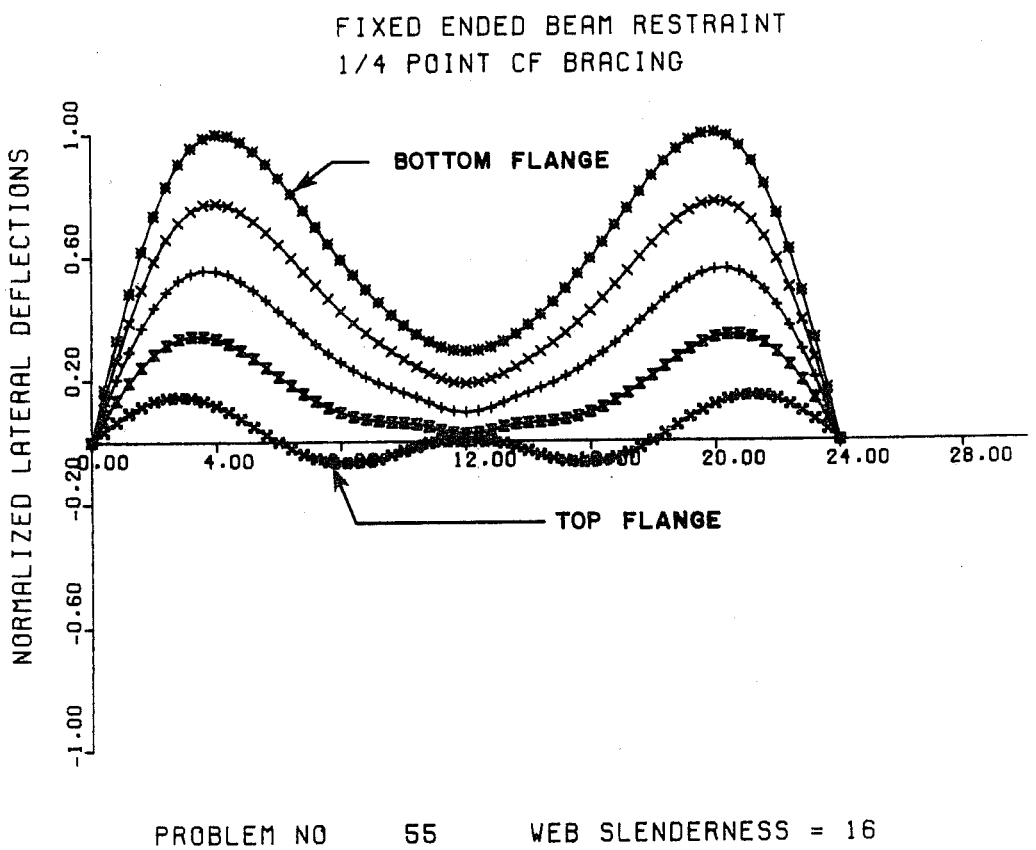

Fig. 3.11 BASP output--bottom flange movement of fixed end beam with very stocky web

(3) The addition of a brace on the tension flange does little to increase the theoretical buckling load for simply supported beams.

(4) When a beam with an unbraced bottom flange has negative end moments, the "buckling" part of the beam may be the bottom flange rather than the web. In this case the buckling load is greatly reduced and the addition of a brace under the load on the bottom flange greatly increases it.

(5) Basler's and Yura's theories (and extensions) do not accurately predict the buckling of webs under concentrated loads.

CHAPTER 4

DESIGN RECOMMENDATIONS--SIMPLY SUPPORTED BEAMS

The current AISC specification[3] employs Basler's theory,[5] which ignores the bending stress contribution to the local web buckle at a point of concentrated load. In this chapter an interaction equation is developed that incorporates both a bending stress term and a vertical stress term.

4.1 Tension Flange Braced

The equation to be developed must predict the buckling load at the limits of design situations. Short beams have very low bending stresses and at the buckling load, the vertical stress distribution is the dominant factor causing the instability. Quite the opposite occurs in long beams, where the bending stresses overshadow the vertical stresses. BASP was used to determine the buckling loads for these two extreme conditions.

Figure 4.1 shows the manner in which the buckling load of a beam with no bending stress was determined. A distributed moment was applied in the opposite sense to the bending moment caused by the vertical load. In this manner, a beam with very low bending moments under a concentrated midspan load is obtained. The beam cross section of Model 1 (Fig. 2.7) was used in the buckling analysis. The bracing system adopted prevents all flange lateral movement; only local web buckling can occur. The results are shown in Table 4.1 for two model beam lengths, 24 in. and 48 in. These show that with the bending stresses suppressed, the buckling load of 86.4 lb. is independent of length. Basler's theory suggests that P_{cr} = 57.8 lb. and this is conservative in this case by 49 percent. Hence, a more

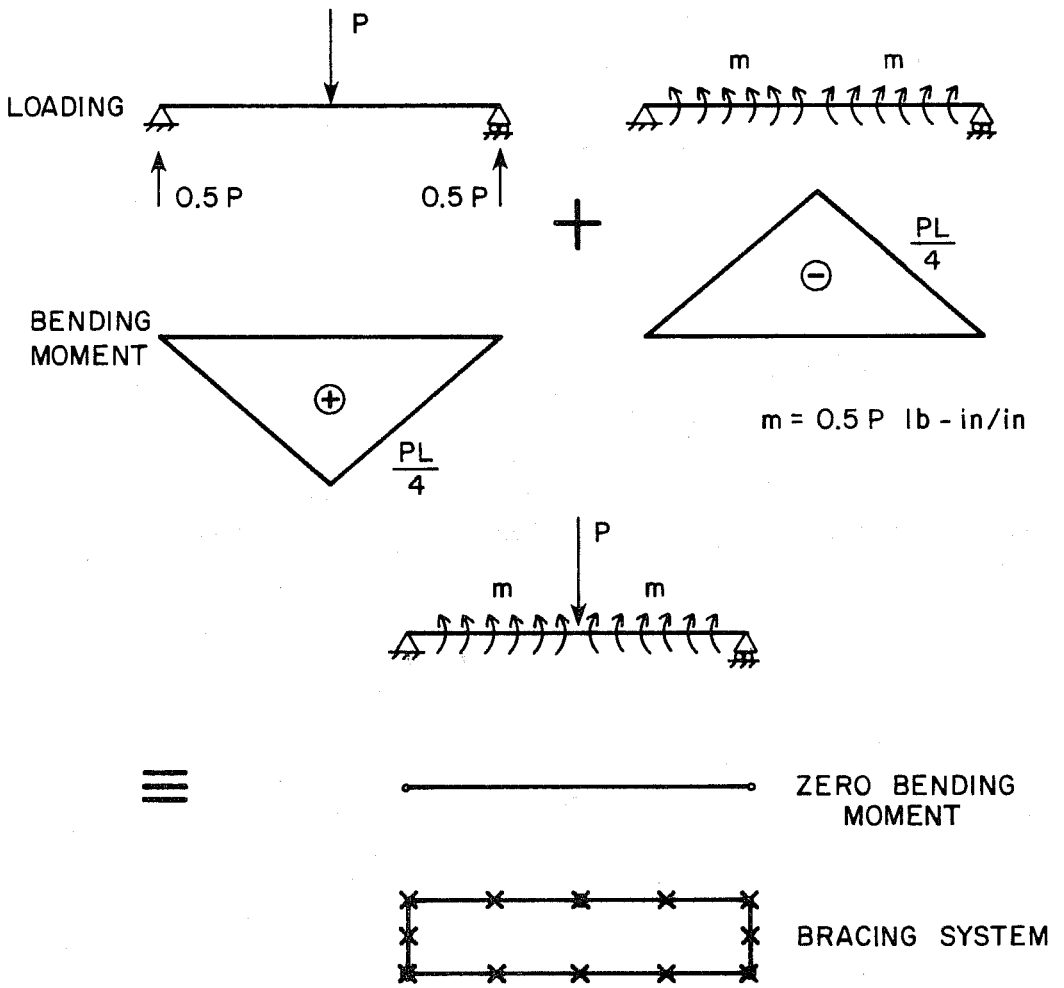

Fig. 4.1 Beam under concentrated load with no bending stresses

TABLE 4.1 EFFECT OF BENDING STRESSES ON WEB BUCKLING

Problem Number	Length, L (in.)	Bending Stresses Present	P_{cr} (lb.)
13	24	Yes	62.3
70	24	No	86.4
15	48	Yes	37.0
71	48	No	86.5

realistic estimate of the buckling load with only vertical stresses present is 1.5 times the Basler load, P_{BAS}, given in Eq. (1.2):

$$P_{VC} = 1.5P_{BAS} = \frac{8.2\pi^2 E}{12(1 - \nu^2)} \frac{t_w^3}{h} \qquad (4.1)$$

To obtain the limit whereby the web buckles solely under flexure with no vertical stresses, the configuration shown in Fig. 4.2 was adopted. This beam had a state of uniform moment and, so as to prevent premature web buckling at a particular location, the compression flange was continuously braced against lateral movement and twist. End stiffeners prevented local buckling at the supports. The cross section of Model 1 (Fig. 2.7) was used over a 24 in. span. The buckled shape in Fig. 4.2 shows the web has buckled everywhere in flexure between the undisplaced flanges at a moment of 526 lb.-in., which gives a critical stress for the web buckling in bending, σ_{bc}, of 8730 psi. If σ_{bc} is expressed in terms of the usual plate buckling parameters, the following equation can be used:

$$\sigma_{bc} = 39.8 \frac{\pi^2 E}{12(1 - \nu^2)} \left(\frac{t_w}{h}\right)^2 \qquad (4.2)$$

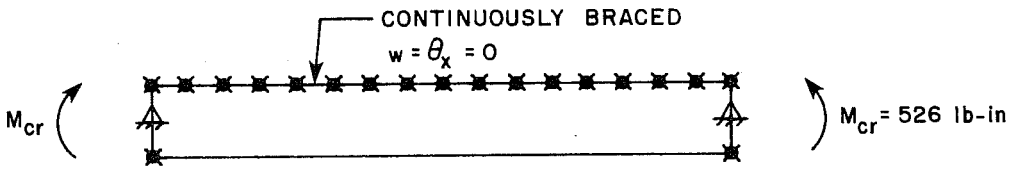

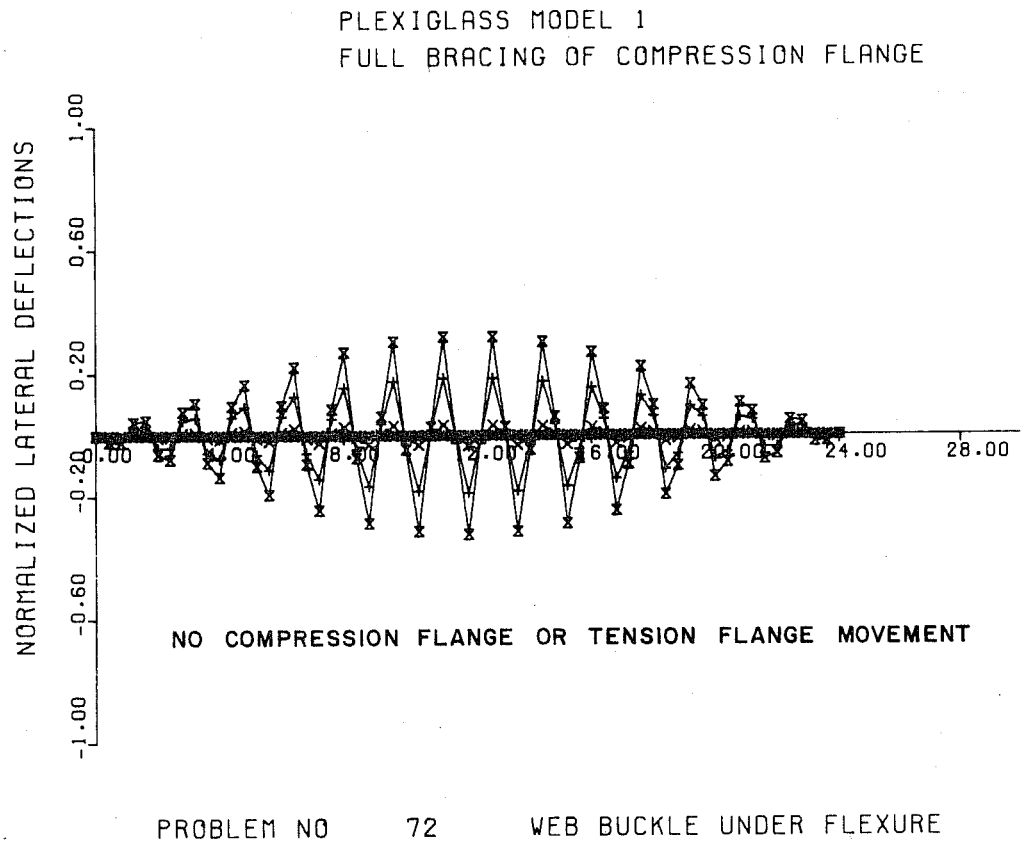

Fig. 4.2 BASP output--web buckling of beam under uniform bending with no vertical stresses

The coefficient 39.8 compares with published values[10] of 39.7 to 43.0 for rectangular plates of aspect ratio 0.5 to 2.0 subjected to bending stresses applied on the two opposite simply supported sides ($w = 0$) and clamped top and bottom ($w = \theta_x = 0$).

An interaction equation was formulated using the two limits given by Eqs. (4.1) and (4.2). The trial equation is

$$\left(\frac{\sigma_b}{\sigma_{bc}}\right)^2 + \left(\frac{P_{LOC}}{P_{VC}}\right)^2 = 1 \tag{4.3}$$

where σ_b is the bending stress at web-flange junction under the critical load to cause local web buckling, P_{LOC}. Equation (4.3) can be converted to the following form by using Eqs. (4.1) and (4.2) and substituting for σ_b in terms of P_{LOC}, h, L and bending axis moment of inertia, I.

$$P_{LOC} = \frac{\frac{\pi^2 E}{12(1-\nu^2)}\left(\frac{t_w}{h}\right)^2}{\sqrt{\left(\frac{hL}{318I}\right)^2 + \left(\frac{1}{8.2t_w h}\right)^2}} \tag{4.4}$$

For doubly symmetric sections h is the depth of the web. For singly symmetric cross sections in the plane of bending, h should be taken as twice the depth of web in compression, d_{wc}.

The first term in the denominator of Eq. (4.4) represents the bending stress contribution and the second, the vertical stress contribution. Table 4.2 shows the comparison between this equation and the BASP results of Chapter 3, the details of which are given in Appendix 4.

The predictions of Eq. (4.4) are all within 7 percent of the BASP buckling load except for problem 39. The cross section of this beam, which is very stocky, is shown in Fig. 4.3. Using

TABLE 4.2 COMPARISON OF BASP AND APPROXIMATE SOLUTIONS FOR BRACED TENSION FLANGES

Problem Number	Buckling Load BASP (lb.)	Buckling Load P_{LOC}, Eq. (4.4) (lb.)	% Error
5	62.4	61.4	- 1
11	78.3	77.4	- 1
12	69.4	69.4	0
13	62.3	61.4	- 1
14	46.0	38.3	+ 5
15	37.0	39.0	+ 6
19	62.3	61.4	- 1
20	62.4	61.4	- 1
21	62.4	61.4	- 1
33	62.4	61.4	- 1
38	154	161	+ 4
39	106	126	+18
40	32.9	32.7	- 1
41	23.1	22.0	- 5
44	29.2	29.3	0
45	176	177	0
47	72.5	77.4	+ 7
50	6230	6140	- 1
51	30.5	28.6	- 6

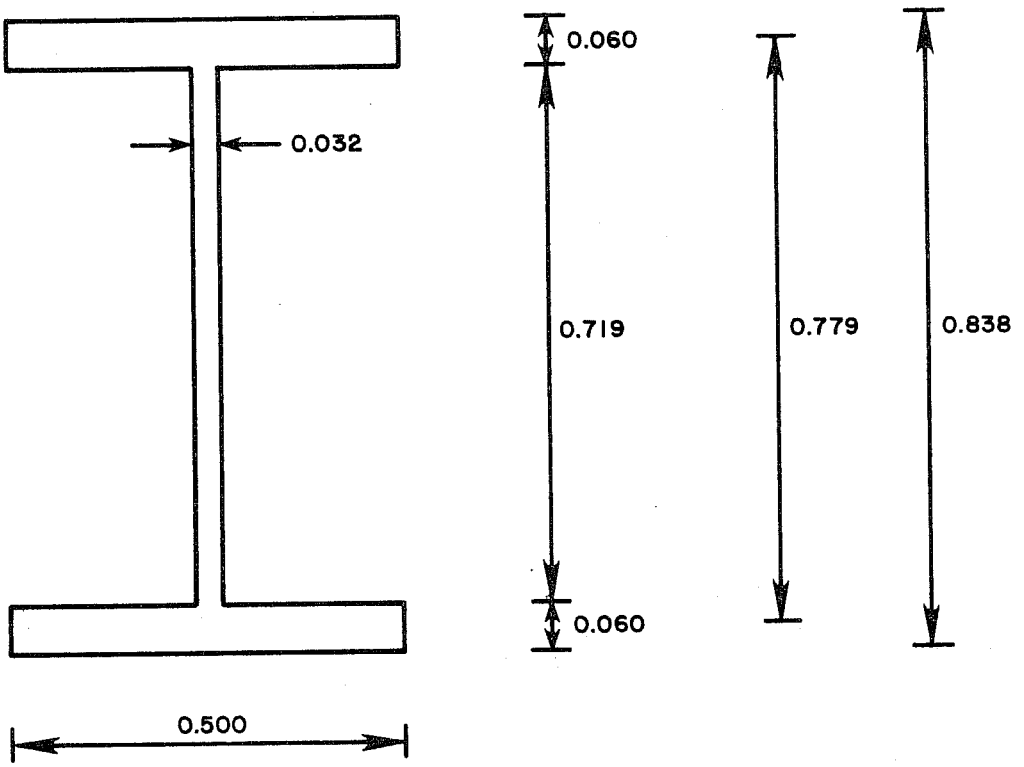

Fig. 4.3 Stocky beam cross section
(dimensions in inches)

the correct definition of h (0.719 in.), Eq. (4.4) gives P_{cr} = 126 lb., an 18 percent error. In BASP, however, the web elements have a total depth d = 0.779 in., while the flanges are line elements separated by this distance. Any shortening of the web elements to accurately model the length of the web would result in a significant reduction in the moment of inertia of the section. If h = d = 0.779 in. is used in Eq. (4.4), then P_{cr} = 106 lb., an error of less than 0.1 percent. Thus, the difference between BASP and Eq. (4.4) is mainly due to computer modeling of the web depth as the distance between the flange centroids. Equation (4.4) appears to be valid and can be easily used.

4.2 Tension Flange Unbraced

For web buckling at a point of concentrated load, the current AISC specification makes no distinction between this case and the tension flange "braced" problem of the previous section. In Chapter 3, nineteen cases were observed in which significant movement of the tension flange occurred in the buckled state. The solutions are summarized in Table 4.3. The average difference between the buckling loads for tension flange braced (Table 4.2) or unbraced was 13 percent with a range of 1 percent to 23 percent. The tension flange movement buckling load is always less than the local web buckling load. After trying various approaches, it is recommended when the tension flange is laterally unsupported, the buckling load P_{TFU} be determined by applying a reduction factor of 0.8 to the equation developed previously for braced tension flanges.

$$P_{TFU} = 0.8P_{LOC} \tag{4.5}$$

In this manner both bending stress effects and vertical stress effects are modelled again. Table 4.3 shows the comparison between this equation and the BASP results of Chapter 3.

TABLE 4.3 COMPARISON OF BASP AND APPROXIMATE SOLUTIONS FOR UNBRACED TENSION FLANGES

Problem Number	Buckling Load BASP (lb.)	Ratio of Buckling Loads BASP $\left(\frac{\text{Unbraced Tens. Fl.}}{\text{Braced Tens. Fl.}}\right)$	Buckling Load P_{TFU}, Eq. (4.5) (lb.)	% Error
4	51.8	0.83	49.1	- 5
6	68.8	0.88	61.9	-10
7	59.5	0.86	55.5	- 7
8	52.9	0.85	49.1	- 7
9	42.8	0.93	38.6	-10
10	36.6	0.99	31.2	-15
16	54.7	0.88	49.1	-10
17	52.7	0.84	49.1	- 7
18	51.1	0.82	49.1	- 4
32	56.8	0.91	49.1	-14
34	129	0.84	129	0
35	82.3	0.78	101	+22
36	28.8	0.88	26.2	- 9
37	17.8	0.77	17.6	- 1
42	25.9	0.89	23.4	- 9
43	170	0.96	142	-17
46	55.9	0.77	61.9	+11
48	5290	0.85	4910	- 7
49	30.2	0.99	22.9	-24

The predictions of Eq. (4.5) are conservative on all but two occasions: problems 35 and 46. In problem 35, the same section as shown in Fig. 4.3 was used. For reasons discussed in the previous section, BASP may also considerably underestimate P_{TFU} when beams are stocky. In problem 46, a singly symmetric cross section was used. When the tension flange was braced, Eq. (4.4) overestimates P_{LOC} by 7 percent. For an unbraced tension flange, Eq. (4.5) overestimates P_{TFU} by 11 percent. Both these exceptions to the conservativism of Eq. (4.5) should have little concern to the user.

4.3 New Plexiglass Models

Equations (4.4) and (4.5) predict the loads to cause local buckling and tension flange movement, respectively. Still, experimental verification of both these equations and the BASP results was needed. It was decided to build a new plexiglass model beam that could demonstrate the following phenomena: lateral-torsional buckling in a conventional S-shape when braced at midspan only (Configuration 1, Fig. 2.6), and tension flange movement when the compression flange is braced at the 1/4-points (Configuration 2, Fig. 2.6) at a lower load than that which causes lateral-torsional buckling in a double S-shape.

The beam, Model 2, had very similar dimensions to those of Model 1, the main difference being a thinner web. By reducing the web thickness, the load to cause either local buckling or tension flange movement should be considerably lessened, whereas the load to cause lateral-torsional buckling would be relatively unaffected. Model 2 dimensions are shown below with Model 1 dimensions in parentheses.

b = 0.500 in. (0.500 in.)
t_f = 0.065 in. (0.060 in.)
h = 1.497 in. (1.498 in.)
t_w = 0.025 in. (0.032 in.)

TABLE 4.4 MODEL 2 BUCKLING LOADS

Bracing Configuration	Buckling Mode	P_{cr} (lb.)		
		Experiment	BASP (Problem No.)	Estimate (Eq. No.)
1	Lateral-Torsional	14	12.9 (73)	14.2 (1.1)
2	Lateral-Torsional	--	36.3 (74)	37.8 (1.1)
2	Tension Flange	26	29.5 (75)	26.4 (4.5)
2	Local Web	--	32.8 (76)	33.0 (4.4)

The tension flange movement occurred prior to lateral-torsional buckling in Configuration 2. The buckled shapes were very similar to those of Model 1 both experimentally and on the computer, with a slight exception: when tension flange movement occurred in configuration 2, there was more of a bulge underneath the load, indicating the local buckle effect (Fig. 4.4). This was not so apparent in Model 1, even though BASP had always shown it (Fig. 2.12). The thinner web enhanced the visual indication of this phenomenon. Illustrations of the BASP buckled shapes will not be repeated because of their similarity with those of Model 1 (Figs. 2.10, 2.11 and 2.12).

A third beam, Model 3, was built. It had identical dimensions to those of Model 2, however, it had a significant initial lateral deflection (sweep). The sweep was 0.03 in. at the midspan which is slightly in excess of the sweep tolerance that standard mill practice permits.[2] The permissible sweep is 1/8 in./10 ft. or 0.025 in. over the 24 in. span. This geometrically imperfect beam displayed tension flange movement at only 18 lb., 30 percent lower than the load under which Model 2 buckled. This dramatic lowering of the buckling load for the imperfect beam shows the importance of keeping within the tolerance levels set by AISC and supports the use of a larger factor of safety in design criteria that guard against this stability-related phenomenon.

4.4 Other Considerations

BASP performs an elastic analysis, and Eqs. (4.4) and (4.5) predict the BASP results accurately. The elastic results, however, may be far from the true buckling loads. Inelastic effects and post-buckling strength of the web plate are now discussed.

4.4.1 Inelastic Effects. Beams with very stocky webs ($h/t_w < 50$) may yield under the load point at loads considerably less than the elastic buckling load. If yielding proceeds into the web, local buckling or tension flange movement, depending on whether

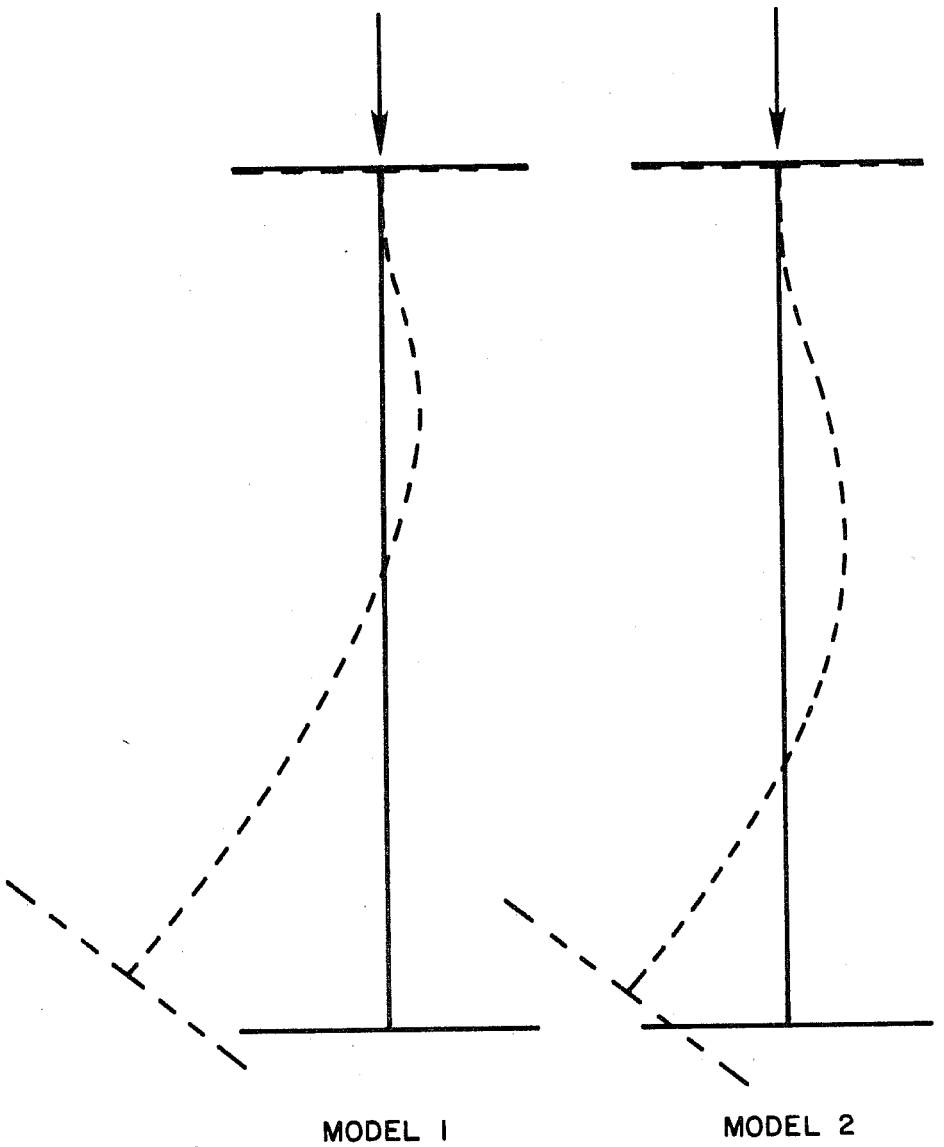

Fig. 4.4 Local buckle effect on plexiglass Models 1 and 2 during tension flange movement

the bottom flange is braced or not, may occur immediately. This is because yielding at the web-flange junction causes a zone of plasticity, and the torsional rigidity of the flange ($\theta_x = 0$) at the load point does not restrain the web. That is, a plastic hinge is formed in the web plate (Fig. 4.5a) and rotational restraint of the web is lost (Fig. 4.5b). In this case, Eqs. (4.4) and (4.5) may considerably overestimate the buckling load.

Lyse and Godfrey[15] conducted tests in the 1930's on six 22-in., 58-lb., rolled steel sections. These beams had a web slenderness ratio, h/t_w, of about 50. The central load was applied over nominal bearing lengths of 7 to 11 in. The beams were very short having a span:depth ratio of only about 3. The steel used had a yield point of 50 ksi and the ultimate loads were about 220 kips. BASP analyses were performed both with and without torsional restraint at the load point. Furthermore, BASP could predict the maximum vertical compressive stress, $\sigma_{v\ max}$, in the web underneath the load for this very short beam.

Results are shown in Table 4.5. They indicate that buckling occurred in the test virtually as soon as the web yielded. Basp overpredicts the load even when rotational restraint at the load point is ignored. This is because BASP allows stresses in excess of the yield stress. Still, problem 78 ($w = 0$ at load point) provides a much better estimate than problem 77 ($w = \theta_x = 0$ at load point). The buckled shape, in both BASP and the test, showed little tension flange movement despite it being unbraced. This is because the beam was so short; the flange was very stiff and was not forced out by the buckling web, the shape being that of Fig. 4.5(b). The theoretical load, P_{TFU}, predicted by Eq. (4.5) was 9 percent below that obtained with BASP, problem 77, indicating an accurate prediction even for such a short beam. This load, however, is far in excess of the actual buckling load because of the inelastic effects. Furthermore, for short beams, Eqs. (4.4) and (4.5) cannot

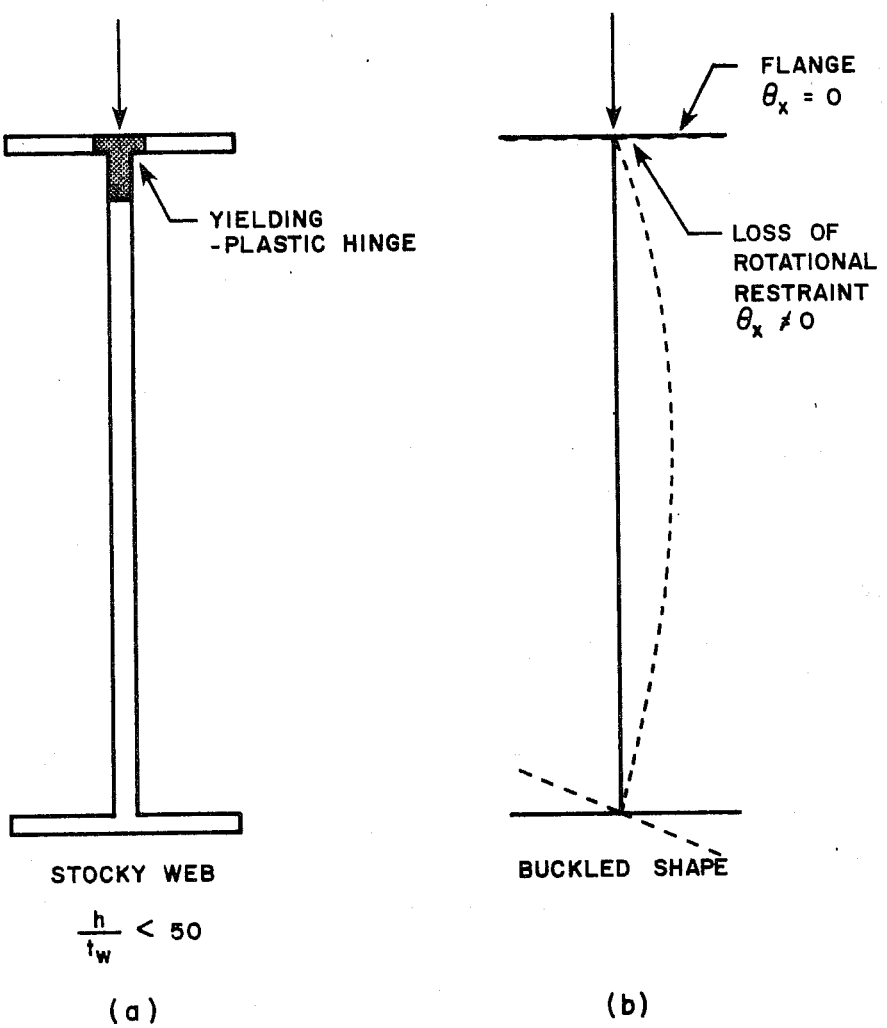

Fig. 4.5 Effect of plasticity on twist restraint of the web

TABLE 4.5 COMPARISONS WITH LYSE AND GODFREY[15] TEST RESULTS

	P_{cr} (kips)	$\sigma_{v\ max}$ (ksi)
Lyse and Godfrey test (average)	220	51*
BASP $w=\theta_x=0$ at load (Prob. 77)	559	130
BASP $w=0$ at load (Prob. 78)	305	71
P_{TFU} (Eq. (4.5))	506	--

*from BASP analysis indicating $\sigma_{v\ max} = 0.232$ ksi for each P = 1 kip.

be implicitly relied upon, since they model bending stresses at the load point with ordinary beam theory, which is really only valid for longer beams.

The composite beam of Daniels and Fisher[11] (Fig. 1.1) also had a very stocky web ($h/t_w = 46$). Because of the concrete slab, the neutral axis was just below the web-flange junction. BASP was employed using an equivalent area of steel to model the concrete slab. Results were far in excess of the actual test load to cause tension flange movement. At this load, the elastic stresses would have been approximately 700 ksi. During the test it was noted that the concrete slab had crushed to its full depth and there was widespread yielding of the W21x62 steel beam prior to tension flange movement. Hence it was considered that the steel beam was acting independently of the slab, and that there was no torsional restraint of the web by the slab because of plasticity. Even with a W21x62 beam model and with only $w = 0$ on the compression flange, BASP predicted P_{cr} to be considerably higher than the test load. Clearly yielding was too widespread for an elastic analysis to be accurate. Again, the significance of inelastic effects is seen.

4.4.2 Post-Buckling Strength. The elastic analysis of BASP is based on small-deflection theory whereby the buckled position is in unstable equilibrium, close to the flat unbuckled original position. Such a small out-of-plane displacement occurs in the web plate at buckling. However, after this small displacement occurs, tensile membrane stresses may arise in the mid-thickness plane which tend to stabilize the plate. Any given element of a plate is constrained by adjacent elements. Because these membrane effects arise gradually during the loading of a plate girder, the sudden buckling as for a compressed bar does not appear. The web of a plate girder cannot collapse without the flanges surrounding it also collapsing. The result of web buckling is to cause a redistribution of stresses. As long as the flanges are capable of resisting an increased share of the load, the web plate cannot fail until yielding occurs. This phenomenon is known as post-buckling strength, and is of course not modelled by the linear-buckling analysis program BASP.

Post-buckling strength usually only occurs in plate compression elements that have edges supported. Free edges tend to move during buckling and, hence, diminish the ability of membrane tensile stresses to form. So, when the web buckles under the action of a concentrated load, post-buckling strength can be expected when the web remains elastic and the tension flange movement is minimal. This tension flange movement can be prevented by bracing or by the flanges being very stiff relative to the web. In this case, Eq. (4.4) may be quite conservative in predicting P_{LOC}. If, however, the tension flange is free to move and is not that stiff relative to the web, little post-buckling strength can be expected, and then both Eq. (4.5) and BASP would accurately predict P_{TFU}.

Bergfelt and Hövik[7] conducted a number of tests on short beams (L/h = 5 to 8) with exceptionally slender webs (h/t_w = 150 to 350). All plate girders had the same extremely thin web, t_w = 2 mm. The girders were unbraced on the bottom flange, but because of the

extreme flexibility of the web, this flange would not move during buckling anyhow. Results are given in Table 4.6 for analyses of Bergfelt and Hövik's test no. 16 which has $h/t_w = 350$.

Both BASP and Eq. (4.4) considerably underestimate the actual test result. They predict only 35 percent of the true load. This can be attributed to the post-buckling strength of the web plate. Note that at the BASP buckling load, the web is indeed elastic and in the test, failure only occurs after yielding under the load point. This time Eqs. (4.4) and (4.5) are vastly conservative in error.

TABLE 4.6 COMPARISONS WITH BERGFELT AND HÖVIK[7] TEST RESULTS

	P_{cr} (kips)	$\sigma_{v\ max}$ (ksi)
Bergfelt and Hövik test no. 16	13.0	45*
BASP $w=\theta_x=0$ at load (Prob. 77)	3.68	13.3
P_{LOC} (Eq. (4.4))	3.86	

*from BASP analysis indicating $\sigma_{v\ max} = 3.61$ ksi for each P = 1 kip.

CHAPTER 5

DESIGN RECOMMENDATIONS--FIXED ENDED BEAMS

5.1 Bottom Flange Braced

As in the case of simply supported beams, the failure mode of interest for fixed ended beams with both top and bottom flanges braced at the load point is that of a local web buckle between these braces. The end restraint simply reduces the midspan positive moment and flexural stresses, resulting in a higher buckling load, as seen in Fig. 3.9. End restraint has little effect on the vertical stress distribution under the load so Eq. (4.4) can be used with one change. The span of the beam, L, is replaced by the length between inflection points, L_1. This is because the bending stress at the web-flange junction under the load, σ_b, is the same function of L_1 in fixed ended beams as it is of L in simply supported beams. With this change, Eq. (4.4) becomes

$$P_{LOC} = \frac{\frac{\pi^2 E}{12(1 - \nu^2)} \left(\frac{t_w}{h}\right)^2}{\sqrt{\left(\frac{hL_1}{318I}\right)^2 + \left(\frac{1}{8.2t_w h}\right)^2}} \qquad (5.1)$$

Once again, for singly symmetric cross sections use $h = 2d_{wc}$. Table 5.1 shows the comparison between this equation and the BASP results of Chapter 3, the details of which are given in Appendix 4. The results show that Eq. (5.1) can predict the web buckling loads over the variety of conditions considered to within an accuracy of ±8 percent. Therefore, it successfully models the web behavior.

TABLE 5.1 COMPARISON OF BASP AND APPROXIMATE SOLUTIONS FOR BRACED BOTTOM FLANGES

Problem Number	Buckling Load BASP (lb.)	Buckling Load P_{LOC}, Eq. (5.1) (lb.)	% Error
30	79.6	77.4	- 3
61	56.9	61.4	+ 8
62	39.8	39.1	- 2
63	89.8	94.6	+ 5
66	35.1	34.1	- 3
67	9.0	8.6	- 4
68	1.2	1.1	- 8
69	0.36	0.33	- 8

5.2 Bottom Flange Unbraced

When the bottom flange is unbraced, the buckling loads are significantly lower than those for simply supported beams (Fig. 3.9) and the buckled shapes are completely different (Fig. 3.10). In the simply supported beam, tension flange movement was observed, but it was usually accompanied by significant local distortion under the load. This indicated a relationship between local buckling and tension flange movement and justified the use of Eq. (4.5). However, if the beam has end fixity, there is little hint of local buckling and the movement of the bottom flange is much more pronounced. Also, the load is considerably lower than that predicted by either Eq. (4.5) or Eq. (1.1). The important difference between a beam with end fixity and one which is simply supported is that the former has compression in its bottom flange

near the supports whereas the latter has a bottom flange that is purely in tension. In fact, under concentrated loading the beam with end fixity has tension in the bottom flange in only the middle half of the beam (Fig. 3.8). The instability in this case could easily be caused by the unbraced bottom flange itself buckling laterally with the web trying to restrain it, instead of, as in the simply supported case, the web buckling with the bottom flange trying to restrain it.

BASP was used to determine the critical buckling stress in the bottom flange, σ_{fc}, under a variety of conditions, and to establish the effect of vertical stresses on it. Figure 5.1 shows the three cases considered: (a) concentrated loading and the associated high vertical stresses under the load (problem 25, Fig. 3.10); (b) uniform loading producing small vertical stresses (problem 80); and (c) moment loading with no vertical stresses (problem 81). All three have similar bending moment diagrams under unit loading in the regions where the bottom flange is in compression. The cross section of Model 1 (Fig. 2.7) was used over a 24 in. span with bracing configuration 2 of Fig. 2.6.

The results show that all three have very similar buckled shapes exhibiting pronounced bottom flange movement. The buckled shape for case (a) of Fig. 5.1 is shown in Fig. 3.10. Furthermore, the critical moments and buckling stresses are also quite similar, considering the huge differences in the vertical stress distribution under the load point. This suggests that vertical stresses under the load have far less to do with the phenomenon of bottom flange movement in fixed ended beams than they do in simply supported beams.

5.2.1 Bottom Flange Models. If the bottom flange compressive stress near the supports is the principal reason for beam buckling, then it may be possible to predict the critical buckling stress in the bottom flange by isolating the bottom flange and applying

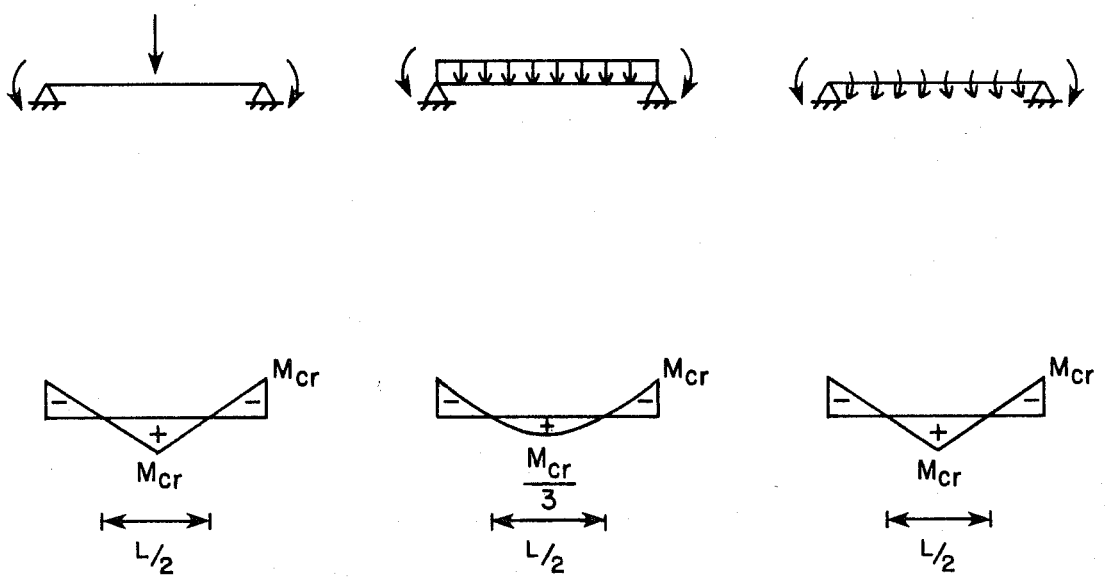

VERTICAL STRESSES UNDER LOAD

High	Low	None
σ_{fc} (psi)		
1020	1180	1290
(a)	(b)	(c)

Fig. 5.1 Effect of vertical stresses on critical buckling stress in the bottom flange of fixed ended beams

both the loads and lateral springs that match conditions in the real beam. Figure 5.2 shows the bottom flange modelled as a column with the same stress distribution in it as was the case when it was part of the beam, supported by springs of variable lateral stiffness, k, which represent the web's ability to restrain the flange.

Two cases were considered to see if this model could predict the buckling loads. The cross section and length of plexiglass Model 1 was used. Case 1 (problem 82) is shown in Fig. 5.3. The top flange of the beam is continuously braced against twist and lateral movement. In this manner, the web provides a uniform lateral support for the bottom flange and the stiffness of the springs, k, is constant per unit length of the flange. The spring constant is taken as the stiffness of the web acting as a cantilever supported at the top flange midsurface, $k = 1/\Delta = 3EI_w/d^3$ where I_w = moment of inertia of a unit width of web. The results show close agreement; the model prediction of σ_{fc} is 12 percent higher than the true stress at which the beam buckles. This is because the model does not take into account the effect of vertical and torsional stresses.

Case 2, shown in Fig. 5.4, is the beam of problem 25, whose buckled shape was presented in Fig. 3.10. Because the web is restrained against twist only at the supports and at midspan, the springs k will clearly be of variable stiffness along the length of the flange. k may be estimated as $1/(\Delta_1 + \Delta_2 + \Delta_3)$ where Δ_1 = translation of compression flange which is assumed to be zero for Case 2 based on an examination of the buckled shape, and Δ_2 = rotation of the compression flange, θ, multiplied by depth of the web. Here $\theta = 0$ at the ends and at midspan. At the other points along the length, assume that rotation θ has a linear distribution between the 1/4-points and the ends and midspan. At the 1/4-point, $\theta = (L/2)^2/8GJ_{tf}$, which is the angle of twist associated with uniform torsion in a bar.[8] J_{tf} is the torsion

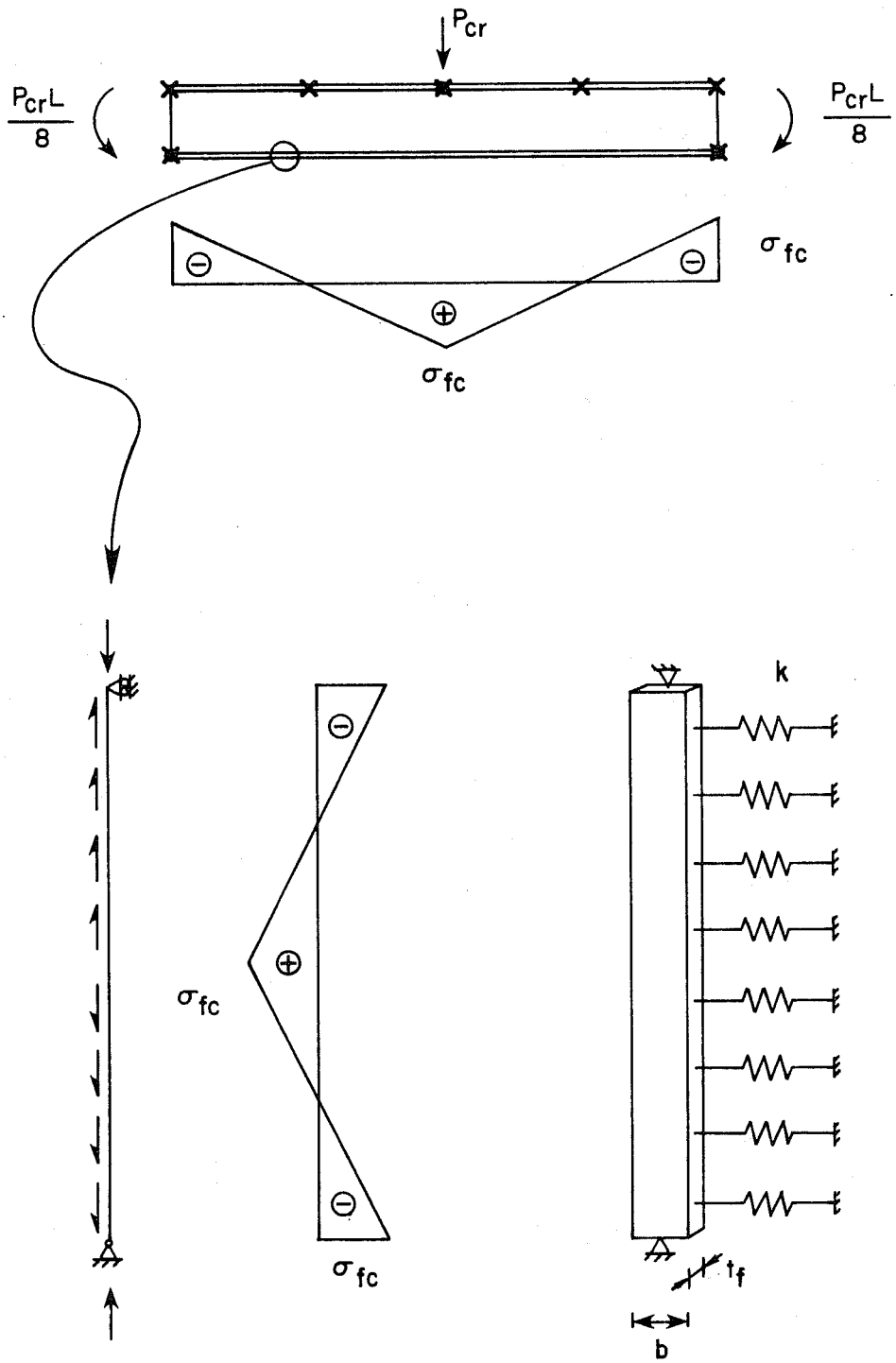

Fig. 5.2 Model of bottom flange

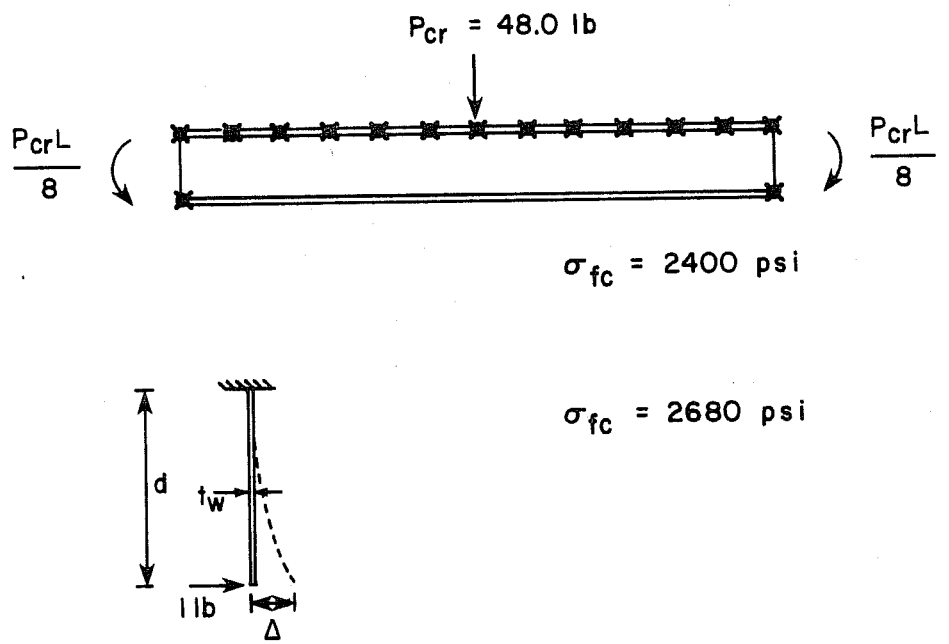

Fig. 5.3 Case 1--fixed ended beam braced continuously on top flange, multispring model

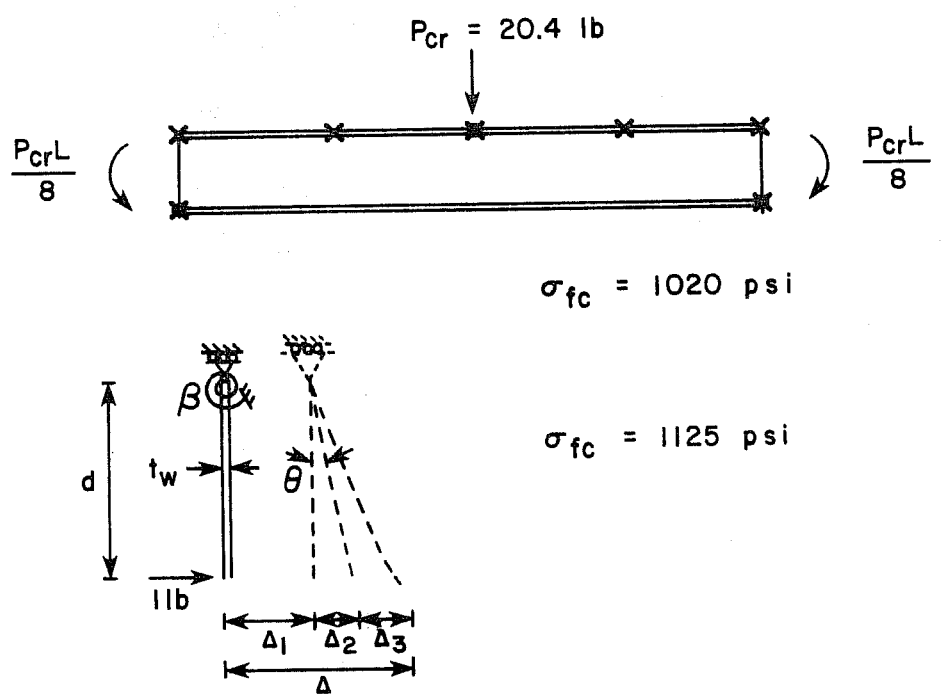

Fig. 5.4 Case 2--fixed ended beam braced at 1/4-points on top flange, multispring model

constant of the top flange which is equal to $bt_f^3/3$. Δ_3 is defined in Fig. 5.3 as Δ.

Using this variation in k, good correlation was obtained between beam and model. The model prediction was 10 percent higher than the beam buckling load and this again can be attributed to the omission of the effect of the vertical stresses in the flange model.

5.2.2 Single Spring Model. The previous section suggests that if the variation in lateral support spring stiffness along the flange length is accurately determined, then an excellent prediction of the critical buckling stress can be obtained. This procedure, however, is not suited for design purposes. Simple parameters are required to model the rest of the beam's ability to support the buckling bottom flange. The beam of Fig. 5.4 has rotational restraint of the top flange at midspan only. Consequently, in the calculation of $\Delta = \Delta_1 + \Delta_2 + \Delta_3$ it was found that at all locations except those near the supports or midspan, Δ_2 was by far the major component of Δ since the torsional resistance of the top flange was not high. Furthermore, most of the spring stiffnesses were less than 20 percent of the spring stiffness at the load point, with the springs adjacent to midspan being only 40 percent of this value. This suggested that a buckling model consisting of the flange with a stress distribution as shown on Fig. 5.2, but supported laterally only at one central location by a spring as in Fig. 5.5, could be applicable. This figure also shows the buckling curve nondimensionalized by σ^* and k^*, two reference values defined below. The curve was generated using BASP. Note that up to $k \simeq 15k^*$, an increase in k results in an increase in σ_{fc} and the buckled shape of the flange is symmetric. However, for $k > 15k^*$, the buckled shape is that of an anti-symmetric S-shape with no lateral movement at the brace point. Also, no increase in σ_{fc} is obtained for an increase in k. The reference value $\sigma^* = P^*/A_f$ where P^* = load at which an axially compressed flange would buckle in the second mode = $4\pi^2 EI_f/L^2$,

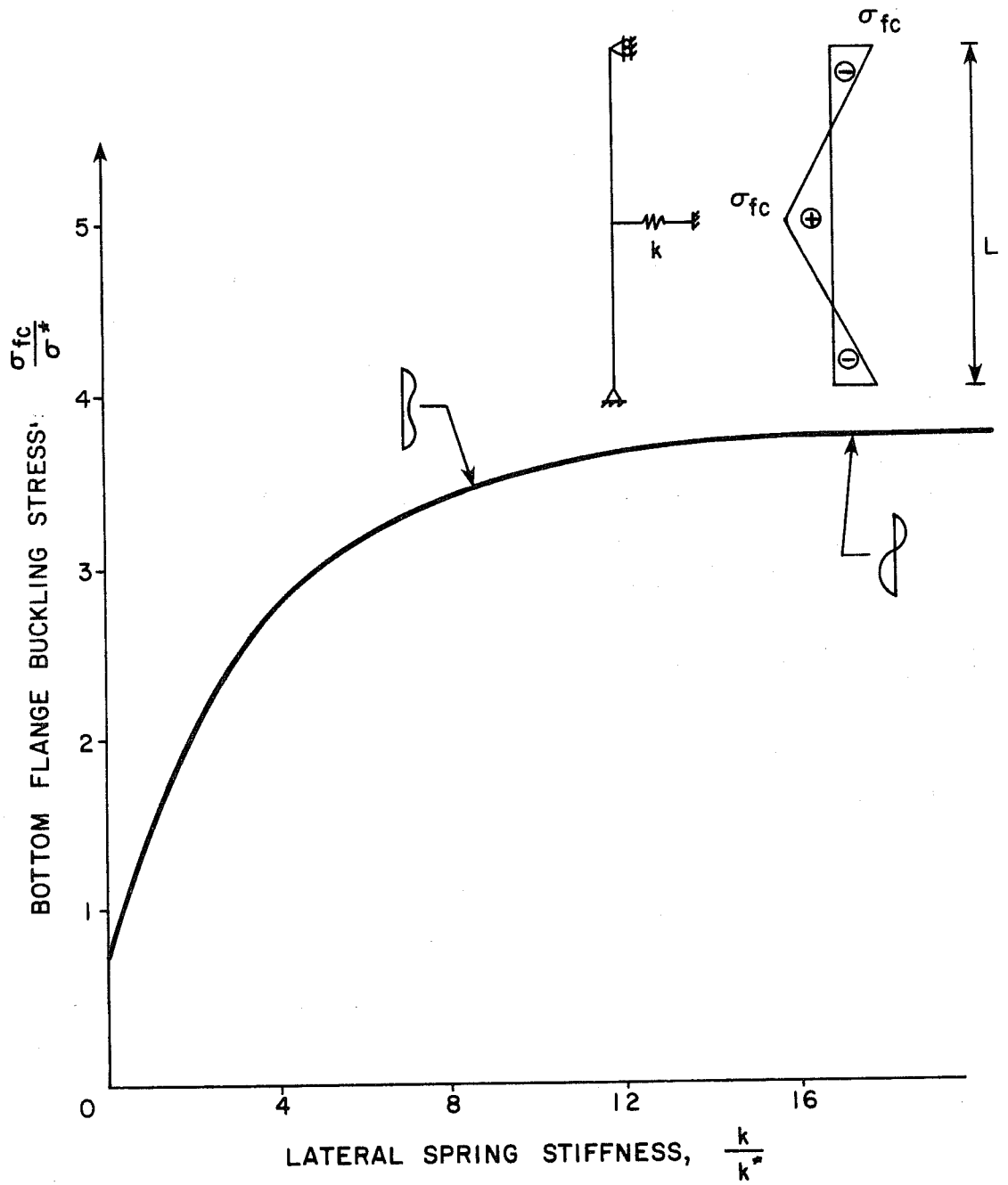

Fig. 5.5 Single spring model--bottom flange buckling stress versus lateral spring stiffness

A_f = area of flange and I_f = moment of inertia of the flange for bending out of the plane. Also k^* = minimum spring stiffness required to force buckling into the second mode of an axially compressed flange = $4P^*/L$.

The spring stiffness k is estimated as the cantilever bending stiffness of a portion of web supported at the top flange, using an effective length of web, b_{eff}, of 2d. In this manner

$$k = \frac{3E(I_w b_{eff})}{d^3} = \frac{Et_w^3}{2d^2} \tag{5.2}$$

Use of Eq. (5.2) and Fig. 5.5 result in an estimate for σ_{fc}. This critical buckling stress for the bottom flange of fixed ended beams can be converted to a buckling load for fixed ended beams with the bottom flange unbraced, P_{BFU}, given by

$$P_{BFU} = \frac{8\sigma_{fc} I}{LC_b} \tag{5.3}$$

where C_b is the distance from the neutral axis to the mid-thickness plane of the bottom flange. For doubly symmetric sections, $C_b = d/2$. Table 5.2 shows the comparison between Eq. (5.3) and the BASP results of Chapter 3. The results were conservative with the exception of problem 53. In this case the beam is very deep with $L/h = 8$. By taking b_{eff} to be 2d, far too much of the beam is considered to be supported by the brace under the load. For cases such as these, b_{eff} should be considerably reduced due to the long length of the web cantilever and hence, reduced effect of the torsional stiffness of the top flange. Taking b_{eff} to be zero, the buckling load prediction is only 5 percent in error.

A very stocky web ($h/t_w = 16$) was used in problem 55. So much support is offered by the web that the anti-symmetric buckling mode is obtained with both BASP and the model. Since this is

TABLE 5.2 COMPARISON OF BASP AND APPROXIMATE SOLUTIONS FOR UNBRACED BOTTOM FLANGES

Problem Number	Buckling Load BASP (lb.)	Buckling Load P_{BFU}, Eq. (5.3) (lb.)	% Error
25	20.4	20.4	0
52	7.3	5.3	-27
53	15.5	26.4 (16.3^{x})	+70 ($+5^{x}$)
54	8.7	7.1	-18
55	72.7	52.1	-28
56	48.3	44.1	- 9
57	14.0	13.6	- 3
58	6.9	8.7 (6.9^{*})	(0^{*})
59	1.14	7.1 (1.10^{+})	(-4^{+})
60	0.36	6.9 (0.33^{+})	(-8^{+})

^{x}obtained using $b_{eff} = 0$

*obtained using P_{LOC} (Eq. (5.1)) x 0.8

$^{+}$obtained using P_{LOC} (Eq. (5.1))

equivalent to full bracing at midspan, Eq. (1.1) could be used to predict the buckling load. Indeed, this is a lateral-torsional buckle between brace points and Eq. (1.1) yields P_{cr} = 65 lb.

The buckled shapes of problems 58, 59 and 60 indicate that local web buckling effects are dominating because of the slenderness of the web (h/t_w = 100, 200 and 300, respectively). In this case, Eq. (5.3) is grossly unconservative and Eq. (5.1) for P_{LOC} (or strictly speaking, 0.8 x P_{LOC}) should be used. These results indicate that local buckling can still occur in a fixed ended beam with an unbraced bottom flange.

5.2.3 Limitations. Equations (5.2), (5.3) and Fig. 5.5 are only valid as an estimate of the buckling load for fixed ended beams with twist restraint at the load, but at no other point in the span. Lateral restraint is assumed to be present at the load and also at some other points on the top flange along the span. This prevents appreciable lateral movement of the top flange during buckling, which is assumed in the derivation in Eq. (5.2). The predictions of the model are for elastic behavior and are based upon very simple assumptions. Real behavior, however, is a complicated interaction of many factors.

Several points must be made concerning the validity of the model:

(1) Beams with slender webs ($h/t_w > 100$) must also be checked for local web buckling, which may occur at loads lower than those to cause movement of the bottom flange. Equation (5.1) can be used to check web buckling for extremely slender webs ($h/t_w > 200$) as in problems 59 and 60 where the bottom flange will not move anyway. For slenderness ratios in the range $100 < h/t_w < 200$, it is recommended to take P_{cr} as 0.8 times the value obtained from Eq. (5.1), as in problem 58 because of bottom flange movement.

(2) For deep beams ($L/h < 10$), b_{eff} should be taken as considerably less than the recommended value for ordinary beams, 2d. Conservatively, take $b_{eff} = 0$, thus considering the flange as unbraced along its length. Note also that for very deep beams, the beam theory used in Eq. (5.3) becomes questionable.

(3) The model becomes very conservative for stocky webs ($h/t_w < 25$) because of significant torsional resistance .

(4) The model is conservative for stocky top flanges since the contribution of its torsional stiffness has been ignored. It was, however, considered in Case 2 of Sec. 5.2.1.

(5) As the thickness of the web increases, so does the stiffness of the supporting spring, k (Eq. (5.2)). In the limit this is equivalent to the bottom flange being braced at the load point. At this stage, the model (Eqs. (5.2), (5.3), and Fig. 5.5) should give the same buckling load as Eq. (1.1) for lateral torsional buckling between brace points. It is found that the model is conservative for web slenderness ratio $h/t_w < 25$, but unconservative for $h/t_w > 25$, because of the manner in which torsional resistance is considered. Nevertheless, it is reasonably accurate, but should not be used in place of Eq. (1.1).

CHAPTER 6

DESIGN RECOMMENDATIONS--BEAMS WITH VARYING END MOMENTS

6.1 Bottom Flange Braced

The interaction equation developed for simply supported beams and modified for fixed ended beams can accurately model local web buckling between top and bottom flanges braces in a beam with any degree of end restraint. Equation (5.1) can be used with L_1 the length between inflection points. Hence, as the end restraint approaches zero, length L_1 approached span length, L, and Eq. (5.1) becomes the original equation for P_{LOC}, Eq. (4.4). Table 6.1 shows the comparison between Eq. (5.1) and the BASP results shown previously in Fig. 3.9.

The results show that Eq. (5.1) can accurately predict the local web buckling load over the full range of end moments, M_N, between 0 and PL/6. As expected, increasing end moment increases the buckling load, P_{LOC}, because the bending stresses under the load are reduced.

6.2 Bottom Flange Unbraced

For a simply supported beam, the phenomenon of tension flange movement seems related to web buckling. Although the movement is pronounced, there is a clear local distortion under the load (Fig. 2.12). The buckling load, P_{TFU}, is predicted by Eq. (4.5) which is 80 percent of the load to cause local web buckling. For fixed ended beams, however, the bottom flange movement is almost unrelated to web behavior, and is caused by lateral buckling of the bottom flange. Equations (5.2), (5.3), and Fig. 5.5 predict the load that causes this movement of the bottom flange, P_{BFU}.

TABLE 6.1 COMPARISON OF BASP AND APPROXIMATE SOLUTIONS FOR BRACED BOTTOM FLANGES

Problem Number	M_N	L_1 (in.)	Buckling Load BASP (lb.)	Buckling Load P_{LOC}, Eq. (5.1) (lb.)	% Error
13	0	24*	62.3	61.4*	-1
27	PL/32	21	66.4	65.3	-2
28	PL/16	18	70.8	69.4	-2
29	PL/12	16	73.8	72.1	-2
30	PL/8	12	79.6	77.4	-3
31	PL/6	8	84.1	81.9	-3

*Can alternatively be obtained using $L_1 = L$ and P_{LOC} (Eq. (4.4)).

Quite clearly, beams with end restraint between zero and PL/8 (i.e., beams in between simple spans and complete fixity) will exhibit behavior that is an interaction of these two effects. With increasing end restraint, the bottom flange compressive stresses increase and cause the bottom flange instability to dominate over the web instability. Note that simultaneously the web becomes less likely to buckle because of reduced bending stresses under the load. An interaction equation is proposed to model this behavior. The negative end moment, M_N, is represented by the coefficient, α, defined by $M_N = \alpha(PL/8)$. A linear interaction is proposed between P_{TFU} for simply supported beams (Eq. (4.5)) and P_{BFU} for fixed ended beams (Eq. (5.3)). The buckling load for any α, $P_{BFU\alpha}$ is

$$P_{BFU\alpha} = \alpha P_{BFU} + (1 - \alpha)P_{TFU} \qquad (6.1)$$

This equation is only suggested in the range from simply supported beams up to complete fixity, and not beyond (i.e., $\alpha \leq 1$). Table 6.2 shows the comparison between this equation and the BASP results shown in Fig. 3.9. The results show reasonable correlation between BASP results and the estimate of Eq. (6.1). They, however, reaffirm that the equation should not be extrapolated beyond $\alpha = 1$. Problem 26 where $\alpha = 1.33$ is conservatively but inaccurately modelled by Eq. (6.1) with a 28 percent error.

6.3 Continuous Beams

Tests on continuous steel beams performed at the University of Texas at Austin and reported by Bansal[4] and Yura[18] are now examined. The estimate of the buckling loads given by BASP and Eq. (6.1) will be compared to the test results.

The test set-up of the 20 ft. main span beams is described in Chapter 1, and cases of both elastic and inelastic buckling were reported with movement of the flange primarily in tension (Figs. 1.2 and 1.3). The results of the tests of four of the beams are shown

TABLE 6.2 COMPARISON OF BASP AND APPROXIMATE SOLUTIONS FOR UNBRACED BOTTOM FLANGES

Problem Number	M_N	α	Buckling Load BASP (lb.)	Buckling Load $P_{BFU\alpha}$, Eq. (6.1) (lb.)	% Error
8	0	0.0	52.9	49.1*	- 7
22	PL/32	0.25	46.8	41.9	-10
23	PL/16	0.50	35.9	34.8	- 3
24	PL/12	0.67	29.3	29.9	+ 2
25	PL/8	1.00	20.4	20.4+	0
26	PL/6	1.33	15.3	10.9	-28

*$P_{BFU\alpha} = P_{TFU}$ (Eq. (4.5))

+$P_{BFU\alpha} = P_{BFU}$ (Eq. (5.3))

in Table 6.3. For convenience, these tests are numbered 83, 84, 85 and 86. Problems 83 and 84 have configurations as shown in Fig. 6.1. Problem 85 has the 1/4 point main span braces removed and problem 86 has the concentrated loads applied 3 ft. each side of the centerline and braced there instead of at the 1/4 points. BASP analyses were performed twice for each problem. Once with twist restraint at the load point enforced ($\theta_x = 0$) and once without. This is in light of the discussion of Sec. 4.4.1 which suggests yielding at the web-flange junction under the load allows rotation of the web to occur despite fixity of the flange, as shown in Fig. 4.5. All the buckled shapes from the BASP analyses were similar to that shown in Fig. 6.1.

At first glance, it appears that the test results are not similar to those obtained with the computer program. This, however, is not the case, and all can be explained by virtue of the degree of inelasticity present in each test.

Problem 83, shown in Fig. 6.1, was highly inelastic with a theoretical flange compressive stress of 77 ksi and a vertical web compressive stress of 59 ksi at the buckling load given by BASP of

TABLE 6.3 COMPARISONS WITH UNIVERSITY OF TEXAS CONTINUOUS BEAM TESTS[4,18]

Problem Number	Section	Buckling Load Test Result (kips)	Buckling Load, BASP (kips)	
			$w=\theta_x=0$	$w=0$
83	M14x17.2	26.8	52.3	44.5
84	M12x11.8	15.8	22.1	16.1
85	W12x14	27.8	34.5	23.7
86	M12x11.8	13.2	14.4	8.1

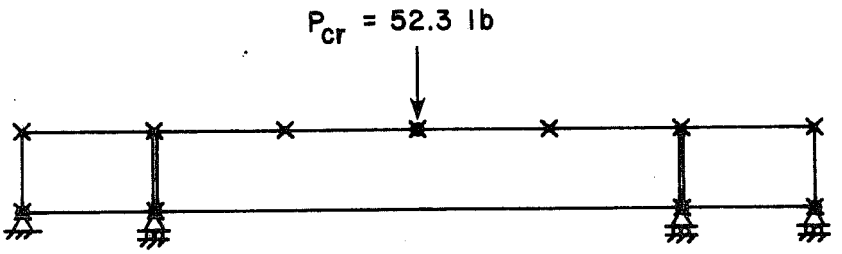

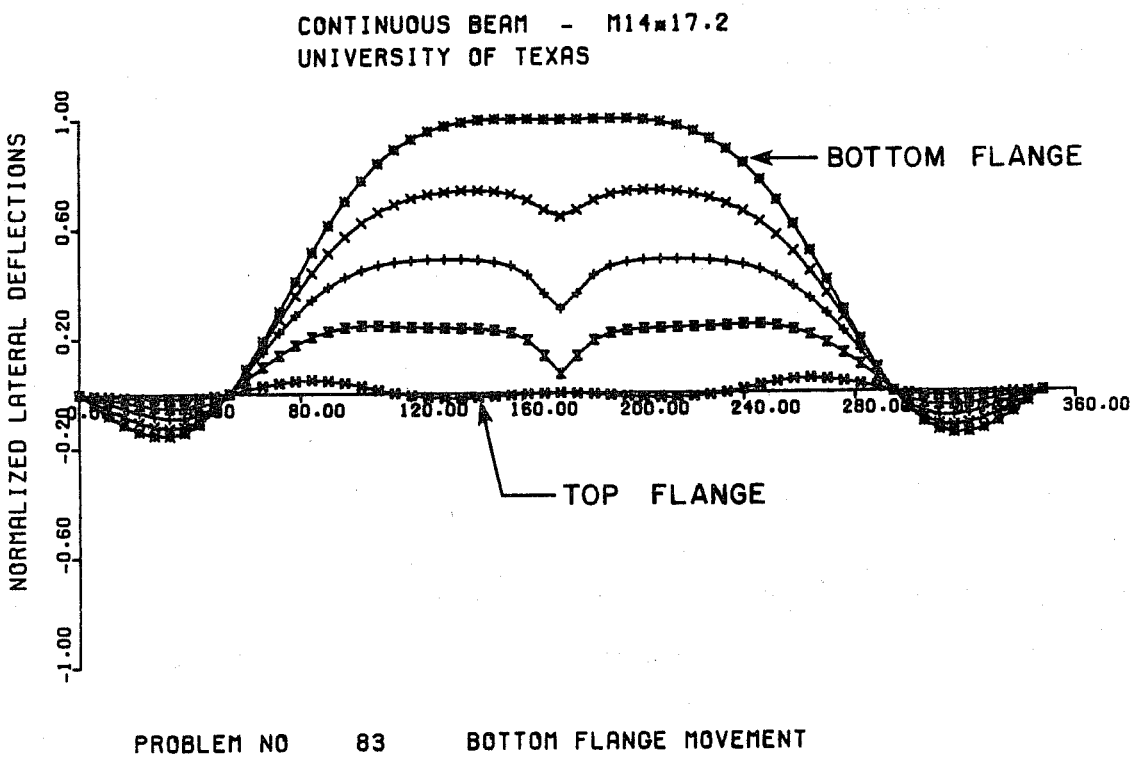

Fig. 6.1 BASP output--bottom flange movement of three-span continuous steel beam test[18]

52.3 kips. The yield stress of the material was 38 ksi. Theoretically yielding commenced at a load of only 25 kips and most certainly twist restraint of the web at the load point was lost. In such a highly inelastic problem, the elastic buckling program is grossly unconservative. However, the test result of 26.8 kips may also be low, as a 0.25 in. sweep was noted, which is at the tolerance limit of standard mill practice.[2]

Test beam 84 had a yield stress of 38.5 ksi. At the BASP buckling load for twist restraint removed, 16.1 kips, the flange stress is 43 ksi, slightly greater than the measured yield point. Hence, the BASP estimate should be valid; the comparison with the test result of 15.8 kips is very favorable.

The load to buckle the beam of test 85 was midway between the two BASP estimates. At the BASP estimate for the case $w = 0$, the flange stress is 48 ksi whereas when $w = \theta_x = 0$, the flange buckling stress is 72 ksi. The yield stress for this beam, 65 ksi, is between these two values and so is the buckling load.

Finally, test beam 86, which is just over yield when buckling occurs (39.6 ksi and 38.5 ksi for buckling stress and yield stress, respectively) is accurately predicted by BASP with rotational restraint enforced.

The buckling load $P_{BFU\alpha}$ given by Eq. (6.1) is compared to the BASP result for problem 83 in Sec. 6.4 following

6.4 Design Example

The buckling load for the beam of Fig. 6.1 will be calculated using the design recommendations presented in the previous sections. The beam is an M14x17.2 with $\sigma_y = 65$ ksi. The central span is 20 ft. and the outside spans are 4 ft.- 6 in. Relevant data are

$E = 29000$ ksi	$b = 4.000$ in.	$I = 149$ in.^{4}
$\nu = 0.3$	$t_f = 0.272$ in.	$I_f = 1.451$ in.^{4}
	$t_w = 0.231$ in.	$A_f = 1.09$ in.^{2}
	$d = 13.728$ in.	
	$h = 13.456$ in.	

In accordance with Eq. (6.1) α, P_{TFU} and P_{BFU} must be determined.

From statics, $L_1 = 138$ in. and $\alpha = 0.85$

From Eq. (4.4), $P_{LOC} = 98.2$ kips

From Eq. (4.5), $P_{TFU} = 0.8 \times 98.2 = 78.6$ kips

Also, $$P^* = \frac{4\pi^2 EI_f}{L^2} = 28.83 \text{ kips}$$

$$\sigma^* = \frac{P^*}{A_f} = 26.5 \text{ ksi}$$

$$k^* = \frac{4P^*}{L} = 0.481 \text{ k/in.}$$

From Eq. (5.2), $k = 0.948$ k/in.

From Fig. 5.5, $\sigma_{fc} = 54.7$ ksi

From Eq. (5.3), $P_{BFU} = 39.6$ kips

Thus, substituting α, P_{TFU}, P_{BFU} into Eq. (6.1),

$$P_{cr} = P_{BFU\alpha} = 0.85 \times 39.6 + 0.15 \times 78.6$$

$$= 45.5 \text{ kips}$$

This is 13 percent on the conservative side of the BASP estimate, 52.3 kips. Note that at P_{cr} = 45.5 kips, the flange stress is 67 ksi which is just above σ_y = 65 ksi. The final estimate for P_{cr} would conservatively be taken as 45.5 x 65/67 = 44 kips. The beam would remain elastic up to this load.

CHAPTER 7

SUMMARY AND CONCLUSIONS

A research program was carried out to study the phenomenon of lateral movement of the bottom flange of W-shaped beams under concentrated loading. The purpose of the study was to examine this phenomenon and determine whether or not the movement of this flange, primarily in tension, significantly affects the strength of the beam. Beams examined were simply supported or end restrained to any degree in the plane. Laterally, the ends were free to warp. The beams were loaded at midspan by a single concentrated load applied on the top flange, which was braced at this point both laterally and against twist. Plexiglass model beams were tested, analytical studies were undertaken using an elastic finite element linear-buckling program, and the results were compared to full-scale tests performed by others. Design recommendations for the control of this behavior were presented. It was discovered that the provisions in the AISC specification[3] for local web buckling under a concentrated load at midspan were unsatisfactory. Alternative recommendations were given.

The results of the study are:

(1) When the bottom flange of either simply supported or restrained beams is braced at the load point, then local web buckling can occur. The bending stresses at the load point, as well as the direct vertical stresses, heavily influence the buckling of the web plate. The load at which local buckling occurs is given by Eq. (4.4) for simply supported beams and Eq. (5.1) for restrained beams. The current AISC specification assumes that bending stresses do not

affect the local web buckling load and may, at times, be grossly unconservative.

(2) If the bottom flange of a simply supported beam is not braced at the load point, movement of this flange may occur together with a varying amount of local web distortion. Despite movement of the flange, the phenomenon is still related to the local web instability. The tension flange movement reduces the web buckling load by 20 percent (Eq. (4.5)), and hence, the costly addition of a brace may be unwarranted. However, with the bottom flange braced, significant post-buckling strength could be expected if the beam remained elastic, whereas, if the bottom flange were unbraced, none could be relied upon. This observation could be the subject of a future study.

(3) When the bottom flange of a fixed ended beam is unbraced under the load, its movement may be pronounced with little hint of local web distortion. The cause of this bottom flange movement is different than that in a simply supported beam. The end fixity induces compression in the bottom flange between the supports and the 1/4-points. The flange itself, being unbraced, triggers the beam buckling at loads considerably lower than those at which buckling occurs when the bottom flange is braced. Equations (5.2), (5.3), and Fig. 5.5 present some guidelines for calculation of this load. The addition of a brace on the bottom flange under the load may definitely prove worthwhile.

(4) If the beam is continuous, or has any degree of end restraint between zero and complete fixity, the interaction equation (6.1) can be used when the bottom flange is unbraced. In this case, the phenomenon is an interaction between web buckling and compression buckling of the bottom flange.

(5) Slender webbed beams with end restraint must also be checked for local web buckling.

(6) Beams with significant initial lateral deflection (sweep) displayed movement of the bottom flange at loads considerably lower than those without this sweep. It is important to keep within tolerance levels set by AISC, and to use a larger factor of safety to guard against this stability-related phenomenon.

(7) If yielding of the beam at the web-flange junction occurs, the twist restraint at this point can be lost, as a plastic hinge is formed. In this case, significantly lower buckling loads can be expected. Generally speaking, slender webs remain elastic at buckling, whereas stocky webs become inelastic under the load and should be examined carefully. Inelastic buckling may also be the subject of future research.

A P P E N D I X I

BASLER THEORY

The AISC Specification[3] uses theory developed by Basler[5] to check local web buckling under a concentrated load. Equation (1.2) is the unfactored version of the formula for the critical buckling load when no transverse web stiffeners are present. Basler considered both flanges to be braced laterally against movement and, in this case, the loaded flange is also braced against twist. He assumed that the loaded area of the web underneath the concentrated load is triangular as shown in Fig. A1.1(a), and then approximated this area by a square under a triangular stress distribution. This triangular distribution of stress along the length of the column is similar to a uniform column loaded under its own weight. A buckling analysis shows that problem to be equivalent to a uniform fixed-pinned column, end loaded by a force of 0.38 times the total force of the triangular stress distribution, as shown in Fig. A1.1(b). A fixed-pinned column has an effective length factor of approximately 0.7. Thus,

$$0.38P_{cr} \simeq \frac{\pi^2 EI}{(0.7L)^2}$$

or

$$P_{cr} \simeq \left(\frac{1}{0.38}\right) \pi^2 E \left(\frac{1}{0.7h}\right)^2 \left(\frac{ht_w^3}{12}\right)$$

$$= \frac{5.4\pi^2 E}{12} \times \frac{t_w^3}{h}$$

Allowing for the Poisson's ratio effect in plates, Eq. (1.2) results.

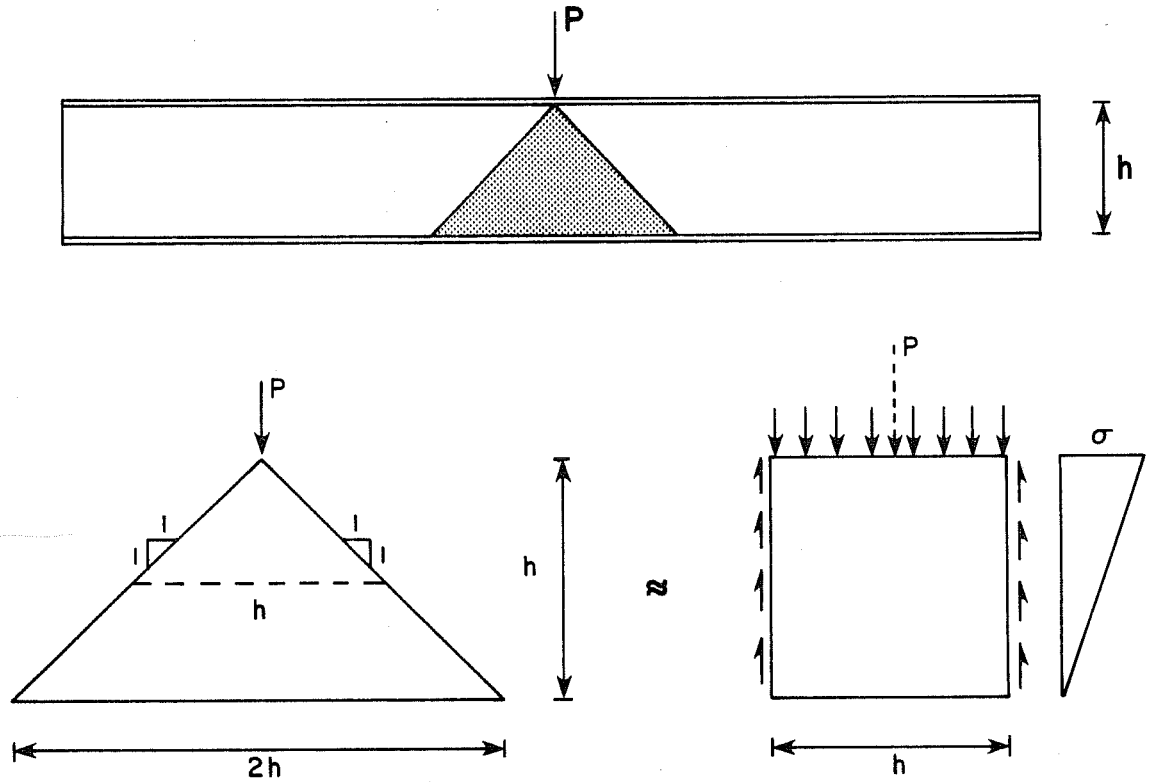

(a)

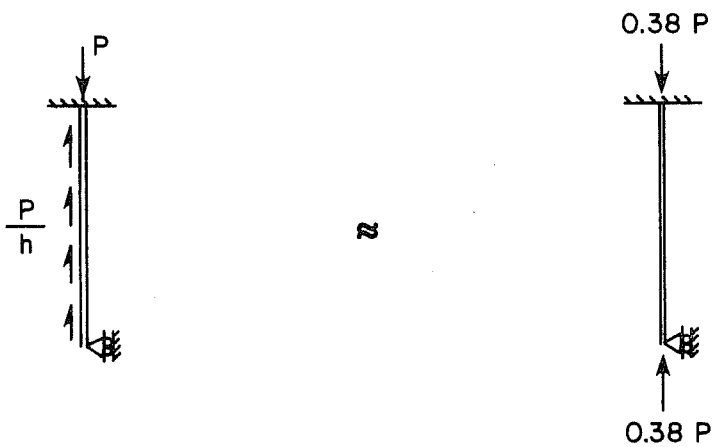

(b)

Fig. A1.1 Basler's theory

A P P E N D I X II

YURA THEORY

Yura's theory[18] employs the same stress distribution in the web as assumed by Basler, but the bottom flange is permitted to move laterally under the action of the concentrated load. The lateral stiffness of this flange controls the movement of point "B" in Fig. 1.8. The lateral spring stiffness, T, can be calculated for beams unbraced along the tension flange and with ends free to warp, as shown on Fig. A2.1, as

$$T = \frac{1}{\delta} = \frac{48EI_f}{L^3} \qquad \text{(A2.1)}$$

where δ = lateral deflection of flange under a unit load

I_f = moment of inertia of the flange for out-of-plane bending

$\simeq \frac{I_y}{2}$

A buckling analysis for the model of Fig. 1.8 yields the nondimensional plot of P_{cr}/P_E versus $t = Th/P_E$ shown in Fig. 1.9, where P_E = reference Euler buckling load of a pinned-pinned column = $\pi^2 E t_w^3/12h$.

As an example of the use of this theory, consider the 24 in. long plexiglass Model 1, the dimensions of which are shown in Fig. 2.7. The load to cause movement of the tension flange is calculated as follows:

$T = 1.08$ lb./in. from Eq. (A2.1)

$P_E = 9.00$ lb. from above definition

Therefore, $t = \frac{Th}{P_E} = 0.18$ and from Fig. 1.9,

$\frac{P_{cr}}{P_E} = 1.25$, hence $P_{cr} = 11.3$ lb.

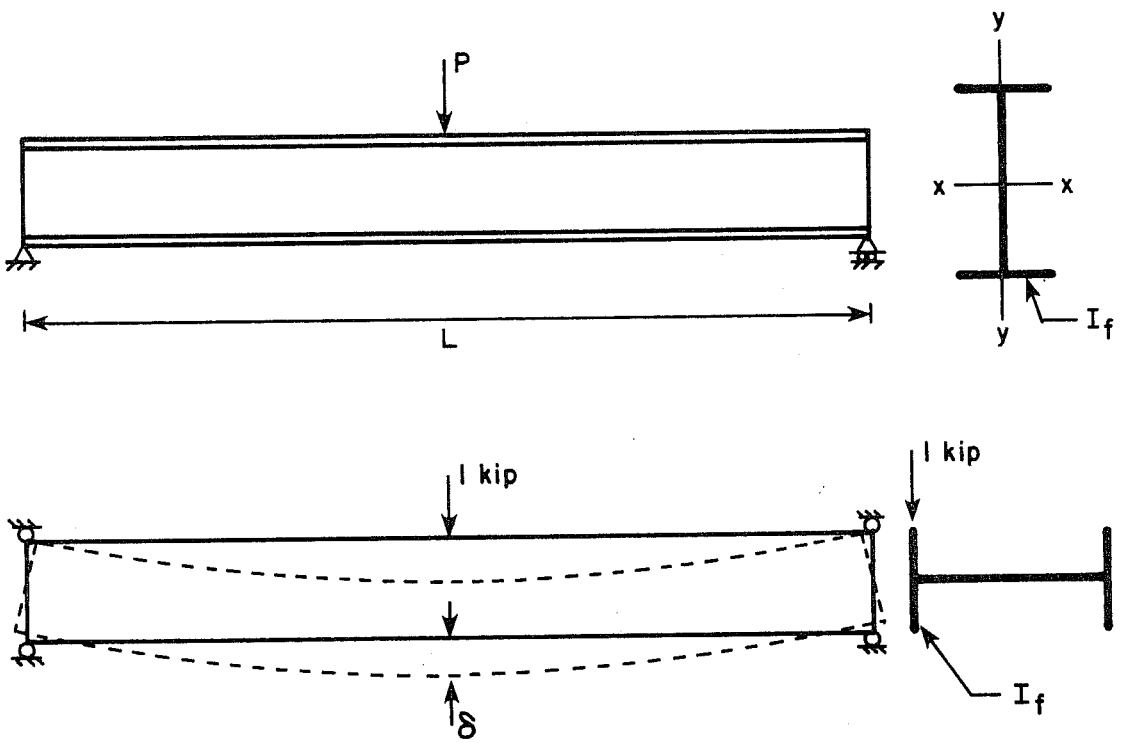

STIFFNESS OF TENSION FLANGE,

$$T = \frac{1}{\delta} = \frac{48EI_f}{L^3}$$

Fig. A2.1 Calculation of spring stiffness in Yura's theory

A P P E N D I X 3

LATERAL-TORSIONAL BUCKLING EXAMPLES

As examples of the use of Eq. (1.1) consider the plexiglass Model 1 (Fig. 2.7), simply supported over a 24 in. span and braced in the two configurations of Fig. 2.6.

First consider configuration 1 where the compression flange is braced at midspan and at the supports. The unbraced length, ℓ, is 12 in. The buckling coefficient, C_1, is 1.83 for this problem.[16] Use of Eq. (1.1) yields M_{cr} = 77.2 lb.-in. and hence, P_{cr} = 12.9 lb.

The calculation of P_{cr} for Configuration 2 (1/4-point compression flange bracing) can be conservatively estimated using ℓ = 6 in. and C_1 = 1.32 since in the critical central quarter-spans, the moment ratio M_{sm}/M_{1a} = -0.5, as shown in Figs. A3.1(a) and (b).[16] This yields M_{cr} = 188 lb.-in. and hence, P_{cr} = 31.4 lb. This is lower than the value of 35.2 lb. given by BASP (Fig. 2.11).

A better estimate, however, can be made using an effective unbraced length in Eq. (1.1). When the central quarter spans, BC and CD, shown in Fig. A3.1(b) try to buckle, the outside quarter spans, AB and DE, are not on the verge of buckling because of reduced stresses in these regions. The outside spans can offer restraint to the central buckling portions. For the whole beam to buckle, however, all portions must be on the verge of buckling and so P_{cr} is greater than the conservative estimate of 31.4 lb. given above.

The effective unbraced length can be estimated by the following alignment chart procedure, in which the beam is treated as a continuous column.[19]

In BC, CD $\quad \dfrac{M_{sm}}{M_{1a}} = -0.5$

In AB, DE $\quad \dfrac{M_{sm}}{M_{1a}} = 0$

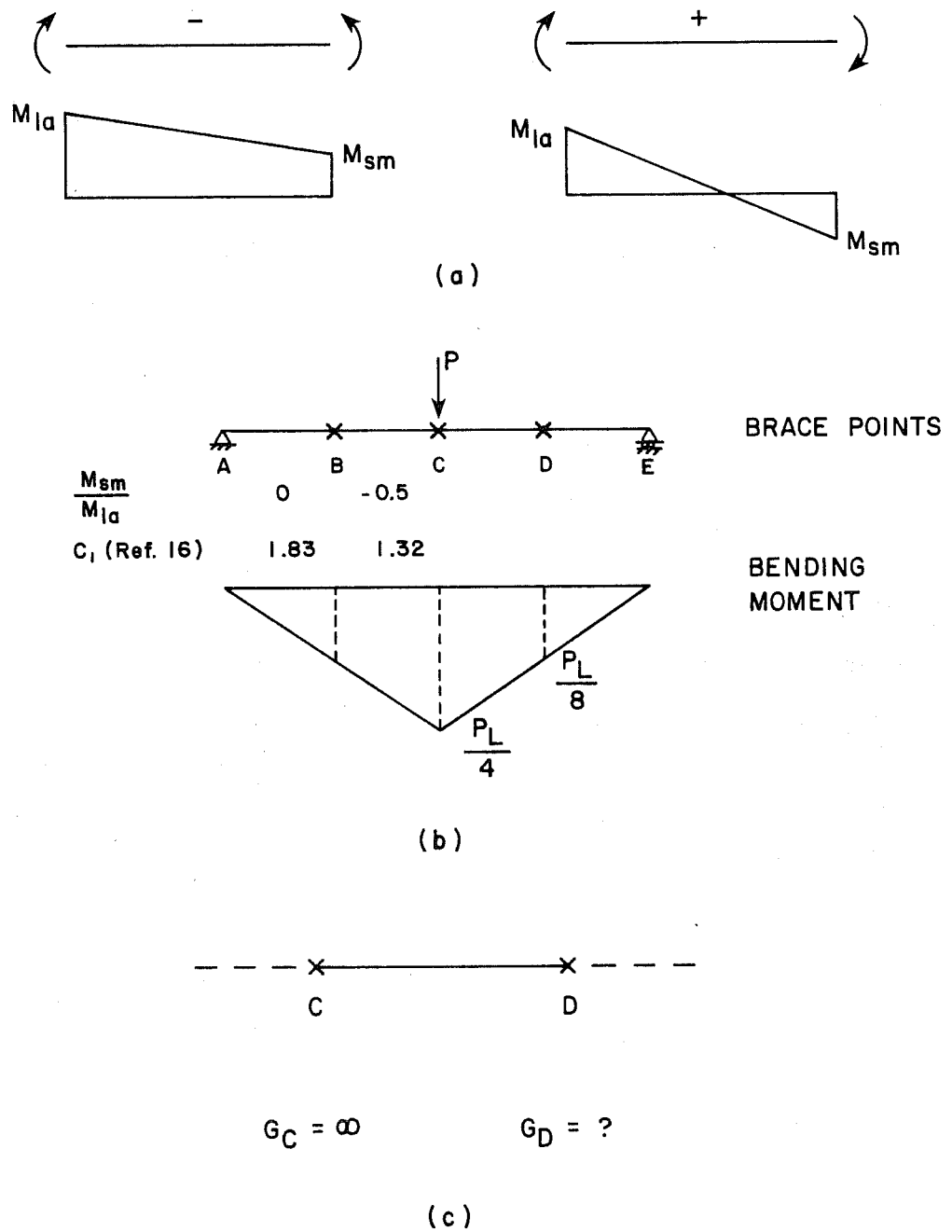

Fig. A3.1 Accurate use of Eq. (1.1) to calculate lateral-torsional buckling load for plexiglass Model 1 in configuration 2

Consider segment CD on the verge of buckling, Fig. A3.1(c). The joint stiffness bending ratio, G,[17] defined as

$$G = \frac{(I/L) \text{ buckling member}}{(I/L) \text{ restraining member}}$$

can be taken as ∞ at joint C as BC is simultaneously on the verge of buckling. However, at joint D, G_D is a finite value and can be estimated as

$$G_D = \frac{\left(\frac{I}{L}\right)_{CD}}{\left(\frac{I}{L}\right)_{DE}\left[1 - \frac{M_{CD}}{M_{DE}}\right]}$$

where M_{CD} = critical buckling moment of CD as a beam under the stresses present and M_{DE} = critical buckling moment of DE as a beam under the stresses present.

M_{CD}/M_{DE} can be approximated using the buckling coefficient ratio $(C_1)_{CD}/(C_1)_{DE} = 1.32/1.83 = 0.721$. Hence, $G_D \simeq 1/(1 - 0.721) = 3.59$. Using the alignment chart[17] for sidesway prevented frames with $G_C = \infty$ and $C_D = 3.59$, an effective length factor of 0.95 is obtained. Thus, taking $\ell = 0.95 \times 6$ in. = 5.7 in., in Eq. (1.1) yields $M_{cr} = 207$ lb.-in. and $P_{cr} = 34.6$ lb., which is very close to the BASP result.

One final observation should be made. For moment ratios $M_{sm}/M_{1a} = 1.0$ (reverse curvature), use of Eq. (1.1) with coefficients given by Salvadori[16] resulted in an estimate of the critical load (38.4 lb.) considerably higher than the BASP prediction (32.9 lb.) for a fixed ended 24 in. beam with the cross section of plexiglass Model 1 (Fig. 2.7), buckling between the supports and midspan in an antisymmetric S-shape. Note, however, that use of the design approximation to Salvadori's coefficients[17] given by

$$C_1 = 1.75 + 1.05\left(\frac{M_{sm}}{M_{1a}}\right) + 0.3\left(\frac{M_{sm}}{M_{1a}}\right)^2 \leq 2.3 \qquad \text{(A3.1)}$$

results in an accurate estimate of the buckling load (32.4 lb.). At other moment ratios considered in this study, Salvadori's coefficients resulted in accurate predictions of P_{cr}. Further investigation needs to be done to establish the extent of the inaccuracies.

A P P E N D I X 4

RESULTS OF PARAMETRIC STUDY

The parametric study presented in Chapter 3 involved the BASP analyses of 64 problems, designated as problems 6 through 69. The standard beam dimensions were those of plexiglass Model 1 (Fig. 2.7) over a 24 in. simple span, but for each problem one of more parameters were varied. The bracing configuration was that of Fig. 3.3 with the tension flange either braced or unbraced at location A. The results are shown in Table A4.1.

TABLE A4.1 RESULTS OF PARAMETRIC STUDY

Problem Number	Bottom Flange Bracing	Parameter Variation (Dimensions in Inches)	P_{cr} (lb.)
6	No	L=12	68.8
7	No	L=18	59.5
8	No	Standard	52.9
9	No	L=36	42.8
10	No	L=48	36.6
11	Yes	L=12	78.3
12	Yes	L=18	69.4
13	Yes	Standard	62.3
14	Yes	L=36	46.0
15	Yes	L=48	37.0
16	No	b=1.000,t_f=0.030*	54.7
17	No	b=0.250,t_f=0.119*	52.7
18	No	b=0.125,t_f=0.238*	51.1
19	Yes	b=1.000,t_f=0.030*	62.3
20	Yes	b=0.250,t_f=0.119*	62.4
21	Yes	b=0.125,t_f=0.238*	62.4
22	No	M_N=PL/32	46.8
23	No	M_N=PL/16	35.9
24	No	M_N=PL/12	29.3
25	No	M_N=PL/8	20.4
26	No	M_N=PL/6	15.3
27	Yes	M_N=PL/32	66.4
28	Yes	M_N=PL/16	70.8
29	Yes	M_N=PL/12	73.8
30	Yes	M_N=PL/8	79.6
31	Yes	M_N=PL/6	84.1
32	No	b=0.250,t_f=0.119	56.8
33	Yes	b=0.250,t_f=0.119	62.4
34	No	L=12,h=0.719	129
35	No	h=0.719	82.3
36	No	h=3.055	28.8
37	No	L=48,h=3.055	17.8
38	Yes	L=12,h=0.719	154
39	Yes	h=0.719	106
40	Yes	h=3.055	32.9
41	Yes	L=48,h=3.055	23.1
42	No	t_w=0.024	25.9
43	No	t_w=0.048	170
44	Yes	t_w=0.024	29.2
45	Yes	t_w=0.048	176
46	No	Singly symmetric+	55.9

TABLE A4.1 (Cont.)

Problem Number	Bottom Flange Bracing	Parameter Variation (Dimensions in Inches)	P_{cr} (lb.)
47	Yes	Singly symmetric+	72.5
48	No	Dimensions x 10	5290
49	No	Dimensions x 10, t_w=0.048	30.2
50	Yes	Dimensions x 10	6230
51	Yes	Dimensions x 10, t_w=0.048	30.5
52	No	M_N=PL/8, L=48	7.3
53	No	M_N=PL/8, h=3.055	15.5
54	No	M_N=PL/8, Singly symmetric+	8.7
55	No	M_N=PL/8, t_w=0.096	72.7
56	No	M_N=PL/8, t_w=0.064	48.3
57	No	M_N=PL/8, t_w=0.024	14.0
58	No	M_N=PL/8, t_w=0.015	6.9
59	No	M_N=PL/8, t_w=0.0075	1.14
60	No	M_N=PL/8, t_w=0.005	0.36
61	Yes	M_N=PL/8, L=48	56.9
62	Yes	M_N=PL/8, h=3.055	39.8
63	Yes	M_N=PL/8, Singly symmetric+	89.8
64	Yes	M_N=PL/8, t_w=0.096	No local
65	Yes	M_N=PL/8, t_w=0.064	No local
66	Yes	M_N=PL/8, t_w=0.024	35.1
67	Yes	M_N=PL/8, t_w=0.015	9.0
68	Yes	M_N=PL/8, t_w=0.0075	1.2
69	Yes	M_N=PL/8, t_w=0.005	0.36

*Tension flange only

+Fig. 3.6

Standard dimensions (Fig. 2.7) are:

b = 0.500 in.

t_f = 0.060 in.

h = 1.498 in.

t_w = 0.032 in.

L = 24 in.

B I B L I O G R A P H Y

1. Akay, H. U., Johnson, C. P., and Will, K. M., "Lateral and Local Buckling of Beams and Frames," Journal of the Structural Division, ASCE, Vol. 103, No. ST9, Proc. Paper 13226, Sept. 1977, pp. 1821-1832.

2. American Institute of Steel Construction, Manual of Steel Construction, 8th ed., Chicago, Illinois, 1980.

3. American Institute of Steel Construction, Specification for the Design, Fabrication and Erection of Structural Steel for Buildings, Chicago, Illinois, 1978.

4. Bansal, J. P., "The Lateral Instability of Continuous Steel Beams," unpublished Ph.D. dissertation, The University of Texas at Austin, Austin, Texas, 1971.

5. Basler, K., "New Provisions for Plate Girder Design," Appendix C, 1961 Proceedings, AISC National Engineering Conference, pp. 65-74.

6. Bathe, K., Wilson, E. L., and Peterson, F. E., "SAP IV: A Structural Analysis Program for Static and Dynamic Response of Linear Systems," Earthquake Engineering Research Center, University of California, Berkeley, California, Report No. EERC 73-11, June 1973, Revised April, 1974.

7. Bergfelt, A., and Hövik, J., "Thin-Walled Deep Plate Girders under Static Loads," IABSE, 8th Congress, New York, 1968, pp. 465-478.

8. Blodgett, O. W., Design of Welded Structures, The James F. Lincoln Arc Welding Foundation, Cleveland, Ohio, July 1976.

9. Clark, J. W., and Hill, H. N., "Lateral Buckling of Beams and Girders," Trans. ASCE, Vol. 127, Part II, 1962, pp. 180-201.

10. Column Research Committee of Japan, Handbook of Structural Stability, Corona Publishing Company, Ltd., Tokyo, Japan, 1971.

11. Daniels, J. H., and Fisher, J. W., "Static Behavior of Composite Beams with Variable Load Position," Fritz Engineering Laboratory Report No. 324.3, Lehigh University, Bethlehem, Pennsylvania, March 1967.

12. Hendry, A. W., Elements of Experimental Stress Analysis, SI Ed., Pergamon Press Ltd., Oxford, England, 1977.

13. Johnson, C. P., "Lateral Buckling of Rigid Frames by Finite Element Procedure," CESM Report, No. 72-1, Department of Civil Engineering, The University of Texas at Austin, Austin, Texas, January 1972.

14. Johnson, C. P., and Will, K. M., "Beam Buckling by Finite Element Procedure," Journal of the Structural Division, ASCE, Vol. 100, No. ST3, Proc Paper 10432, March 1974, pp. 669-685.

15. Lyse, I., and Godfrey, H. J., "Investigation of Web Buckling in Steel Beams," Trans., ASCE Vol. 100, Paper No. 1907, discussion by Lyse, I., and Godfrey, H. J., 1935, pp. 675-706.

16. Salvadori, M. G., "Lateral Buckling of Eccentrically Loaded I-Columns," Trans., ASCE, Vol. 121, 1956, pp. 1163-1178.

17. Structural Stability Research Council, Guide to Stability Design Criteria for Metal Structures, 3rd ed., John Wiley and Sons, Inc., New York, 1976.

18. Yura, J. A., "Web Behavior of Concentrated Loads in Steel Beams," presented at the Annual Meeting of the Column Research Council, March 24-25, 1970, St. Louis, Missouri.

19. Standards Association of Australia, SAA Steel Structures Code, Metric Units, AS1250-1975, Sydney, Australia, 1975.